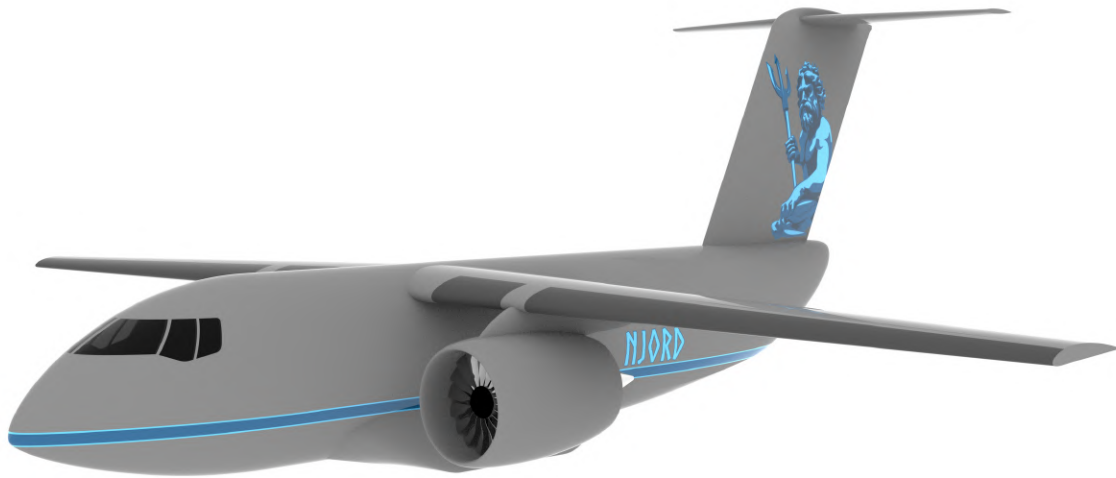# AIAA 2021-2022 Undergraduate Team RFP

Team Njord FDR

Ram Dwarakanath, Maverick Emerson, Nicholas Hall, Alan Hong, Macy Nanda, Nik Wagher, Kuan-Ta Wu

AE 443 - Aircraft Senior Design II
Department of Aerospace Engineering
University of Illinois at Urbana-Champaign
May 14, 2022

The Team

Macy Nanda

Ram Dwarakanth

Maverick Emerson

Nicholas Hall

Alan Hong

Nikhil Wagher

Kuan-Ta Wu
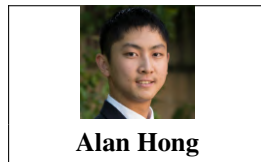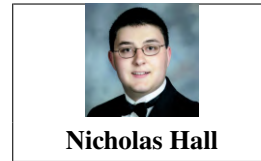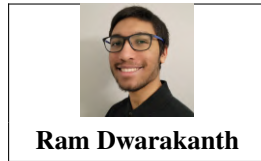
Group Member Responsibilities
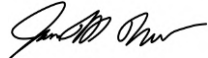
Team Member	Member Responsibilities	AIAA Number	Signature
Macy Nanda	Team Lead Cost Analysis Certification	1229331	
Ram Dwarakanth	Mass Properties Drop & Refill	1356667	
Maverick Emerson	Aerodynamics Systems (Lead) Configuration	1314914	
Nicholas Hall	Performance Propulsion (Lead) Repair & Maintenance	965091	
Alan Hong	Stability & Control Systems (Secondary) Avionics	1069168	
Nikhil Wagher	Structures Propulsion (Secondary) Landing Gear	1356665	
Kuan-Ta Wu	Loads & Dynamics Interior (Payload) Design	1356666	

Professor Jason Merret	Faculty Advisor	155270	

Table of Contents

Nomenclature

Greek Letters

α	=	angle of attack
α_{trim}	=	trim angle of attack
α_{zl}	=	zero lift angle of attack
β	=	side-slip angle
δ_a	=	aileron deflection angle
δ_e	=	elevator deflection angle
δ_r	=	rudder deflection angle
ϵ	=	downwash angle
Λ	=	quarter-chord wing sweep
Λ_h	=	horizontal tail $c/4$ sweep
Λ_v	=	vertical tail $c/4$ sweep
λ	=	Eigenvalue
ω	=	damped frequency
ω_n	=	undamped (natural) frequency
ρ	=	density
σ_{Yield}	=	yield stress
σ_{Ultimate}	=	ultimate stress
ζ	=	damping coefficient

Latin Letters

$c/4$	=	quarter-chord
C_d	=	2D coefficient of drag
C_D	=	3D coefficient of drag
C_{D_O}	=	induced coefficient of drag
C_f	=	coefficient of friction
C_l	=	2D coefficient of lift
C_L	=	3D coefficient of lift
C_{L_α}	=	lift-curve-slope
$C_{l_{\max}}$	=	2D maximum coefficient of lift
$C_{L_{\max}}$	=	3D maximum coefficient of lift
$C_{L_{TO}}$	=	take off lift coefficient
C_m	=	moment coefficient about the CG
C_{m_α}	=	derivative of C_m with respect to α
$C_{m_{\delta_e}}$	=	derivative of C_m with respect to δ_e
h_{cr}	=	cruise altitude
h_p	=	pressure altitude
K	=	drag-due-to-lift factor
M_{cr}	=	cruise Mach number
N_{half}	=	number of cycles to half amplitude
t_{half}	=	time to half amplitude
T	=	period of oscillation
V_H	=	horizontal tail volume coefficient
V_V	=	vertical tail volume coefficient

Acronyms

AA	=	Aluminum Alloy	IPPS	=	Integrated power plant system
AIAA	=	American Institute of Aeronautics and Astronautics	ISA	=	International Standard Atmosphere
AGL	=	Above Ground Level	KCAS	=	Knots Calibrated Airspeed
APU	=	Auxilliary Power Unit	LFL	=	Landing Field Length
AR	=	Aspect Ratio	M	=	Mach Number
ATC	=	Air Traffic Control	MAC	=	Mean aerodynamic chord
AVL	=	Athena Vortex Laboratory	MAFFS II	=	Modular Airborne Firefighting System II
BFL	=	Balanced Field Length	MSL	=	Mean Sea Level
CAD	=	Computer Aided Design	MTOW	=	Maximum Takeoff Weight
CFD	=	Computational Fluid Dynamics	MZFW	=	Maximum Zero Fuel Weight
CFR	=	Code of Federal Regulations	NACA	=	National Advisory Committee for Aeronautics
CG	=	Center of Gravity	NFPA	=	National Fire Protection Agency
DAPCA IV	=	Development and Procurement Costs of Aircraft v.4	NG	=	Nose Gear
			OV1	=	Operational Viewpoint
ECU	=	Engine Control Unit	PW	=	Pratt and Whitney
EIS	=	Entry Into Service	RDTE	=	Research, Development, Testing, and Evaluation
EGI	=	Embedded GPS/INS System			
EW	=	Empty Weight	RFP	=	Request for Proposal
EWIS	=	Electrical Wiring Interconnect System	SAF	=	Sustainable Aviation Fuel
FADEC	=	Full Authority Digital Engine Control	SFC	=	Specific Fuel Consumption
FAR	=	Federal Aviation Regulation	S.M.	=	Static Margin
FBW	=	Fly By Wire	TAWS	=	Terrain Avoidance and Warning System
FEA	=	Finite Element Analysis	TCAS	=	Traffic Collision Avoidance System
FEM	=	Finite Element Method	TCDS	=	Type Certification Data Sheet
GE	=	General Electric	TOC	=	Top of Climb
GEnx	=	GEnx 2B-67	TOS	=	Time on Station
GPS	=	Global Positioning System	USDA	=	United States Department of Agriculture
HEPA	=	High Efficiency Particulate Air	VLM	=	Vortex Lattice Method
INS	=	Inertial Navigation System			

List of Figures

List of Tables

I. Introduction

As the effects of climate change take their toll, wildfires have been occurring at an alarmingly increasing rate worldwide. This concerning trend has prompted the American Institute of Aeronautics and Astronautics (AIAA) to call on undergraduate design teams to conceptualize a novel purpose built firefighting aircraft to combat this worldwide crisis[1]. The University of Illinois at Urbana-Champaign (UIUC) based Team Njord proposes Valkyrie in response to this Request for Proposal (RFP). Valkyrie meets all requirements outlined in the RFP, with the majority of the objective requirements also being met. It is a highly modular aircraft with applications beyond firefighting. The design is a high-wing, T-tail, twin-engine tanker aircraft. Valkyrie is multi-drop capable and features a configurable drop system, meaning any volume of retardant up to the total capacity can be dropped. The aircraft outlined can transport 8,000 gallons of nine pounds per gallon retardant at a 400 nmi radius. Additionally, it is capable of performing two 6,500 gal missions at a 200 nmi radius per refueling. Firefighting aircraft must be able to operate in challenging environments, this necessitates the ability to takeoff and land from smaller, rural airstrips. As such, Valkyrie has a rough field Balanced Field Length (BFL) of 5,000 ft.

Valkyrie has an anticipated Entry Into Service (EIS) date of 2030, this is accomplished by using existing and pre-certified systems wherever possible; the proposed powerplant – the General Electric GEnx-2B67 – and the RADS-XXL payload drop system are used for this reason. Additionally, existing, pre-certified systems and avionics packages were selected with special consideration being given to the upgradeability of the avionics package to account for future autonomous operations. To further make Valkyrie a competitive aircraft in the aviation landscape of 2030, environmental implications of Valkyrie's operations were taken into account during the design process. The powerplant was selected in part due to its increased efficiency and compatibility with Sustainable Aviation Fuel (SAF). Additionally, the size of projected fires for 2030-2050 was used to drive Valkyrie's mission profiles.

The proposed aircraft has a wing area of 1,845 ft^2, an aspect ratio of eight, and Maximum Takeoff Weight (MTOW) of 209,000 lb. While the high-payload, dive-drop-dash mission profile associated with firefighting missions is unique, the aircraft capable of performing these missions is not necessarily constrained to it. The market for firefighting aircraft is relatively small, therefore Valkyrie is designed to be modular and can perform regular cargo missions with a 20,000 lb payload at the aircraft's ferry range of 3,000 nmi. This enables Valkyrie to double as a cargo carrier capable of reaching remote areas or transport an extra engine on the ferry mission to alleviate repair and maintenance concerns that arise from operating in remote areas.

The Research, Development, Test, and Evaluation (RDTE) and flyaway cost is $8.14B and the unit cost is $186M. Valkyrie operates primarily in the Very Large Air Tanker (VLAT) sphere due to its payload capacity and, as such, is intended to be owned by a private company and leased to firefighting bodies. Market analysis shows that, when sold at a 15% profit to the manufacturer, Valkyrie is highly financially competitive with similar existing systems to both owners and operators.

II. Concept of Operations

A. Requirements

Wildfires spread fast and unpredictably, thus making combating them in a timely manner of the utmost importance. Accordingly, the design parameters driving the development of the aircraft were the 5,000 ft balanced field length and 8,000 gallon fire retardant capacity. To ensure the aircraft can operate from all airports currently used for firefighting purposes, a span limitation of 132 ft was imposed as this is the wingspan of the C-130 currently used by CAL FIRE. Additionally, the aircraft was designed to be able to perform two 6,500 gal 200 nmi radius missions on a single load of fuel as refueling takes far longer than reloading retardant as typical refuelling procedure mandates that the engines must power off and cool down. The requirements laid out by AIAA and the team's design goals in response to them are laid out in Table 2.

Table 2 RFP Requirements[1]

Category	Requisite Requirement	Objective Requirement	Team's Choice
Entry into Service (EIS)	2030	–	2030
	Existing engines used	–	General Electric GEnx-2B67
Retardant Capacity	4,000 gal	8,000 gal	8,000 gal
Multi-drop capable	2,000 gal per drop	–	Configurable multi-drop capable
Retardant Specific Weight	9 lb/gal	–	9 lb/gal
Payload Drop Speed	150 kts	125 kts	150 kts
Payload Drop Altitude	300 ft AGL	–	300 ft AGL at 5,000 ft pressure altitude
Balanced Field Length (BFL)	8,000 ft at 5,000 ft MSL elevation on +35°F day	5,000 ft at 5,000 ft MSL elevation on +35°F day	5,000 ft at 5,000 ft MSL elevation on +35°F day
Design radius at full payload	200 nmi	400 nmi	One 400 nmi mission or 2×200 nmi
Design ferry range	2,000 nmi	3,000 nmi	3,000 nmi
Dash speed	300 kts	400 kts	300 kts
Certification	FAA Title 14 Code of Federal Regulations - Part 25 Certifiable	–	FAA Title 14 Code of Federal Regulations - Part 25 Certifiable

The team's choice of requirements for Valkyrie informs specific airframe requirements and design choices, as shown in Table 3.

Table 3   Requirement Flow Down

Requirement	Derived Requirement	Allocated Requirement
EIS 2030, powerplant in development by 2028	Where possible, use systems in development by 2028	• Use existing systems and avionics packages • Prioritize system software upgradeability • Design for 2030 environmental legislation
8,000 gal fire retardant at 9 lb/gal (72,000 lb)	• 209,000 lb MTOW • 122,000 lb take off thrust • 45,700 lb fuel	• 1,845 ft^2 Wing Reference Area • 8 AR • Use multi-drop capable payload delivery system with compatible 500 gal/min retardant reloading rate
125 kts drop speed	0.13 M minimum sea level velocity	• Stall angle of attack of 12° • C_{L_max} of 2.27
300 kts dash speed	–	–
400 nmi design mission radius	Additional 2×200 nmi radius firefighting mission	• 6,500 gal payload at 2×200 nmi radius mission • 28,000 ft cruise altitude
5,000 ft at 5,000 ft MSL on a +35 °F day	5,000 ft FAR rough field landing at 5,000 ft MSL on a +35 °F day	• 30% oversized landing gear tires • Takeoff angle of 9° • Compressed tailstike angle of 13° • Span limited by C-130 (132 ft)
3,000 nmi ferry range	–	• 20,000 lb cargo capacity • 28,000 ft cruise altitude • Cruise Mach number of 0.67

B. Operations

A network of airports with fire retardant reloading capabilities that are within the mission range to the fire in question is essential to Valkyrie's operation. Additionally, communication between the aircraft and a lead plane, which is required by the National Fire Protection Association (NFPA) for firefighting aircraft of Valkyrie's size, in order to determine where to strategically deliver fire retardant to mitigate the spread of the fire is also imperative[2]. This communication will be facilitated via radio channel. Additionally, Valkyrie will be able to communicate via radio channel with ground operations and Air Traffic Control (ATC). Valkyrie's operation requires three crewmembers, namely, a pilot, copilot, and drop operator. Communication with the leadplane and ground operations is the primary responsibility of the drop operator, whereas communication with ATC is primarily the responsibility of the pilot and copilot. The many systems which must interact have been synthesized in an Operational Viewpoint (OV1) diagram, shown below in Figure 1.
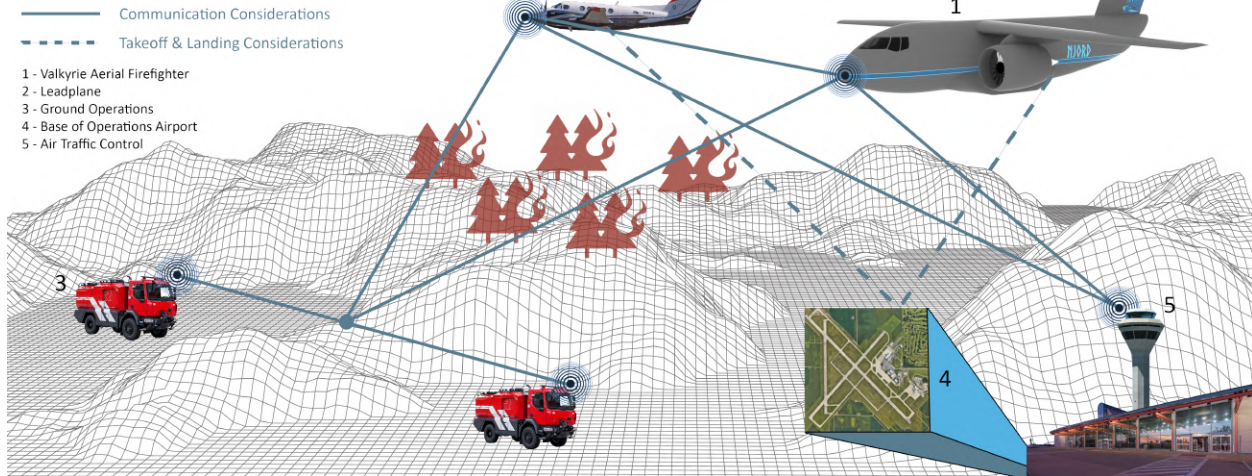
Fig. 1   OV1 Diagram

Valkyrie is designed to both fight fires efficiently and maximize profit for operators by doubling as a cargo aircraft at its ferry range. As such, Valkyrie has three distinct mission profiles. The mission profile for which Valkyrie was designed is the 400 nmi firefighting mission carrying 8,000 gal of payload, shown in Figure 2.
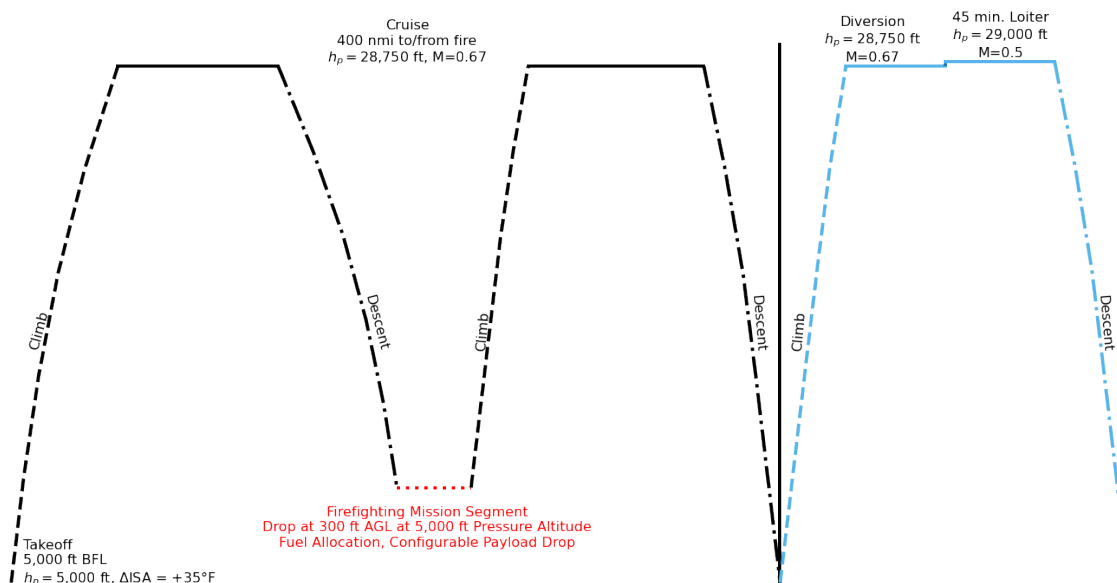
Fig. 2   400 nmi firefighting mission profile

Valkyrie has an alternate firefighting mission profile in which two 200 nmi radius firefighting missions, each carrying 6,500 gal of retardant, can be performed on a single refueling shown in Figure 3.
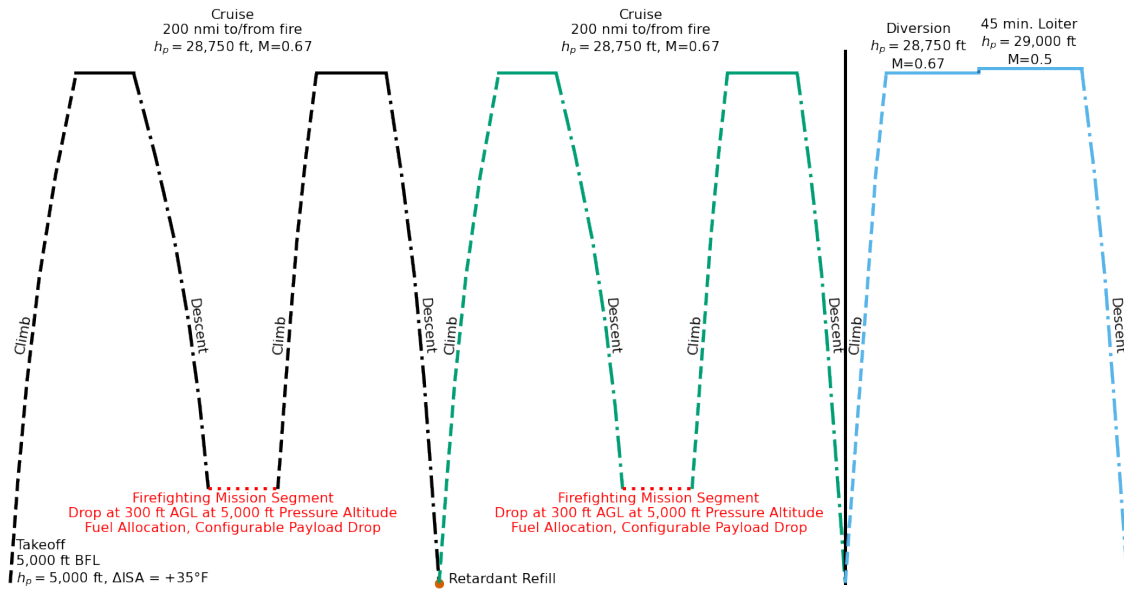
Fig. 3   2 × 200 nmi Firefighting Mission Profile

Valkyrie is intended to be used year round in all fire seasons and thus must be capable of flying a 3,000 nmi ferry range mission. Valkyrie's ferry mission profile is shown below in Figure 4.
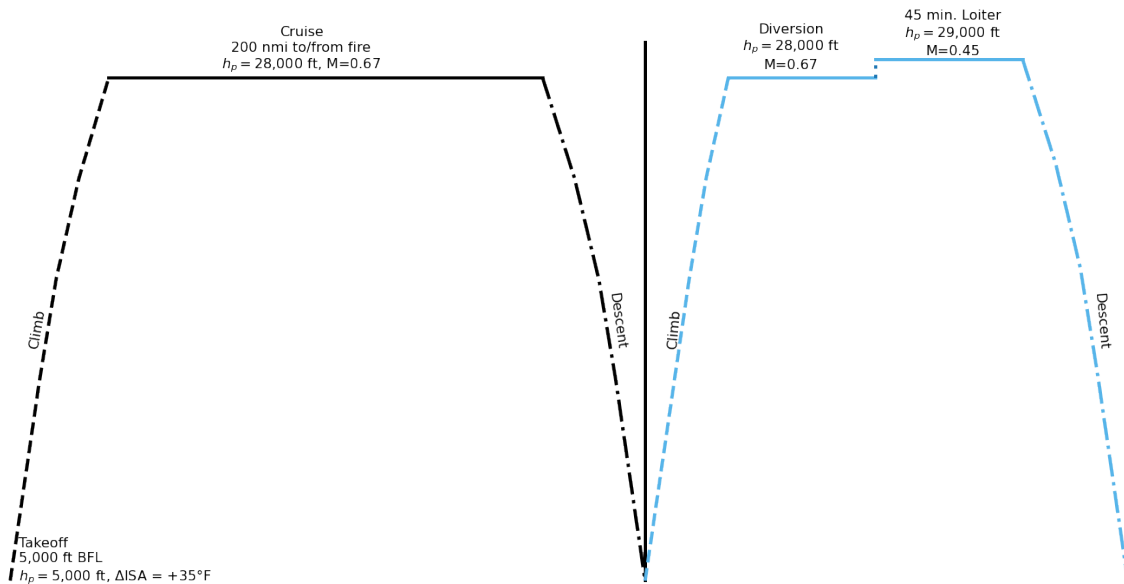
Fig. 4   Ferry Mission Profile

The 3,000 nmi mission was designed in order to allow Valkyrie to operate globally, specifically in the Austrailian fire season. The ferry range allows Valkyrie to travel to Australia as shown in Figure 5.
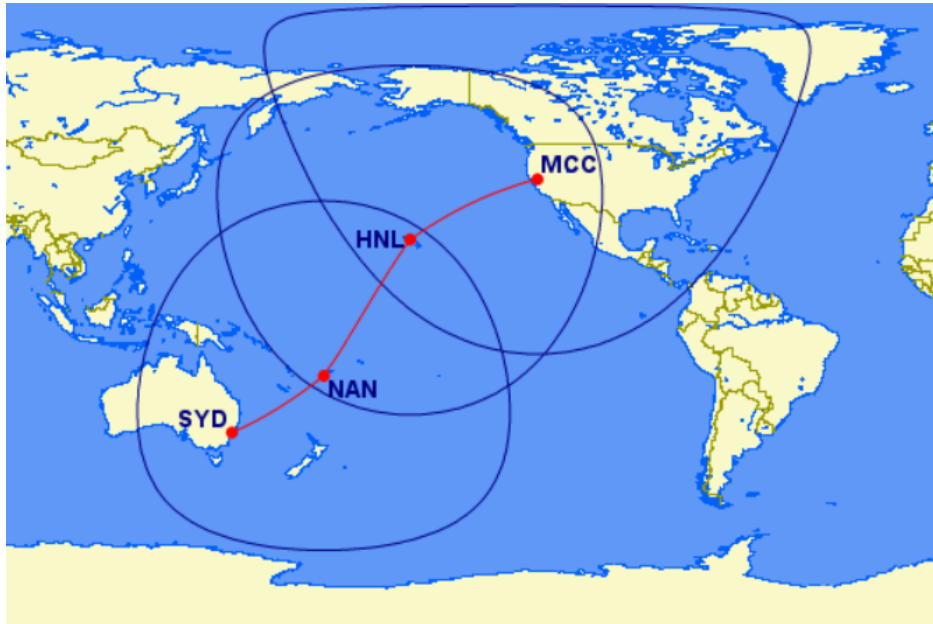
Fig. 5   Potential Valkyrie Ferry Route

C. Fielding and Maintenance

Valkyrie is a VLAT designed assuming that it is a leased aircraft and, thus, designed for year-round use. The RFP outlines that the aircraft should be designed assuming 1,200 flight hours per year, which is in keeping with the year-round assumption. These flight hours shall consist of cargo missions, ferry missions, firefighting missions, and training missions. An assumed flight hour allocation is shown below in Figure 6.
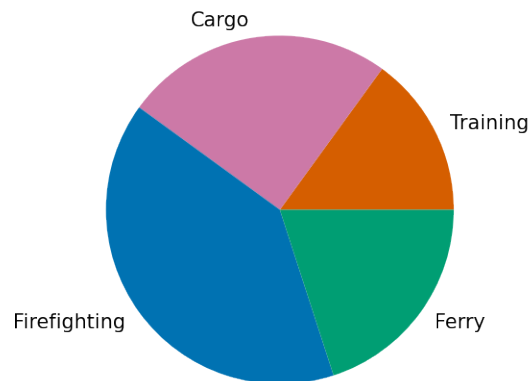
Fig. 6   Assumed Allocation of Valkyrie's Yearly 1,200 Flight Hours

Valkyrie is designed for the harsh firefighting environment it will fly in for the majority of its use. This harsh environment will lead to soot buildup in the engines and increased wear to the airframe. Preventative measures have been taken in the design of Valkyrie including the use of an aluminum fuselage and ten percent excess thrust margin on the engines. As previously mentioned, to account for the lack of resources in the remote locations Valkyrie will likely be operating in, a 20,000 lb cargo capacity was added to the ferry mission to enable Valkyrie to bring a backup engine. Valkyrie will also carry backup equipment such as an engine winch and engine dolly part to add to ease of repair. In addition to these measures, a robust repair and maintenance schedule has been created for the operators of Valkyrie.

III. Sizing Analysis

The foundation of Valkyrie's design was derived from an existing, similarly configured aircraft comparable to a VLAT. The aircraft considered along with their specifications are detailed in Table 4. An initial firefighting aircraft was sized by morphing the Embraer C-390's design. The weight of the derived aircraft was obtained by approximating the weight difference from the C-390 seed using statistical equations, which was used to inform the selection of the engines. The weight was recalculated using a component-wise weight buildup from which the design was iteratively refined to meet the team's goals. The decisions made throughout the design process were guided by the results of trade studies. The influences of wing taper ratio, wing quarter-chord sweep, and cruise Mach number on the aircraft's MTOW, empty weight, fuel weight, and takeoff lift coefficient were investigated. The effects are visualized in the contour plots presented in Figures 7-10.

Table 4   Valkyrie and Similar Aircraft Used in Initial Sizing

Parameter	Valkyrie	C-390[3]	C-2[4]	C-17[5]	A400M[6]	YC-15[7]
Max. Payload (lb)	76,600	57,320	79,370	170,900	81600	78,000
Range w/ Max. PL (nmi)	950*	1,470	2,400	2,400	2,100	1,040
Ferry Range (nmi)	3,000	3,370	5,300	6,230	4,800	–
BFL (ft)	4,910	5,000	7,550	7,440	–	–
TOFL (ft)	3,450	–	–	–	3,215	<2,000
MTOW (lb)	209,000	164,000	311,100	585,000	310,850	216,680
TO Thrust (lb)	122,540	62,660	119,480	161,760	–	64,000
S_w (ft^2)	1,845	1,490	2,620	3,800	2,384	1,740
AR	8.0	8.9	8.1	7.6	8.1	7.0
S_h (ft^2)	335	280	590	845	710	640
S_v (ft^2)	400	340	560	810	560	580
Λ_h (deg)	7.8	30.2	27.4	27.0	32.2	6.2
Λ_v (deg)	25.0	38.6	34.7	41.4	34.2	41.1
V_H	0.616	0.732	0.804	0.756	1.117	1.293
V_V	0.084	0.105	0.096	0.100	0.108	0.167

*Does not include reserves range and assumes payload drop conforming to 400 nmi mission profile
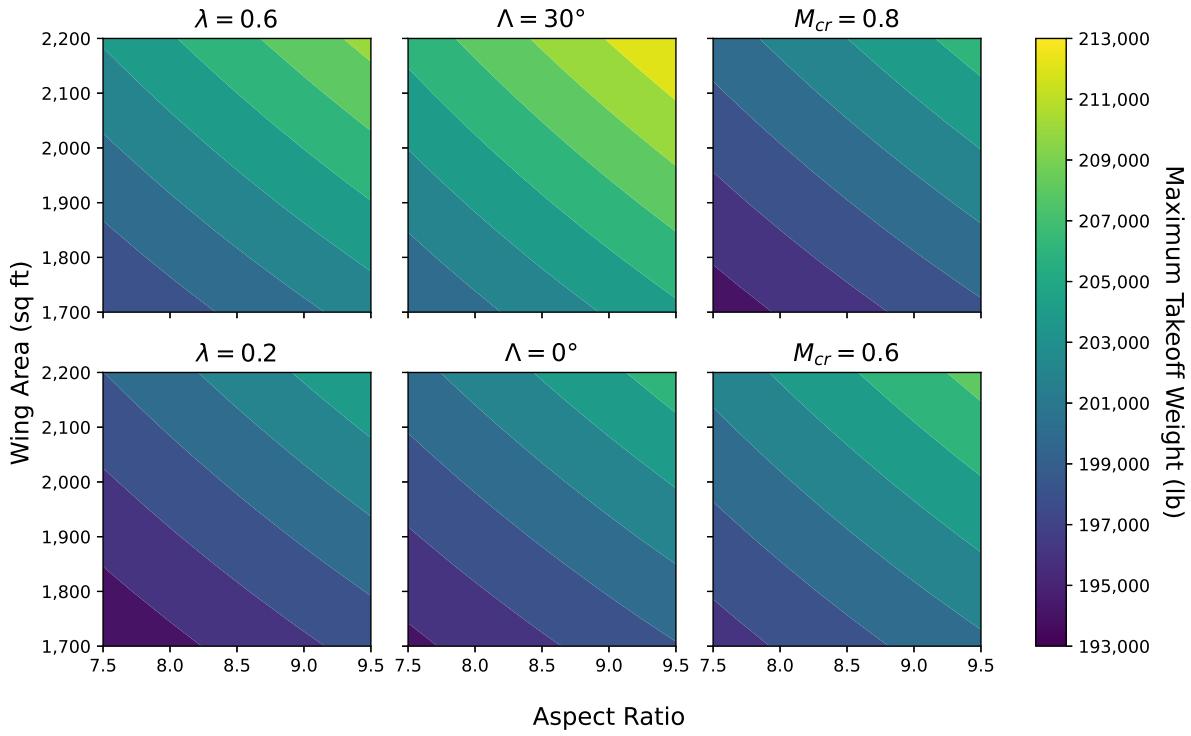
Fig. 7   MTOW for Wing Area and Aspect Ratio Combinations Subject to Changes in Design Parameters
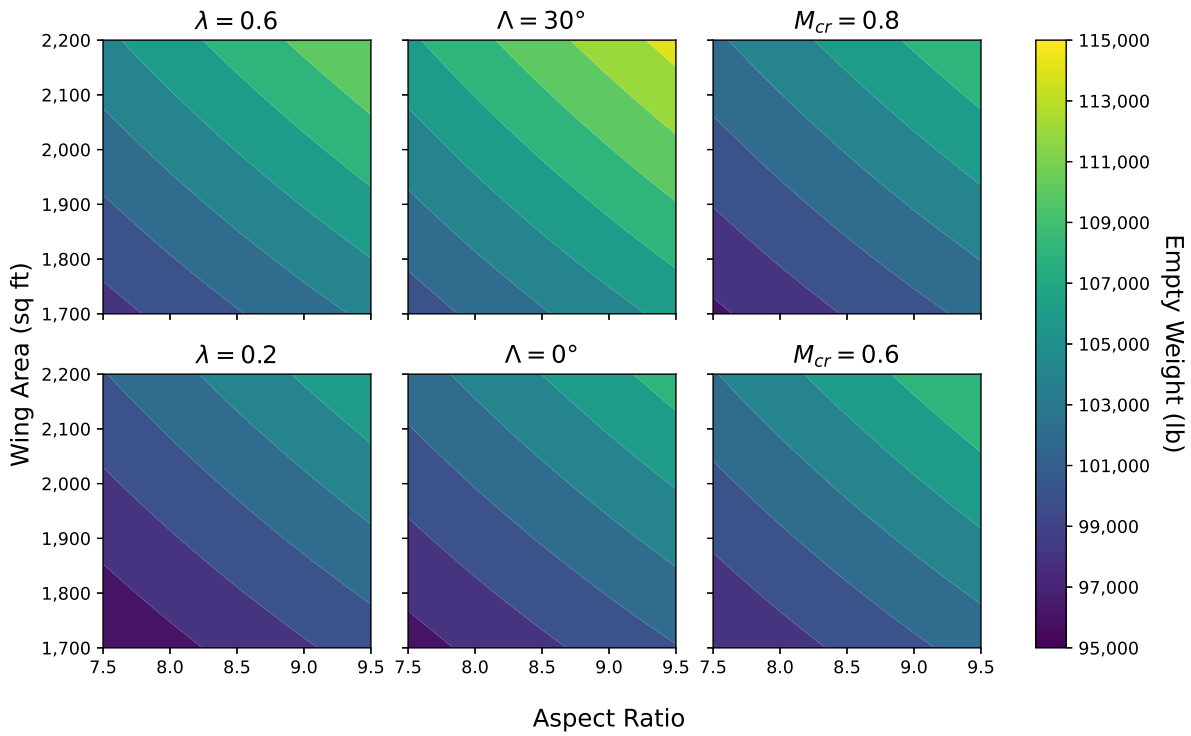
Fig. 8   Empty Weight for Wing Area and Aspect Ratio Combinations Subject to Changes in Design Parameters
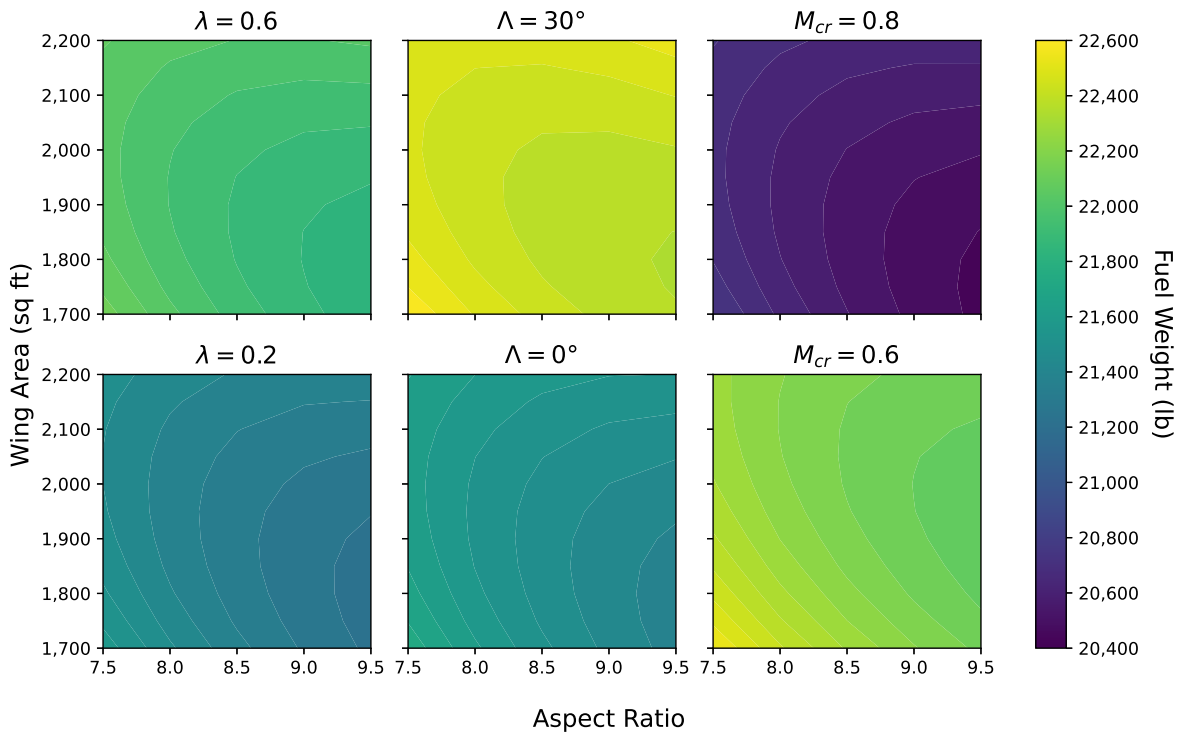
Fig. 9   Fuel Weight for Wing Area and Aspect Ratio Combinations Subject to Design Parameter Changes
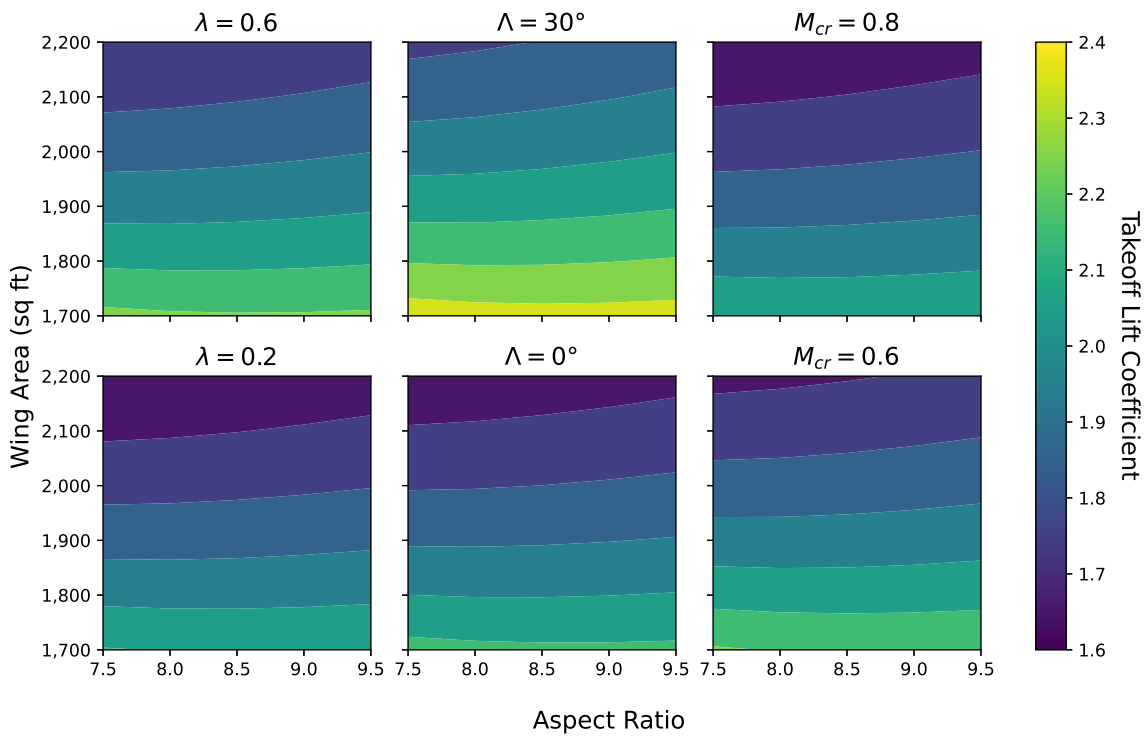
Fig. 10   Takeoff C_L for Wing Area and Aspect Ratio Combinations Subject to Changes in Design Parameters

Table 5   Averaged Variable Sensitivities

	∂MTOW	∂W_{empty}	∂W_{fuel}	$\partial C_{L_{TO}}$
$\partial\lambda$	105.3 lb/%	90.74 lb/%	14.57 lb/%	0.002554 /%
$\partial\Lambda$	188.0 lb/deg	157.7 lb/deg	30.24 lb/deg	0.005961 /deg
∂M_{cr}	-93.67 lb/%	-12.32 lb/%	-81.35 lb/%	-0.003936 /%

The variable sensitivities from the trade studies are quantified in Table 5. Observations about the effects of each design parameter can be quickly made from the sign and magnitude of the sensitivities. To reduce the maximum takeoff, empty, and fuel weights and takeoff C_L, lower taper ratio and wing sweep and a higher cruise Mach number should be designed toward. Across all parameters, wing sweep had the greatest impact, and so Valkyrie was designed around an unswept wing. Consequently, by straight wing aerodynamics, for the same airfoil section, the critical and drag divergence Mach numbers are lower. Valkyrie cruises at its more aerodynamically constrained maximum cruise Mach number of 0.67. The taper ratio was set to 0.4 as is typically ideal for most unswept wings[8]. These, along with other specifications not already listed in Table 4, are expressed in tabular form in Table 6.

Table 6   Additional Aircraft Specifications

λ	0.4	Empty Weight (lb)	105,000
Λ	0	Fire Mission Fuel Weight[†] (lb)	28,300
M_{cr}	0.67	Fuel Capacity (lb)	46,000
$C_{L_{TO}}$	2.00	T/W	0.584
$C_{L_{LDG}}$	2.27	W/S	114

From requirements, a constraint diagram can be constructed that readily determines whether an aircraft design is feasible or infeasible simply by looking at its thrust loading and wing loading. For this RFP, the feasible region can be fully defined by the BFL, drop speed, and dash speed requirements. A minimum 1.2% climb gradient at One-Engine-Inoperative (OEI) condition in accordance with §25.121(c)(1) of 14 Code of Federal Regulations (CFR) Part 25 requirements for twin engine aircraft was accounted for, but was not an active constraint. However, to ensure that the final design would be competitive on the market, the desired outstanding capabilities were to be designed into an aircraft similar in size to the C-130 airframe that is popular among firefighting agencies. This was represented as a constraint in the form of a maximum span of the C-130's 132 ft, which was more constraining than the dash speed. In designing for a 400 nmi operational firefighting radius with 8,000 gal of retardant, the BFL objective of 5,000 ft became the biggest design driver. The nonexistence of modern turbofans that produce between 35,000 and 55,000 lb of thrust meant that BFL could only be met using either a large wing with small engines or a small wing with large engines. The smaller wing configurations were favored because they reduced overall weight and cost.

[†]400 nmi fire mission

The optimal design minimally satisfies the most requirements to minimize over-design. Shown in Figure 11, Valkyrie is optimally designed for the BFL objective. The drop speed requirement (shown as a derived stall speed at a near-fire +45°F ΔISA) was not aggressively optimized for in order to retain a wing large enough to not require enormously powerful engines or high complexity high lift devices to make BFL. A smaller wing would also require either a greater C_L at cruise or a greater cruise velocity, both of which heavily constrain the aerodynamics. Importantly, though, is that Valkyrie lies within the feasible region.
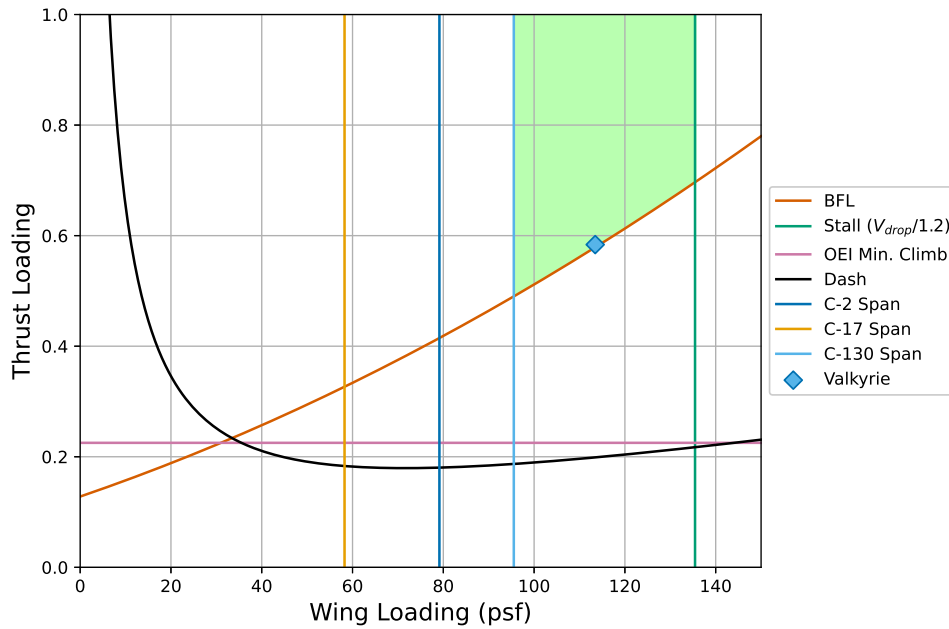
Fig. 11   Constraint Diagram

IV. Configuration

A. External Configuration Alternatives and Design Choices

In considering alternate wing designs, different engine mount locations were considered. An above wing mounted engine as shown in Figure 12 causes structural and aerodynamic issues regarding the large trailing-edge moment arm and added span-wise circulation within the low-pressure flow due to the engine inlet conditions made this option unusable for the purposes of this mission.
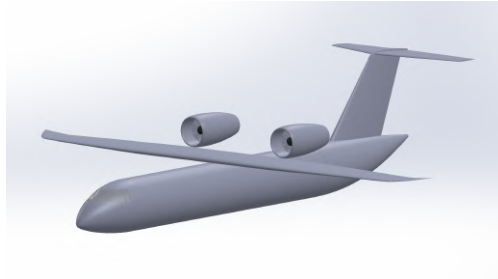
Fig. 12   High-Wing Configuration with Engines Mounted to the Top, Trailing-Edge of the Wing

A low-wing configuration is shown in Figure 13. The size of the selected GEnx-2B67 rendered this option unfeasible as the landing gear would need to be longer than for a high-wing layout, this would present an issue for the rear cargo loading ramp length or angle.

Fig. 13   Low-Wing Configuration with Engines Mounted to the Bottom of the Wing

The team's choice of a high wing, under-wing mounted engine configuration shown in Figure 14 provides added in-flight stability with a well balanced CG location compared to the other considered layouts.

Fig. 14   High-Wing Configuration with Engines Mounted to the Bottom of the Wing

Valkyrie can carry a spare GEnx-2B67 engine, the size of which was accommodated for by a four part rear cargo door. The bottom of the fuselage tail section splits in two parts with the front part being a door that opens downward to act as a ramp for cargo loading and the rear part opening upward to accommodate taller cargo. The sides of the fuselage tail section open outward to allow for wider cargo to be loaded into the central cylindrical section of the fuselage. This cargo door scheme can be visualized in Figure 15.

Fig. 15   Selected Aircraft Rendering with Open Cargo Doors

B. Selected Aircraft Configuration Design

Valkyrie's vertical height is not as critical as some military transport planes as Valkyrie's payload is located on the flat floor of the aircraft. Therefore, the wing structure can run through the top of the fuselage. The sponsons, which house the landing gear, are made large enough to enclose the main landing gear mostly outside of the internal fuselage space, maximizing internal volume. The internal layout can be seen in Figure 16.
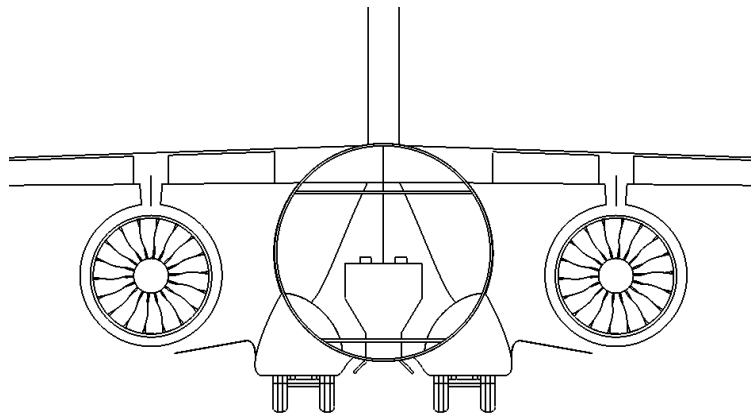
Fig. 16   Cargo and Landing Gear Spacial Accommodation Inside the Fuselage

The finalized Valkyrie design features a high-wing, bottom mounted engine layout. The T-tail configuration was chosen to produce the maximum potential moment from the elevator and minimize wake interference from the engines.

A fuselage length trade study was performed to determine an optimal fuselage length that would provide the necessary internal volume to store the fire retardant payload while minimizing structural weight. This trade study resulted in an optimal fuselage length of 1,167 in. The overall aircraft design and major component dimensions can be found in the provided Three-View in Figure 17.
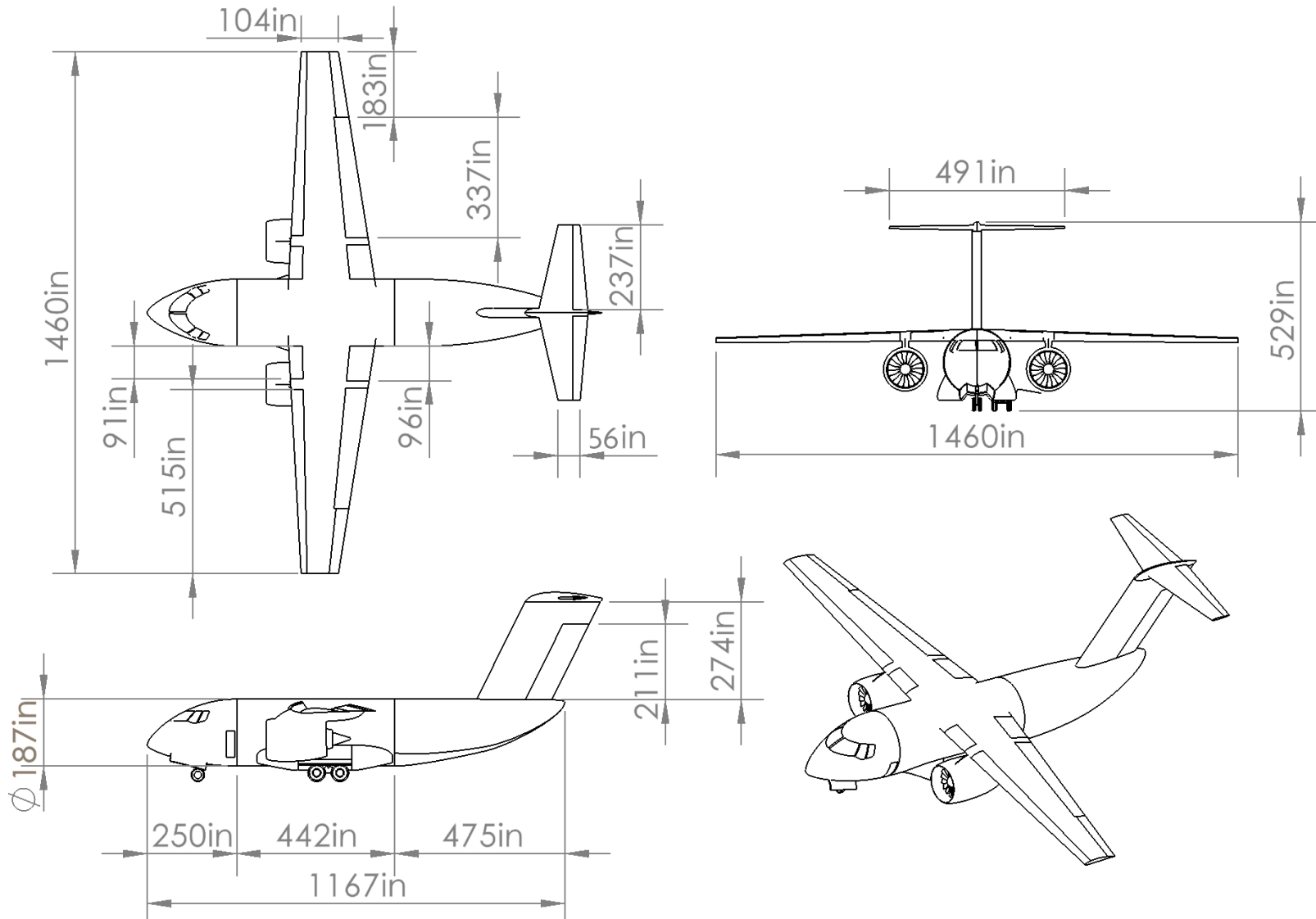
Fig. 17   Three-View of Valkyrie with Dimensions and an Isometric View

C. Fuselage design

When set up in a firefighting configuration, the fire retardant is stored in two RADS-XXL tanks acquired from Coulson Aviation Group, shown in Figure 18 and Figure 19. The tanks are removable and easy to maintain.
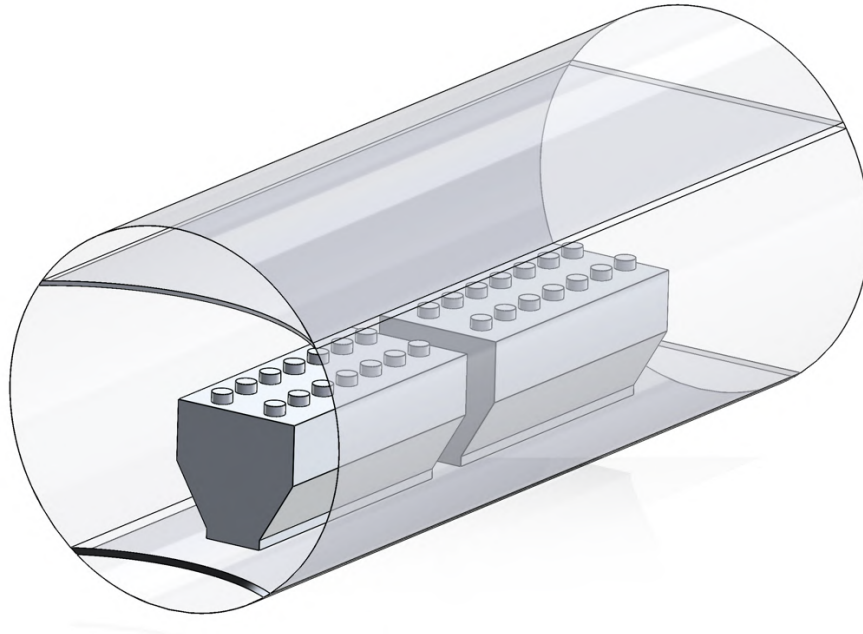
Fig. 18   Internal Tank Configuration (Aft into the Page)
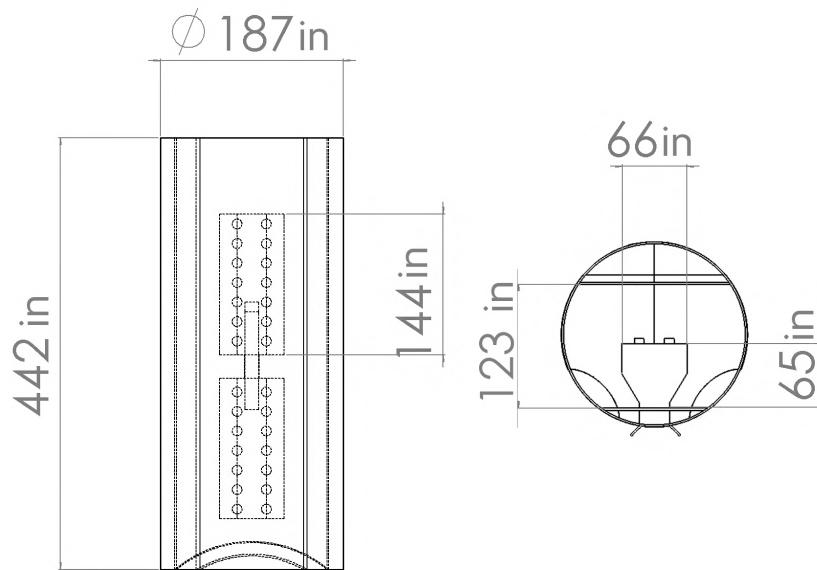
Fig. 19   RADS-XXL Tanks

D. Flight Deck Design

The aircraft is operated by a pilot, copilot, and drop operator. The decision was made to use a traditional yoke to control the aircraft rather than a side stick. This is to aide in ease of pilot training - comparable aircraft such as the C-130 and C-5 Galaxy use yokes for pitch and roll control. Flight deck control knobs were designed to comply with 14 CFR §25.781. The flight deck was designed to include all relevant flight controls and interfaces for radar, weather, and navigation. In addition to the flight deck for the pilot and copilot, the drop system operator station includes the ACLADS cargo management system interface. The interior of the flight deck was designed in accordance with 14 CFR Part 25 and paralax preventative gauge redundancy was incorporated in keeping with parameters outlined in §25.777(a) - 25.777(h). The flight deck layout can be seen in Figure 20.
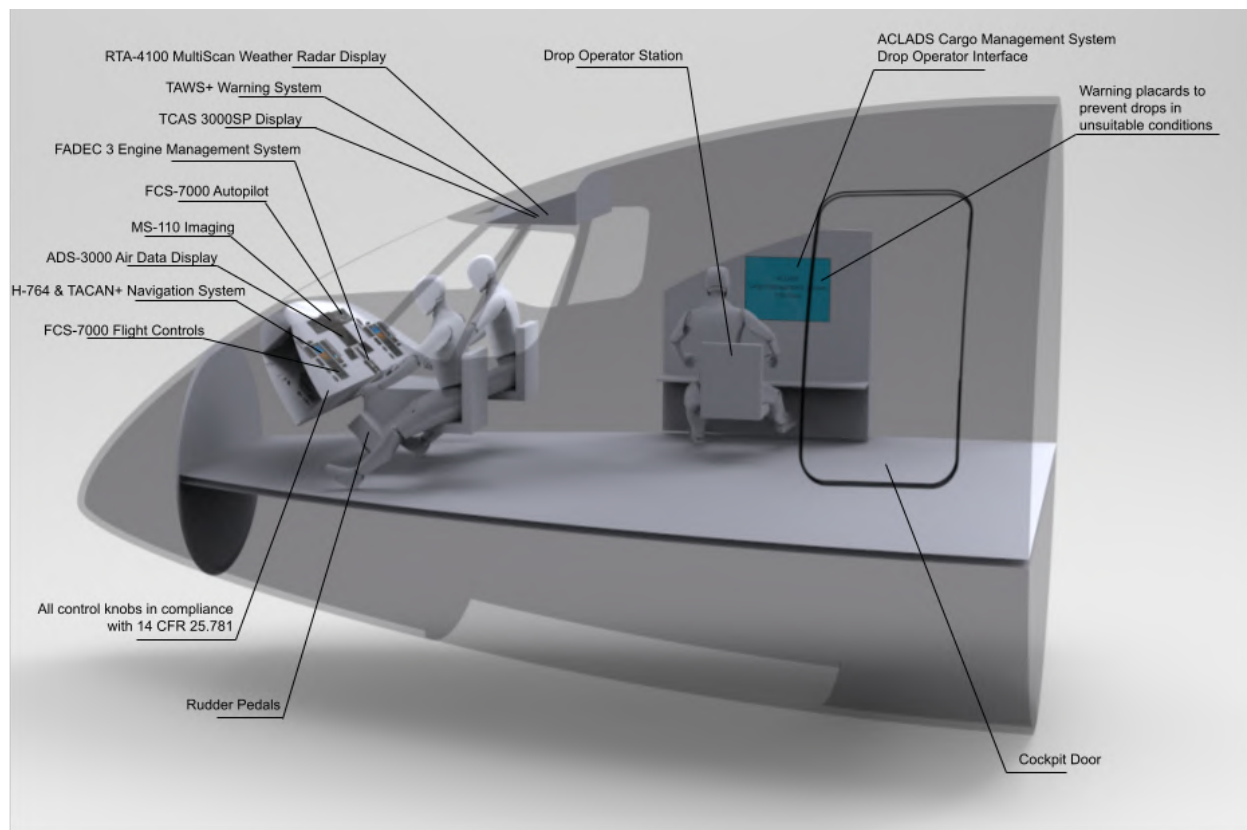
Fig. 20   Flight Deck Layout Schematic

Pilot view angle specifications are outlined in Advisory Circular (AC) 25.773-1 for both level flight and on a 2.5° glideslope. The current design meets specifications in the horizontal field of vision but fails to do so for vertical. However, per the same AC, this can be augmented by cameras, which are integrated into Valkyrie's avionics package.
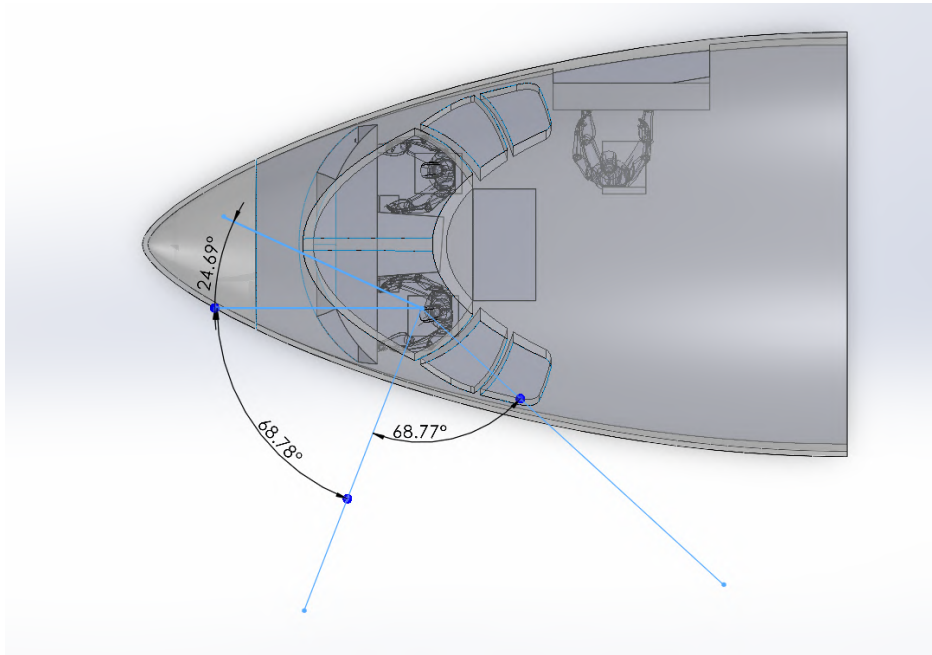
Fig. 21   Horizontal Pilot Viewing Angles
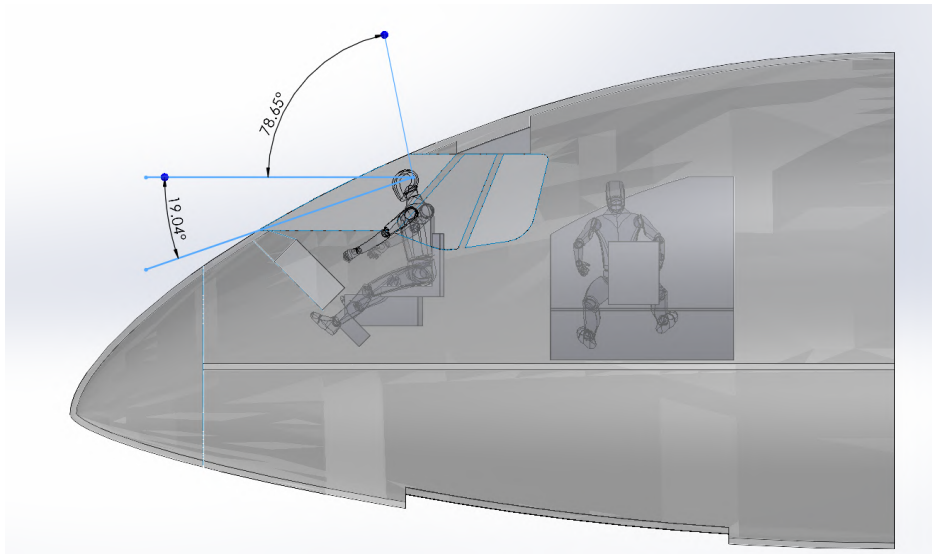
Fig. 22   Vertical Pilot Viewing Angles

V. Mass Properties

A. Weights

Table 7 shows the EW, MTOW, Maximum Zero Fuel Weight (MZFW), and Maximum Landing Weight (MLW). Valkyrie's MLW and MTOW are identical as the landing gear was designed to handle landing at MTOW. This decision was made due to the fact that Valkyrie does not include a fuel jettison system – the inclusion of such a system would be highly problematic on an aircraft designed to fly over wildfire. While the payload delivery system does include an emergency jettison function, this may fail in a scenario where emergency landing at MLW is required, as such, Valkyrie was designed to land with the full maximum fuel and payload weight. Defining maximum weights such as the MTOW and MZFW is imperative to the development of this aircraft. 14 CFR Part 25 §25.25(a) stipulates that an aircraft must have maximum weights corresponding to different operating conditions, such as taxi, cruise, takeoff, and landing, documented along with each weight's loading conditions, such as center of gravity. This is to ensure the CG remains within the CG limits, as defined by either the manufacturer or the structural limitations of the aircraft, as stipulated in §25.27(a) - 25.27(c).

Table 7   Major Weight Parameters

Weight Parameter	Weight (lb)
Empty Weight	105,000
MTOW	209,000
MZFW	182,000
MLW	209,000

1. Methodology

The weight of Valkyrie was determined using statistical methods. Specifically, Roskam's Class II methods, Raymer's method, and Nikolai's method were used. Statistical methods use data from past aircraft to estimate the relationship between the weight of a component and relevant design parameters.

Valkyrie's operation resembles that of a bomber, however, with its dual-purpose as a cargo aircraft, Valkyrie can also be classed as a transport aircraft. From the three methods used, Roskam's Class II was the method of choice as it provided equations that were most relevant to Valkyrie's class of aircraft. Raymer's method is intended for cargo or transport aircraft and Nikolai's method is intended for subsonic conventional, generic metal aircraft. Furthermore, Roskam's Class II Methods provides a conservative estimate compared to Raymer. The difference in weight estimation shown in Table 8 between Roskam and Raymer approximately accounts for the empty weight growth suggested by Raymer[8]. Overall, Roskam's Class II method was chosen because it provided equations that were most relevant to our class of aircraft and also provided a conservative weight estimate.

2. Weight Breakdown

Table 8 shows the breakdown of the MTOW including all the components estimated using the separate statistical methods used. The chosen method, Roskam Class II, is highlighted in blue.

Table 8   MTOW Weights Breakdown

Component	Roskam's Class II Methods (Torenbeek) (lbs)	Raymer's Statistical Weights Method (lbs)	Nicolai's Weight Estimation Methods (lbs)
Fuel	28,300	28,300	28,300
Payload	76,600	76,600	76,600
Wing	23,900	17,100	13,000
Horizontal Tail	1,700	1,900	1,500
Vertical Tail	2,400	1,900	2,300
Fuselage	18,500	21,000	7,800
Nacelle	7,500	7,500	7,500
Engines	24,800	24,800	24,800
Main Landing Gear	7,600	7,600	11,500
Nose Landing Gear	1,300	1,300	
Fuel System	1,100	1,000	2,200
Propulsion System	400	300	700
Flight Control System	3,100	1,700	2,700
Electrical System	6,400	1,400	1,900
Instrumentation, Avionics, Electronics	2,600	6,000	4,000
Air-conditioning, pressurization and anti- and de-icing mechanisms	900	600	600
APU	400	400	400
Cargo Handling System	1,300	1,300	1,300
Paint	1,300	1,300	1,300
Empty Weight	**105,000**	**97,100**	**83,500**
MTOW	**209,000**	**202,000**	**188,400**

B. Center of Gravity

The CG of the aircraft was determined using Roskam's component CG estimation which provided equations that accounted for detailed design differences which were present in our design and not available in other resources[9]. The reference coordinate system sits 1,000 in ahead of the aerodynamic center. Table 9 shows the component breakdown of the CG for the EW and MTOW.

Table 9 Center of Gravity Breakdown

Component	Roskam's Class II Methods (Torenbeek) (lbs)	CG Location (in)	Moment (lbs-in)
Fuel	28,300	1,024	29,013,700
Payload	76,600	1,008	77,194,600
Wing	23,900	1,014	24,445,300
Horizontal Tail	1,700	1,707	2,842,200
Vertical Tail	2,400	1,627	3,944,900
Fuselage	18,500	1,018	18,825,300
Nacelle	7,500	929	6,963,500
Engines	24,800	946	23,417,500
Main Landing Gear	7,600	1,055	8,022,200
Nose Landing Gear	1,300	685	882,100
Fuel System	1,100	986	1,075,100
Propulsion System	400	942	366,500
Flight Control System	3,100	1,018	3,176,300
Electrical System	6,400	1,018	6,496,700
Instrumentation, Avionics and Electronics	2,600	668	1,760,500
Air-conditioning, pressurization and anti-icing and de-icing mechanisms	900	668	607,900
APU	400	1,600	560,900
Cargo Handling System	1,300	962	1,212,100
Paint	1,300	962	1,211,700
Empty Weight	**105,000**	**1008 (31.8% MAC)**	**105,840,000**
MTOW	**209,000**	**1010 (32.9% MAC)**	**212,100,000**

The above table shows that the EW and MTOW CGs are within a percent of each other. This result is by design – the empty weight CG was found then the two retardant tanks were placed in the fuselage such that their average CG lay on the empty weight CG. Thus, if both tanks maintain an equal amount of retardant during the drop then the CG does not shift. The only factor affecting the CG during the mission would be the fuel which is located slightly aft of the EW CG. This greatly simplifies the certification process for Valkyrie as the small variation in CG allows the manufacturer to more easily demonstrate that requirements found in §25.27(a) - 25.27(b) are upheld. Naturally, this theoretical basis is not enough for certification and the results of this analysis will be validated using flight test data as required by §25.21(a)(1).

A visual representation of the major CG components with respect to the reference coordinate system is shown in Figure 23. The circles corresponding to each component are sized in accordance with their contributing weight.
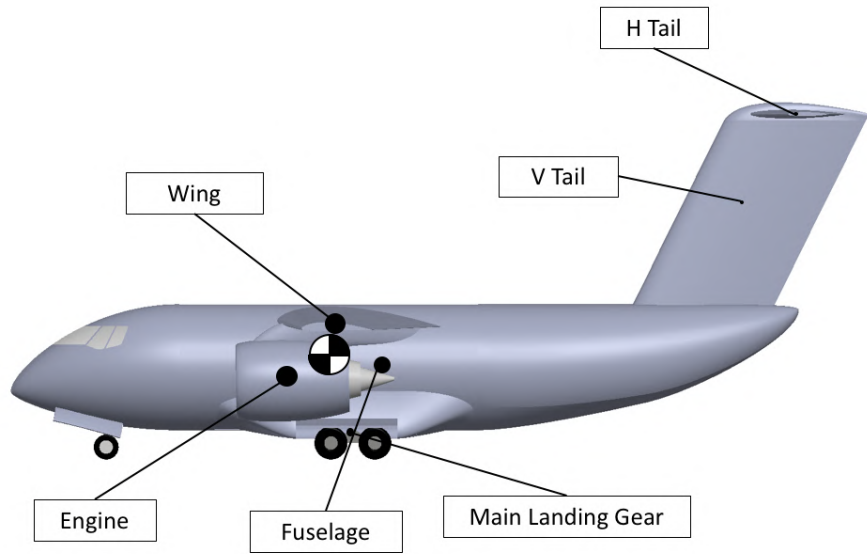
Fig. 23   Major CG Components

1. CG Loading Path

    The difference in the aircraft's CG during ground and flight operations must be accounted for and the corresponding CG limits respected as exceeding loading and flying limits can be dangerous. Figure 24 shows the variations in CG as the empty tanks, retardant, and fuel are loaded onto the aircraft.
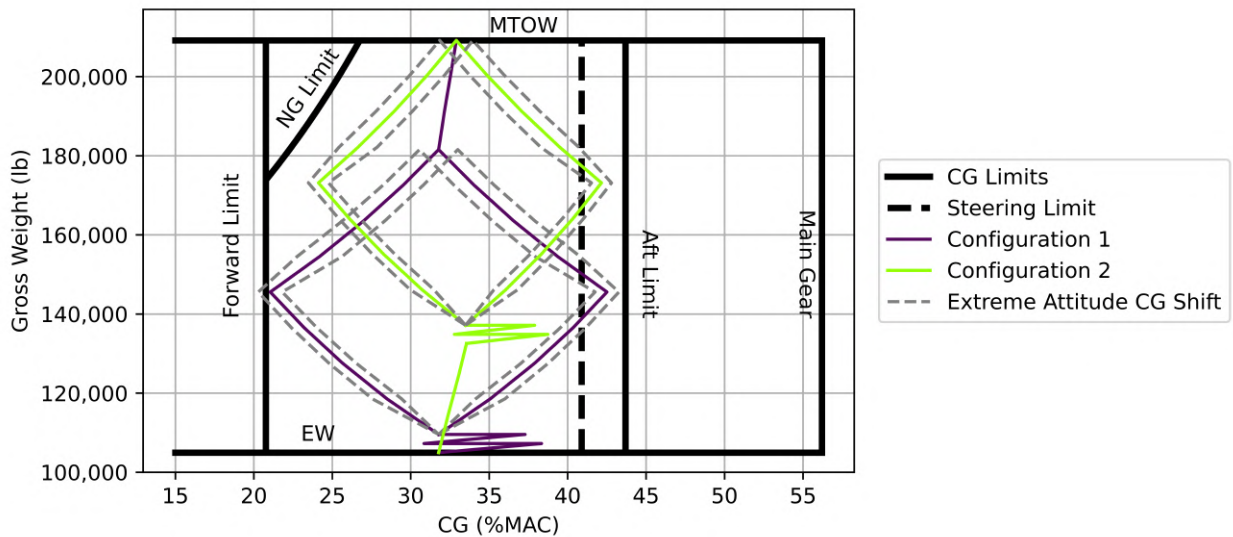
Fig. 24   CG Configurations

Although there are many possibilities for loading fuel, empty tanks, and retardant, only the two extreme cases are shown in Figure 24. The first configuration is when the empty tanks are loaded, followed by the retardant (8,000 gal) and finally the mission fuel. The second configuration is when the fuel is loaded, followed by the empty tanks and finally the retardant. Since the retardant goes in the empty tanks, the empty tanks will always be loaded before the retardant. There are many other configurations in which retardant and fuel can be loaded at the same time, but it was found that these two configurations led to the largest CG range.

The extreme loading CG conditions are important to know so that the aircraft can operate safely on the ground. The extreme loading CG occurs when there is no fuel, the empty tanks are loaded and either the forward or aft tank is loaded with 4,000 gal of retardant whilst the other retardant tank is empty. The choice between forward tank first or aft tank first loading of the retardant is the cause for the diamond shape. Table 10 summarizes the weight, condition and CG for both forward and aft extreme conditions.

Table 10   Extreme Forward and Aft Loading CG

Condition	CG (%MAC)	Gross Weight (lb)
Empty Tanks loaded, Zero Fuel, Forward Tank: 4,000 gal, Aft Tank: 0 gal	21.1	145,600
Empty Tanks loaded, Zero Fuel, Forward Tank: 0 gal, Aft Tank: 4,000 gal	42.5	145,600

As shown in Figure 24, both configurations abide by all limits except the forward limit and the steering limit. Certain procedural rules are set in place keep the aircraft within a safe operating regime.

Throughout normal flight operations, the pitching of the aircraft causes a shift in the CG of the retardant which has an impact on the overall CG of the aircraft. The shift in CG is shown as the 'Extreme Attitude CG Shift' line in Figure 24. The maximum and minimum pitch angles are $\pm 13°$ as determined by performance. Using SOLIDWORKS' centroid feature, fluid could be placed in the retardant tanks and the change in retardant CG could be determined. Given the change in CG, the weight of the retardant and the overall weight of the aircraft, the overall change in CG could be determined. By adding the CG change from the retardant being pitched to the original CG the new CG can be calculated.

2. CG Envelope

The CG Envelope was determined by taking the two previously drawn extreme configurations and all possibilities in between. Figure 25 shows the CG Envelope as well as the mission path. The CG Envelope shows all the relevant flying and operational limits which will be defined in the following section.
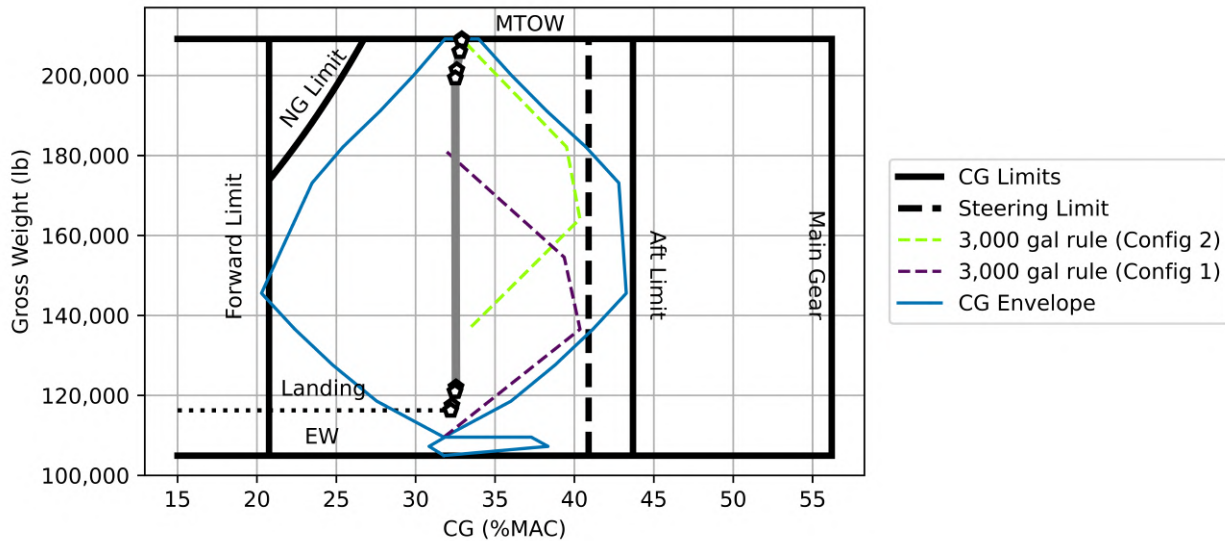
Fig. 25   CG Envelope

3. CG Limits

The nose gear weight limit is the maximum weight that the nose gear can handle before damaging the tires. As the CG moves forward, a greater fraction of the weight is carried by the nose gear. This limit is represented on the CG Envelope as the Nose Gear (NG) Limit, which is driven by the maximum weight the tire is rated for. The nose gear steering limit is the minimum weight the nose gear needs on it so that the aircraft can be steered. Raymer suggests a minimum of 5% of the gross weight, however, the "optimum range" of the Gross Weight (GW) on the nose gear is about 8-15%[8]. The team chose a minimum of nose gear weight of 8% GW.

The main gear limit is defined by the position of the main gear at 57% MAC. If the CG were to fall aft of the main gear then the safety of the aircraft would tip backwards. The CG Envelope shows that the main gear is located far aft of the most aft point meaning that the CG will never go past the main gear. The Forward Limit is defined by the aircraft's controllability at takeoff through a non-stalled tailplane while out of trim. The aft limit is defined such that there is always a positive static margin above 5%.

4. Operational/Procedural Rules

The CG Envelope crosses both the forward limit when there is zero fuel and the forward tank is filled with 4,000 gal of retardant and the steering limit when the aft tank is filled and the forward tank is empty for zero and full fuel configurations. Crossing the forward limit will not occur during takeoff as there will be fuel pulling the CG towards the empty weight CG, however it may occur during landing if all the fuel including reserves have been depleted and the aircraft is landing with only the forward tank filled. In this case, the retardant tanks are equipped with an emergency system in which the retardant can be jettisoned within 2.2 seconds[10]. To address the steering limit, a procedural rule

referred to as the 3,000 gal rule has been added. This rule states that the aft tank may not have in excess of 3,000 gal more retardant than the forward tank. Thus, the worst case scenario would be if the aft tank had 3,000 gal of retardant whilst the forward tank is empty. This limit will be ensured by the sensors in the retardant tanks. Figure 25 shows the loading path of these rules for both configurations mentioned earlier.

C. Trade Study: Retardant Tank Placement

The retardant tanks were placed right on the EW CG to minimize CG variation during the mission. Table 11 shows the position of each retardant tank based on the empty weight CG.

Table 11   Retardant Tank Positions

	CG Location (in)
Valkyrie without Retardant Tanks	1,008 (31.8% MAC)
Forward Tank CG	924
Aft Tank CG	1,092

VI. Propulsion

A. Engine Selection

During the design process, six engines were considered to power Valkyrie: General Electric's CF6 80C2-A5, the PW1100G, the PW1500G, the CFM LEAP-1B, the GEnx-1B54, and the GEnx-2B67. The initial engine choice was based on the seed aircraft, the Kawasaki C-2, which uses two CF6 80C2 engines developed by General Electric Aviation. Because the CF6 is from the 1980s, it has a poor thrust to weight ratio and worse SFC compared to more recent engines. This engine was therefore quickly ruled out. Additionally, the newer engines allow for easier replacement.

The remaining engines were evaluated during the sizing process, the engine specifications are shown in Table 12. The analysis compared both twin and four-engined configurations. The four-engined configurations were powered by the PW1100G, PW1500G, and CFM LEAP-1B, with the GEnx-1B54 and GEnx-2B67 powering the twin-engined configurations. The GEnx-1B54 produces the least amount of thrust of the twin-engined configurations, but is a severely derated version of other GEnx-1B engines, giving it a poor thrust to weight ratio. Therefore the GEnx-1B54 was removed from consideration.

Table 12   Candidate Engine Specification

Engine	Static Thrust for Takeoff [lb]	BPR	Weight (Dry) [lb]
PW1100G[11]	33,110	12.5	6,300
PW1500G[12]	24,400	12.0	4,800
CFM LEAP-1B[13]	29,317	9.0	6,128
GEnx-2B67[14]	67,400	8.0	12,400

To decide between the engines and configurations, a trade study was conducted. The GEnx-2B67 was found to be the overall best option as it had the largest design region while providing repair and maintenance and structural benefits. These benefits are due to the twin-engine configuration. With two engines, the wings do not have to support engine loads farther along the span and there are only two engines to maintain.

Valkyrie is powered by the GEnx-2B67, a turbofan engine developed by General Electric (GE) Aviation. While the majority of fire-fighting aircraft in service today use a reciprocating engine or turbo-prop engine, the high payload weight requires a large amount of thrust. Turbofan engines do come with potential risks associated with flying through smoke. The smoke and embers produced by the wild fires will be ingested into the engine. The turbofan's design helps prevent embers from entering the turbomachinery, instead directing them through the bypass of the engine. Over time soot will be deposited on the turbomachinery, reducing the efficiency, by decreasing the air flow through the core[15]. To combat the drop in efficiency, a ten percent safety margin was applied to the required thrust calculated through sizing analysis. The GEnx-2B67 is a highly reliable system that is well suited for Valkyrie, having been used on numerous aircraft prior. The GEnx is certified under a type certification with the FAA, with Type Certification Data Sheet (TCDS) number E00078NE[14]. Using engines with this certification is required by 14 CFR Part 25 §25.903 (a).

B. Propulsion Architectural Layout

The GEnx-2B67 is a two-spool, high bypass turbofan engine with a dry empty weight of 12,400 lb. It produces 67,400 lb of thrust at takeoff in ISA sea-level static conditions. The engine is used on the Boeing 747-8, which informs the design of Valkyrie's inlet and exit nozzle.

The GEnx-2B67 is capable of powering the aircraft using traditional Jet A-1 fuel as well as SAF – a drop in aviation fuel meeting all safety and technical requirements of Jet A-1 fuel that synthesized from more sustainably sourced hydrocarbons. This process can be viewed in Figure 26 and Table 13. The engine will also be used to drive pumps for the hydraulic and fuel systems and generators for the electrical systems, including avionics. Bleed air is used to pressurize the flight deck, filtering the air first through a High Efficiency Particulate Air (HEPA) filter, and provide deicing capability. Low pressure bleed air is bled off of the final stage of the booster, while high pressure bleed air is bled off of the third stage of the high-pressure compressor.

Table 13   GEnx-2B67 Engine Architectural Configuration

Number of Stages	Engine Section
1	Fan
3	Booster
10	High Pressure Compressor
2	High Pressure Turbine
6	Low Pressure Turbine
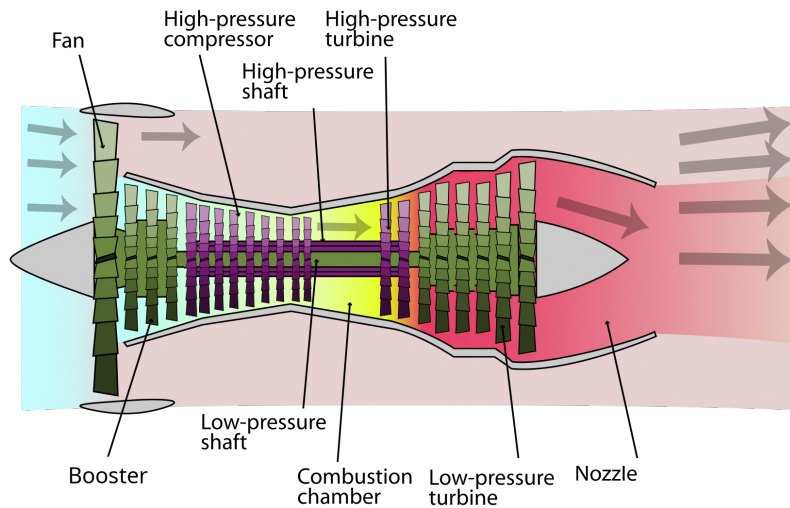
Fig. 26   GEnx-2B67 Configuration Diagram

C. Modelling the GEnx-2B67

GasTurb 14 was used to create a model of the GEnx and to provide propulsion values, namely TSFC (Thrust Specific Fuel Consumption) and F_N (Net Thrust). To create the model, the pressure ratios of each of the engine stages and the mass flow rate were entered. The model was then calibrated to known values. Unfortunately, the TSFC for the GEnx-2B67 is not published. Instead the TSFC has to be estimated. As Mehta explained in his presentation at the 2009 Pacific North West AIAA Symposium, there is a general trend in turbofans of a 0.5% decrease in TSFC per year[16]. The GEnx's predecessor is the GE CF6 80C2, which does have a published TSFC value: 0.576[17]. The CF6 was developed twenty years prior to the GEnx, so a ten-percent decrease in TSFC is expected. The estimated TSFC for the GEnx-2B67 is therefore 0.5184 lb/(lb hr). When GasTurb is run, it computes an TSFC of 0.66 lb/(lb hr), this is clearly wrong. The likely cause of the inaccuracy in the GasTurb model is the non-engine specific compressor maps. To bring the GasTurb model into compliance, the GE90 is used as a stepping stone. Because the GE90 is a recent engine that is architecturally similar to the GEnx for which the TOC TSFC and F_N are known, a correction can be calculated for the outdated GasTurb compressor maps.

A GasTurb model was built for the GE90-85B. While GasTurb still over estimates TSFC, it can be corrected. As explained in Propulsion and Power, to account for the booster stage on newer engines, the bypass ratio must be increased[18]. The GasTurb model produces accurate values when the bypass ratio is set to twelve, which is increased from the design bypass ratio of 8.4. The GasTurb model run at the design bypass ratio can be shifted to align with the GasTurb model run at a bypass ratio of twelve. The points that were used to calculate the required scale factor are shown in Figure 27. The net thrust is scaled down from 20,715 lb to 17,519 lb and the TSFC from 0.6038 to 0.5162. For the GEnx model, there are no points to match as the data is not published, but because the GEnx is based on the GE90, a constant error between the TSFC calculated by GasTurb can be assumed. This process is shown in Figure 28.
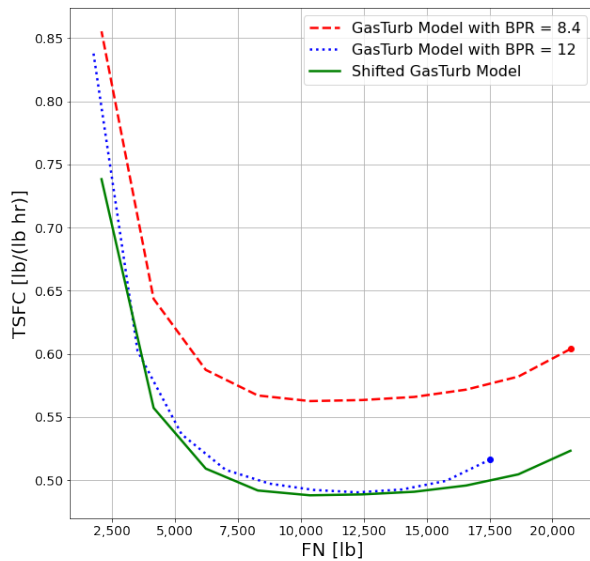
Fig. 27   GE90-85B GasTurb Model Correction for TSFC and F_N Convergence
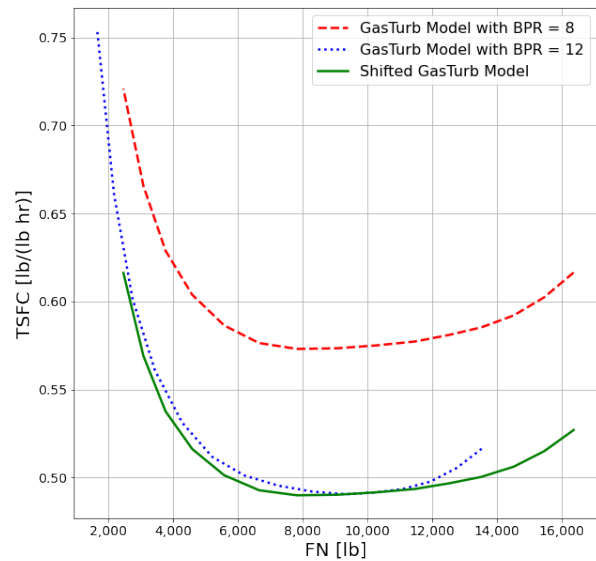
Fig. 28   GEnx-2B67 GasTurb Model Correction for TSFC and F_N Convergence

To check that GasTurb is correct, it can be compared to an analytical method, such as Herrmann[19] informed Howe[20]. Herrmann is first used to find the TSFC at 35,000 ft and Mach 0.8. This is used to calibrate Howe's equation for TSFC[20]. The constant c_1 can be used to calculate TSFC at off design conditions using Howe's off-design TSFC equation[20]. Where T is the thrust available at 35,000 ft and Mach 0.8. T_{OD} is calculated using Equation 1, where the Overall Pressure Ratio (OPR) is assumed to vary linearly.

$$T_{a_{\text{OD}}} = T_{\text{SL}} \delta \frac{\text{OPR}_{\text{SL}}}{\text{OPR}_{\text{OD}}} \tag{1}$$

The comparison between the GasTurb model and Herrmann informed Howe method are shown for TSFC in Figure 29 and for net thrust in Figure 30. Some points of comparison are shown in red and are summarized in Table 14.

Table 14   Herrmann informed Howe and GasTurb Model Comparison

Condition		Herrmann informed Howe Model		GasTurb Model		Marker
Altitude [ft]	Mach Number	TSFC [lb/(lb hr)]	Net Thrust [lb]	TSFC [lb/(lb hr)]	Net Thrust [lb]	
5,300	0.25	0.37	108,085	0.36	98,405	●
28,750	0.67	0.49	37,110	0.48	41,540	■
29,000	0.45	0.42	36,655	0.43	39,905	▲
29,000	0.5	0.41	36,655	0.42	40,165	♦
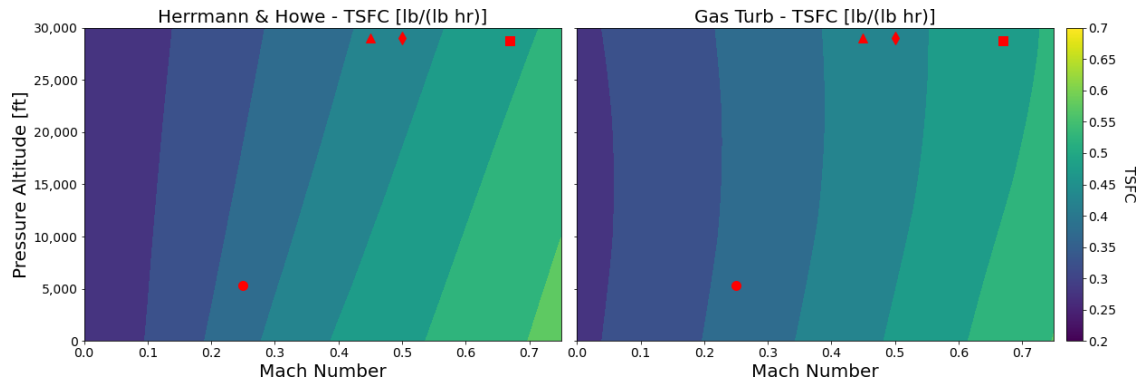
Fig. 29   TSFC Model Comparison
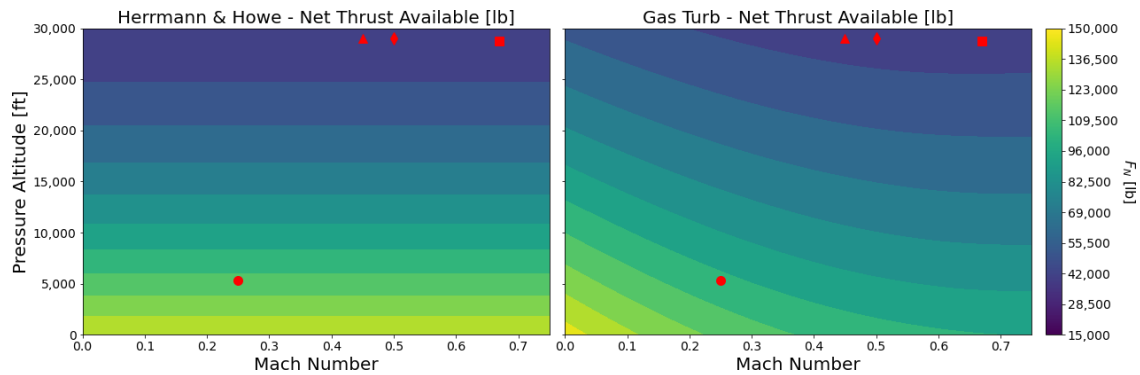
Fig. 30 F_N Model Comparison

D. GasTurb Results

The GasTurb model allows for the calculation of engine parameters at various conditions, with TSFC being shown in Figure 31 and net thrust being shown in Figure 32. As expected TSFC decreases with altitude, but increases with Mach number. The net thrust plot shows the thrust curves of the GEnx-2B67. The curves follow the general trend of net thrust decreasing with both altitude and Mach number. Additionally, when operating under partial power, TSFC and net thrust follow the tends shown in Figure 28. Prior to certification these results will be further validated by flight testing as required by §25.939.

Fig. 31   TSFC vs. Altitude vs. Mach Plot
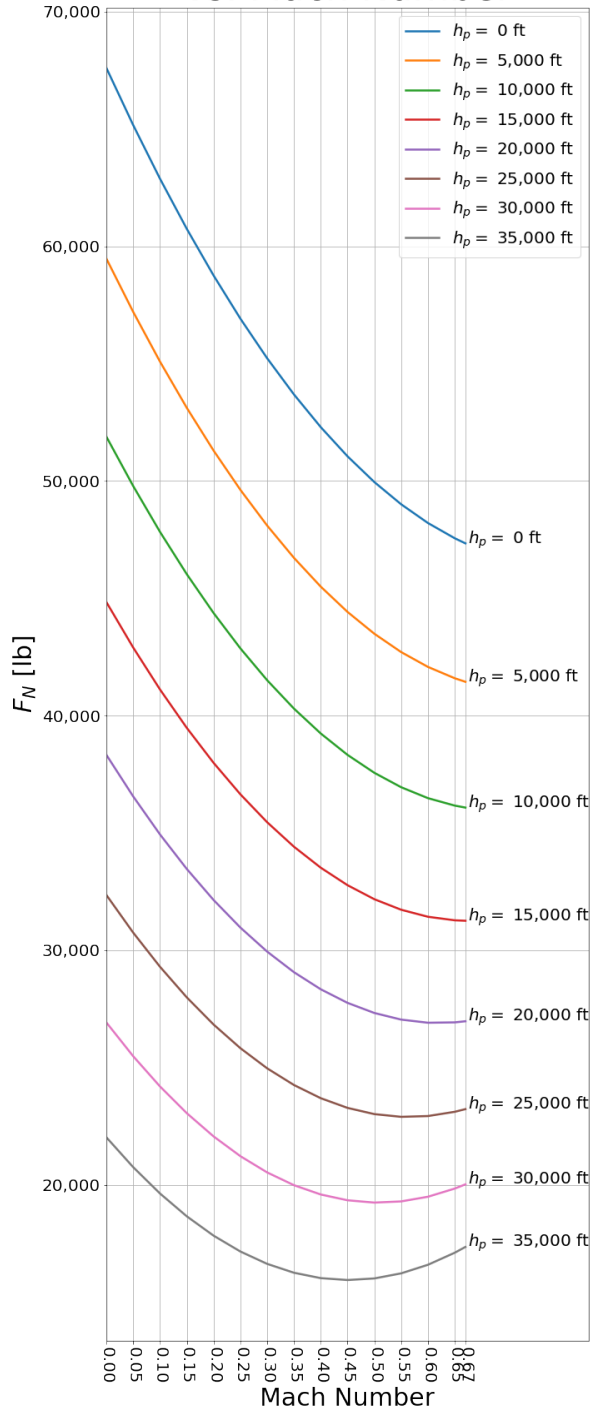
Fig. 32 F_N vs. Altitude vs. Mach Plot

E. Engine Integration

The engine uses the inlet and nozzle present on the GEnx-2B67 when deployed on the Boeing 747-800. To mount the engine to the wing, an engine mount was designed and is discussed in further detail in the structures section. Contained within the engine mount, is a fuel system (connected to tanks within the wing), which is capable of using both Jet A fuel and drop-in SAFs. The majority of operational time is spent at cruise. The propulsive efficiency can be calculated at this position. At cruise, the GEnx has a propulsive efficiency of 0.83. This can be compared to the propulsive efficiency calculated by GasTurb, which is 0.74.

VII. Aerodynamics

A. Airfoil Selection

Using desired values for C_L in cruise and $C_{L_{max}}$ for both landing and takeoff, the NACA 4312-62 airfoil was chosen using a variable XFLR5 setup to account for the change in Mach number at these points within the firefighting mission profile. From sizing analysis, the desired values were determined to be a maximum $C_{L_{max}}$ during landing of 2.27, and a cruise C_L of 0.48. The cruise condition was simulated using a range of Reynolds numbers at a Mach number of 0.67 and the NACA 4312-62 airfoil, achieved the cruise C_L at an ideal α of 0°.

To come to this airfoil shape, XLFR5 was utilized to sweep through maximum camber magnitude and location and maximum thickness magnitude and location with the end goal of achieving the desired C_l values in 2D with minimal pitch sensitivity. Valkyrie can enter highly pitched maneuvers with confidence that stall onset will not be sudden, giving pilots time to react. The XLFR5 setup used to obtain 2D performance values was validated using empirical data from Theory of Wing Sections[21] based around the NACA 4412 airfoil, which was recreated in XFLR5 to compare the lift curve slope with an error within 1%. These results were also checked using Javafoil, a 2D panel solver which makes 3D assumptions about wing geometry to create C_L and C_D values.

The accuracy of the 2D airfoil performance was improved using several Reynolds-Averaged Navier Stokes (RANS) models within the CFD platform Siemens Star-CCM+. Initially, a K-Epsilon turbulence model was run to allow for easier convergence and less computational demand for quick results to compare to XFLR5. Both the final NACA 4312-62 airfoil and the flow field during cruise at an α of 0° can be observed in Figure 33. The mesh for this 2D CFD model was heavily customized to target estimated y+ values along the airfoil surfaces of one using twenty-five growing prism layers, as well as featuring leading-edge and wake refinement regions to focus the finer mesh regions where separation is likely to occur. Once the K-Epsilon model was operational, a K-Omega model was used with the expectation of greater accuracy of flow separation for stall prediction. The results of these models are compared in Figures 34, 35, and 36, with the most conservative estimate still being able to achieve the design goal of a C_L of 0.48 using the Raymer[8] 2D to 3D approximation technique where C_L is 90% of the 2D estimate of C_l.
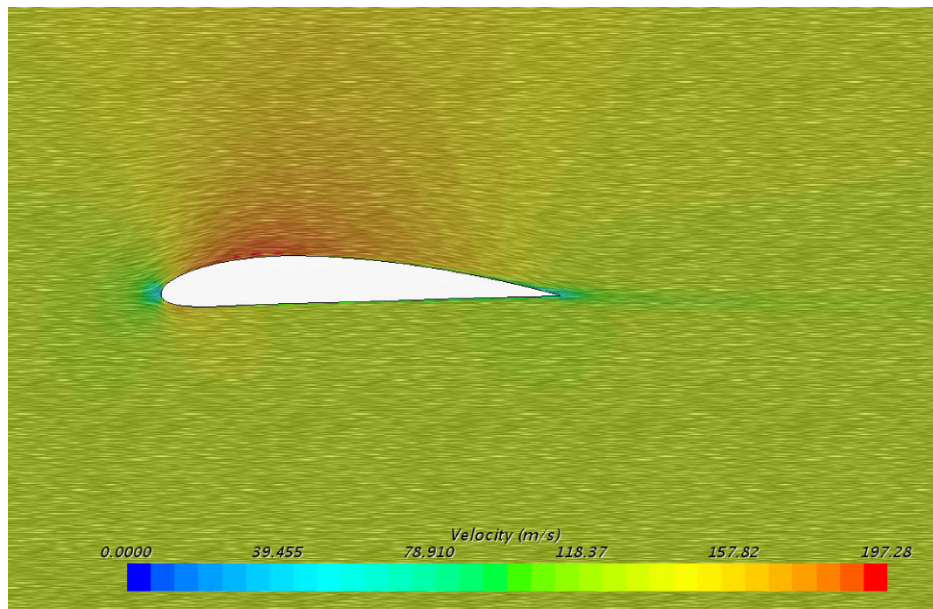
Fig. 33   NACA 4312-62 Airfoil and Respective Flow Velocity Profile at Cruise Conditions ($\alpha = 0°$)
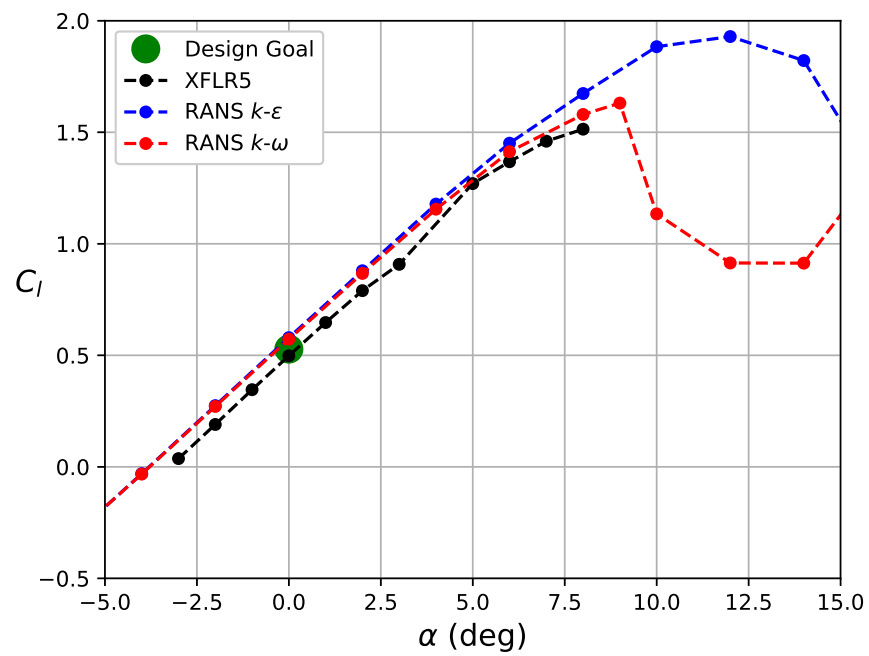
Fig. 34   NACA 4312-62 Airfoil C_l vs. α Curve
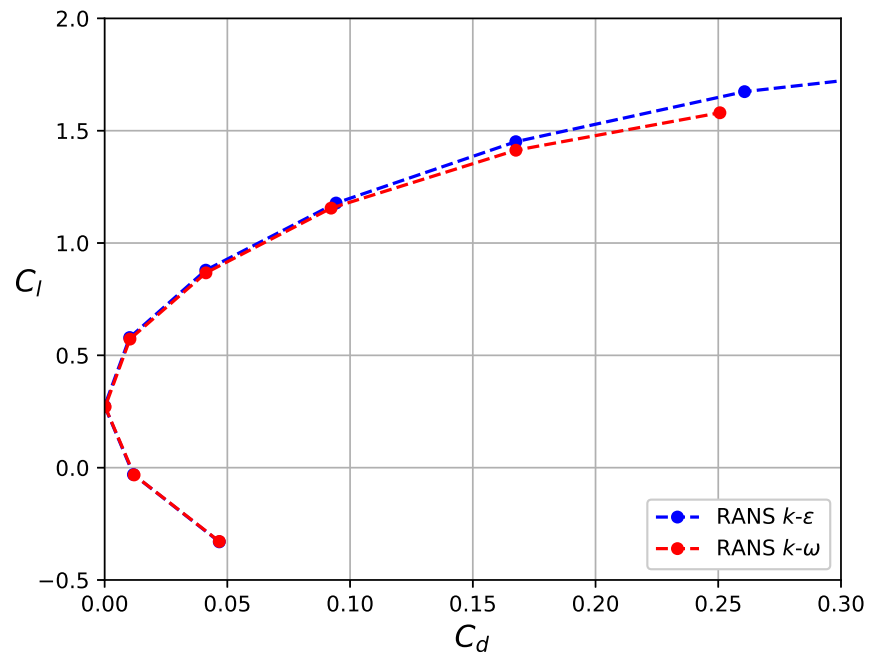
Fig. 35   NACA 4312-62 Airfoil C_l vs. C_d Curve
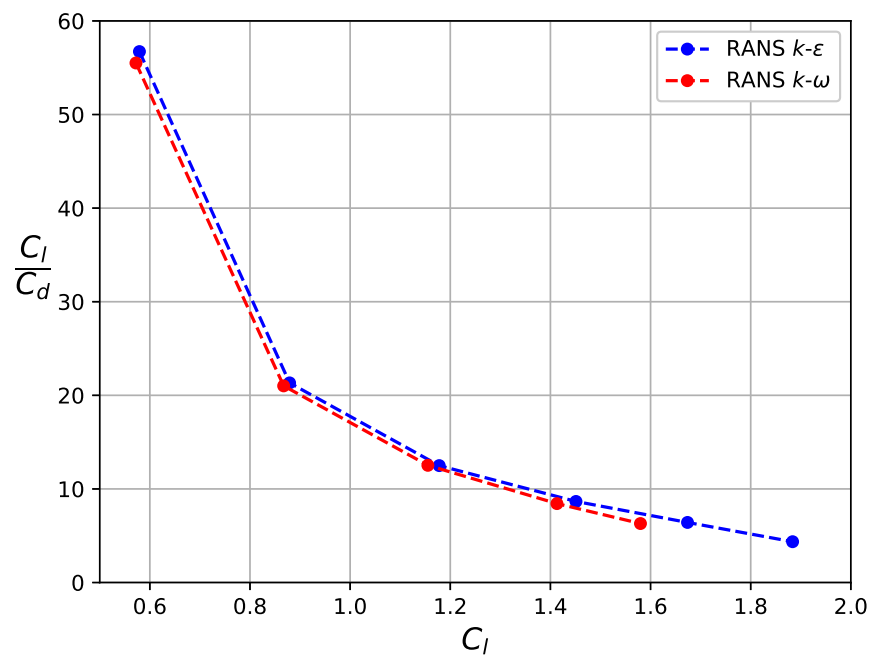
Fig. 36   NACA 4312-62 Airfoil C_l/C_d vs. C_l

B. Wing Design

The wing features no quarter-chord sweep in order to maximize the freestream velocity at the leading edge of the wing with the goal of achieving a maximum $C_{L_{\max}}$. The wing also features a taper ratio of 0.4 in an effort to create a balance between performance and weight. This taper ratio was determined to be an ideal middle-ground through a sizing trade study working around takeoff weight. Continuing with the trade studies carried out by sizing, the optimal aspect ratio is found to be eight, which helps to minimize drag by deviating from a Hershey bar wing shape. To shift the stall bias of the wing toward the root, allowing the control surfaces to stall last, the wing has a twist of 3°. The root incidence is set at 2° to allow for the needed C_L to be achieved during cruise at an ideal neutral α. The wing also features a slight anhedral angle, set to 1°, to increase maneuverability without sacrificing straight-line stability. This angle was determined through a C_{l_β} calculation by stability and control. The resulting wing planform designed is shown in Figure 37.
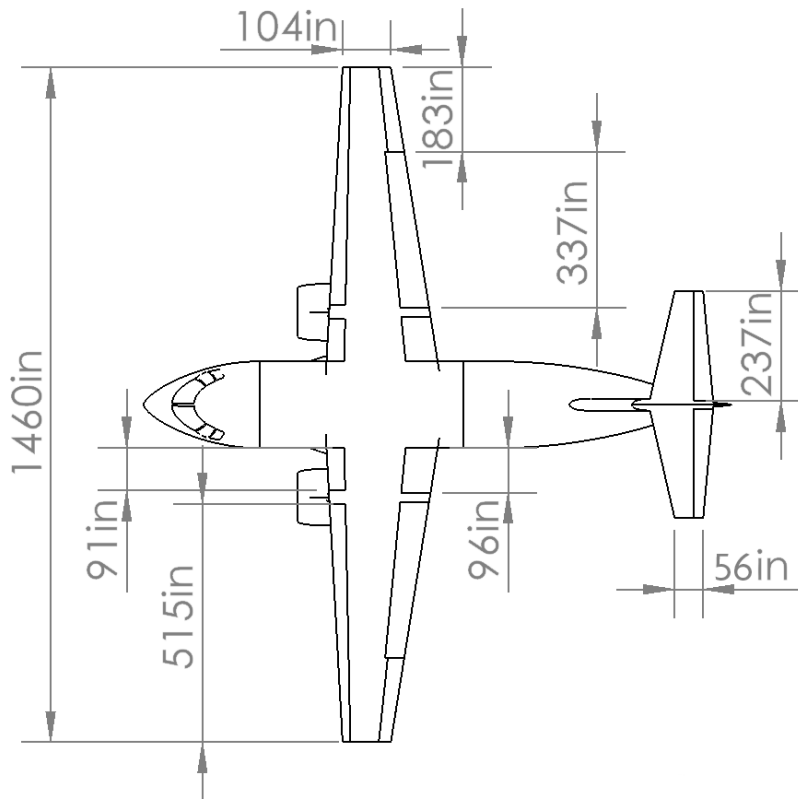
Fig. 37   Wing Top-View with Leading-Edge Slat and Trailing-Edge Fowler Flap Regions

C. High-Lift System

The selected high-lift system for Valkyrie features a leading-edge slat that runs the entire length of the wingspan, as well as a Fowler flap that spans 75% of the wing. The Fowler flap was sized to target a higher overall $C_{L_{max}}$ working off the estimated comparable performance to other single flap configurations giving the highest $\Delta C_{l_{max}}$. The leading-edge slat was chosen to provide a needed lift curve extension to allow for a higher $C_{L_{max}}$ at a higher α.

An initial flap study was done using the selected NACA 4312-62 in XLFR5. These results were produced with a plain flap configuration and no leading-edge slat due to the limitations presented in XFLR5. The 20° flap deflection from the XFLR5 simulation was carried over into a flap model created using SOLIDWORKS and customized in Star-CCM+'s 3D model adjustment tool. The final flap configuration's performance was then calculated in 2D using a Star-CCM+ model similar to the unflapped airfoil using selective mesh refinement. However, in the case of the high-lift system, only a K-Omega turbulence model was utilized due to the adverse pressure gradients present even in non-stall conditions caused by aggressive geometry inclusion, especially regarding the cove needed for flap packaging. The results of the initial XFLR5 with a 20° plain flap deflection and Star-CCM+ simulations for both 20° and 30° Fowler flap deflection can be seen in Figure 39 where the difference in the C_l curves comes from the change in configuration and Fowler flap deflection angle which can be expected going from a plain flap to a Fowler flap with a leading-edge slat. From the Star-CCM+ results it was determined that for takeoff conditions, the slat will be deflected by 8°, while the Fowler flap will be deflection of 20°. For landing this will be increased to 30° for the Fowler flap to allow for a lower α to achieve the $C_{L_{max}}$ of 2.27 needed at this condition. A visual of the landing flap configuration can be seen in Figure 38. The expected $\Delta C_{l_{max}}$ caused by a slatted leading-edge and Fowler flap combination can be found in Raymer[8], which is calculated to be approximately $1.7\frac{c'}{c}$. The Fowler flap contributes a $\Delta C_{l_{max}}$ of $1.3\frac{c'}{c}$, while the slatted leading-edge contributes a $\Delta C_{l_{max}}$ of $0.4\frac{c'}{c}$.
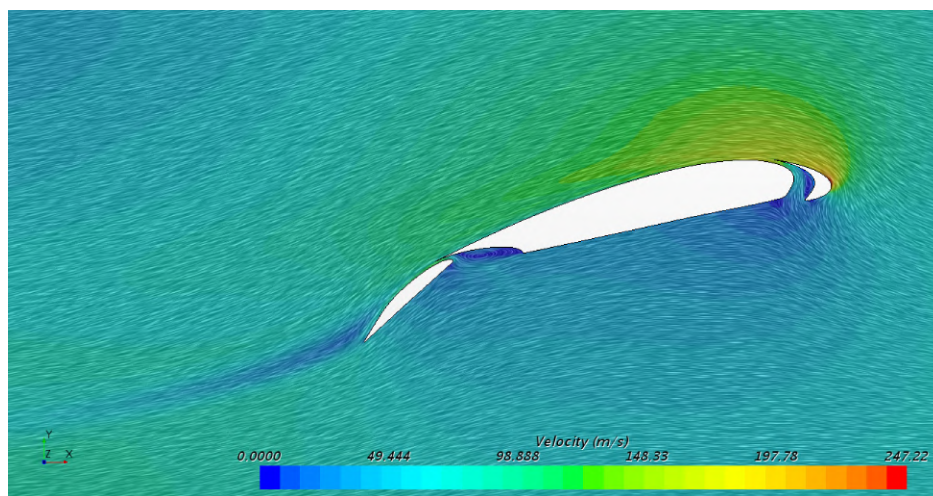
Fig. 38   High-Lift System Configuration Comparison at α = 12°
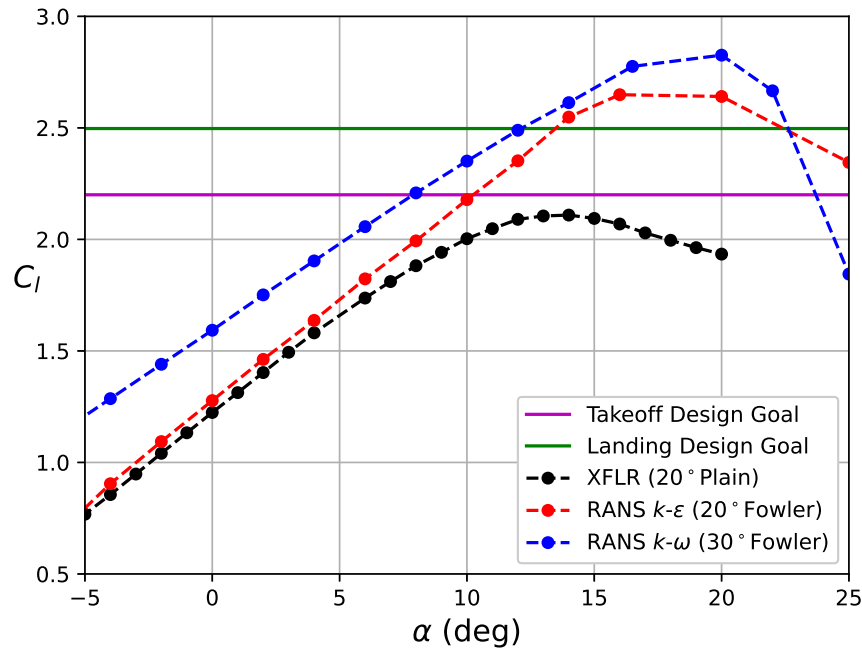
Fig. 39   High-Lift System C_l vs. α Curve

D. Drag Buildup

Using the Raymer[8] drag buildup method, an estimation for the component level parasitic drag contributions can be created. These estimations, along with the overarching design goal C_L values for the different phases of Valkyrie's mission profile. The individual drag contributions of each major component can be seen in Table 16 with the representative dimensions shown in Table 15. These part-level parasitic drag contributions are summed and given a 10% safety factor for doubling the safety factor given by Raymer[8] due to the large degree of unaccounted for parasitic and excrescence drag sources. Induced drag estimates are then added for each flight segment to allow for a total drag estimate to be calculated. The total drag is given an extra twenty count margin for unaccounted for wave drag contributions given that weak shocks may be present, especially at the cruise speed of Mach 0.67. This drag buildup uses a derived span efficiency of 0.81, K value of 0.049, and a $S_{\text{wet}}/S_{\text{ref}}$ of 6.13 measured from the CAD model.

Table 15   Component Sizes For Drag Buildup

Components	Length (in)	Representative Diameter (in)
Fuselage	1167.0	187.4
Wing	193.7	23.2
Horizontal Stabilizer	104.2	10.4
Vertical Stabilizer	210.5	25.3
Engines	167.9	122.4

Table 16   Component Estimated Parasitic Drag Contributions

Part	C_{D_0} Cruise	C_{D_0} Takeoff	C_{D_0} Landing
Fuselage	0.0084	0.0060	0.0064
Wing	0.0083	0.0057	0.0062
Horizontal Stabilizer	0.0017	0.0011	0.0012
Vertical Stabilizer	0.0019	0.0013	0.0014
Engines	0.0021	0.0015	0.0016
Total	**0.025**	**0.017**	**0.018**

The $C_{D_{TOT}}$ estimate for cruise is tabulated to be 0.04 at a C_L of 0.48. During takeoff, the estimated $C_{D_{TOT}}$ increases to 0.22 with an estimated C_L of 2.0 and the estimated $C_{D_{TOT}}$ at landing using a C_L of 2.27 is 0.27. These estimates are reasonable initial overestimates that can be used for aircraft design at the three operating points considered.

E. Aircraft Performance Values

The final design of Valkyrie was simulated using two 3D computational methods, one being the vortex lattice method solver provided by OpenVSP. The C_L, C_D. and L/D curves generated by this initial method can be seen in Figures 40, 41, and 42. These figures also show the tabulated drag values at their respective approximate angles of attack. Also shown at the cruise estimates provided by the RANS K-Omega model for the 3D plane model generated in CAD.
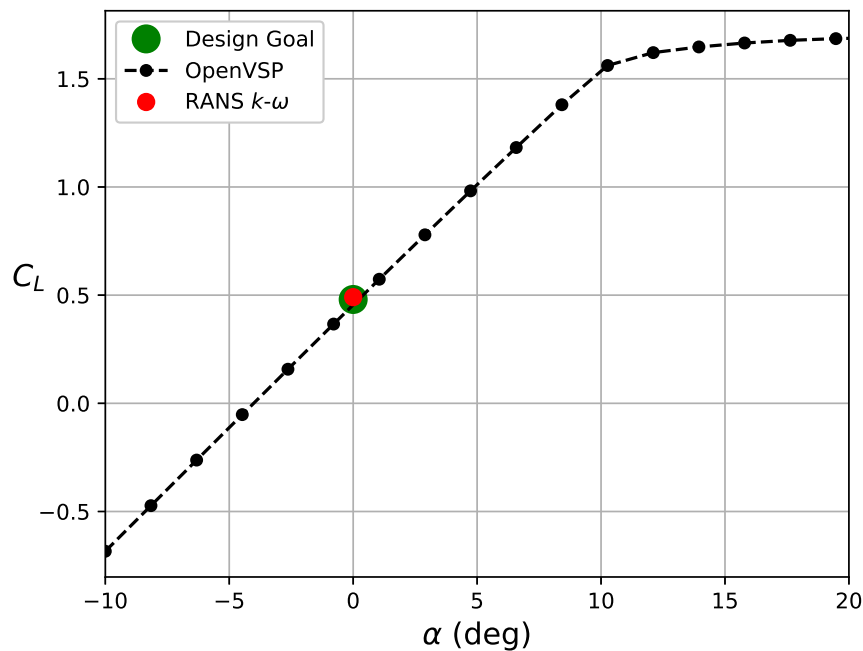
Fig. 40   Full Plane C_L vs α Curve
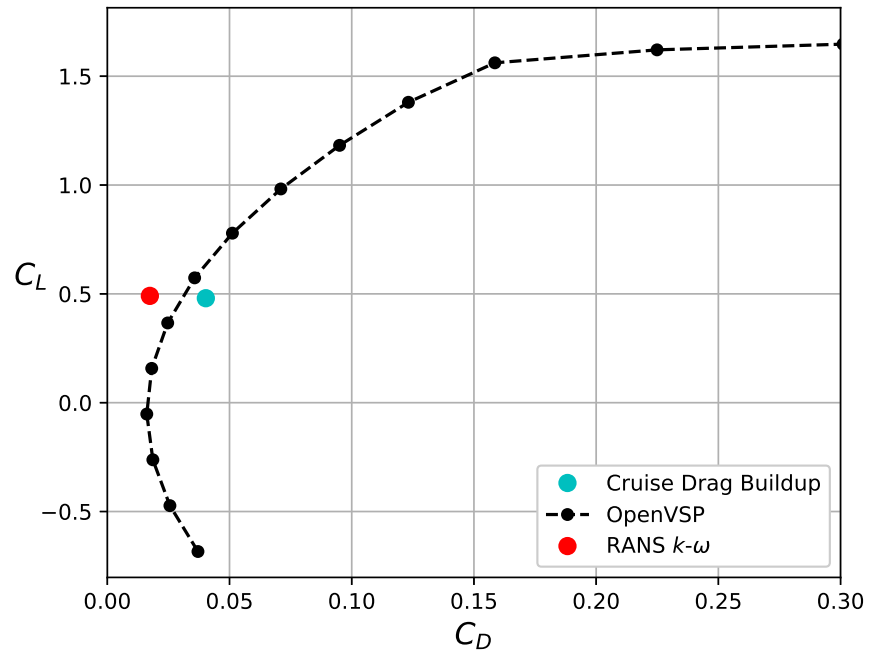
Fig. 41   Full Plane C_L vs C_D Curve
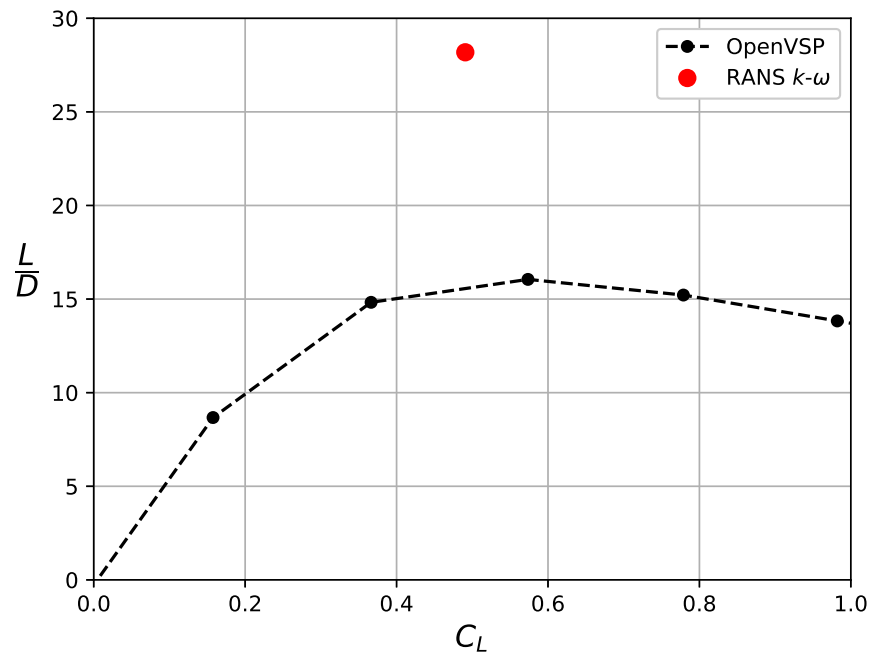
Fig. 42   Full Plane L/D vs C_L Curve

This final model was created using Star-CCM+ to act as a check for the OpenVSP results. To simulate the inlet and outlet conditions, variable boundary conditions were applied for each of the faeces of the fluid domain, the inlet plane was simulated as a velocity inlet with our cruise atmospheric conditions and speed. The top, bottom, outside and outlet faces were all simulated as pressure outlets to not enforce unrealistic conditions along the length of the plane body. Due to computational limitations, the fluid domain was cut in half with a symmetry plane applied to the face running through the middle of the plane model, which is not ideal. These computational limits also called for the application of a selectively refined mesh where there are refined surface, volumetric, and prism layer meshes. The mesh goal was to target a y+ value ideally below one. Prism layer mesh cells were used for the first 1.3 ft (0.4 m) of the mesh moving away from plane surfaces to allow for complete boundary layer treatment, while also maintaining a growth rate of 1.3 between each cell to allow the last prism layer cell to not have a notable change in size as the mesh switches to the minimum cell size for the core mesh as a large cell size change can lead to convergence difficulties. The selective mesh refinement was focused around having the finest mesh located in regions prone to flow separation or having the most aggressive geometry to best capture the local fluid behavior.

Given the complexity of the full plane CFD model setup, only cruise conditions were able to be run with the results shown in the streamline visualization in Figure 43. From Figure 43, the fluid conditions about the exterior surfaces can be observed, showing no major regions of separation that would be cause for performance concern. This especially affects the tail section of the fuselage, which required an iterative design process to ensure minimal flow separation. However, in the future all segments of the mission could be simulated using this model, as well as including a momentum source to simulate the impact of the engines and the induced rotation within the air flow on the performance of the high-pressure surface of the wing. A major source of error in this model is the lack of engine flow impact and nacelle surface area which would impact both lift and drag during each segment of the mission profile. The exclusion of engines from this CFD simulation leads to the notable difference in efficiency estimates between the RANS K-Omega and calculated drag buildup values shown in Figure 42.
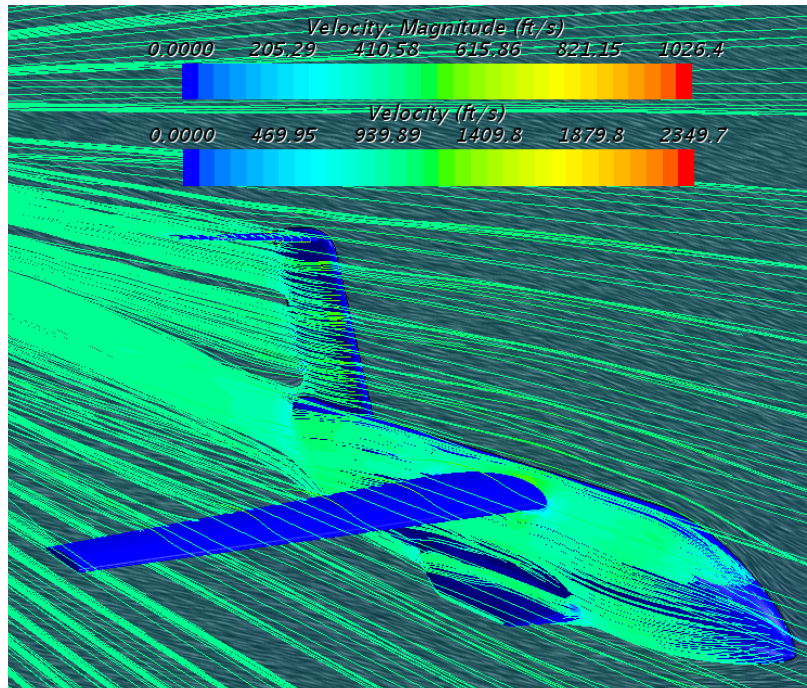
Fig. 43   3D CFD Streamline Visualization at $\alpha = 0°$ During Cruise (Top Legend for Streamline Velocity, Bottom Legend for Background velocity Contour)

VIII. Performance

A. Takeoff and Landing Performance

Valkyrie must be able to meet a BFL of 8,000 ft at $h_p = 5,000$ ft and $\Delta ISA = 35\,°F$, with the team opting to pursue the objective requirement of a 5,000 ft BFL[1]. This requirement is also used as the Landing Field Length (LFL), assuming that if the aircraft takes off from a 5,000 ft runway it should be able to land on that same runway. As Table 17 shows, Valkyrie is able to meet the BFL requirement for all surfaces analyzed. This allows Valkyrie to perform rough-field takeoffs, in the One Engine Inoperative (OEI) condition. BFL distance was calculated through iterating on the V_1 speed until the accelerate stop distance was equal to the takeoff field length. An obstacle height of 35 ft was used based on the required obstacle height for V_r given in 14 CFR §25.107(c)(2).

Valkyrie is unable to meet the LFL requirement for missions on wet concrete and icy concrete. When completing a drop mission, both the 400 nmi and 2×200 nmi mission, Valkyrie is unable to meet the requirement on soft turf and wet grass. Fire season often falls during the warmer months of the year and is typically aided by drought conditions. This means that icy concrete or wet concrete are unlikely. The required LFL and BFL for each of Valkyrie's three mission profiles on a variety of surfaces have been calculated and documented, as is required by §25.1587(b)(7).

Table 17   Takeoff and Landing Performance at 5,000 ft and ΔISA = 35°F

Conditions			400 nmi Drop Mission		2 × 200 nmi Drop Mission		Ferry Mission	
Surface	μ	μ_{brake}	**BFL Distance**	**Landing Distance**	**BFL Distance**	**Landing Distance**	**BFL Distance**	**Landing Distance**
Dry Concrete	0.03	0.3	4,240 ft	3,785 ft	4,185 ft	3,810 ft	3,010 ft	4,180 ft
Wet Concrete	0.05	0.225	4,600 ft	5,760 ft	4,540 ft	5,805 ft	3,230 ft	6,430 ft
Icy Concrete	0.02	0.075	4,895 ft	12,235 ft	4,830 ft	12,340 ft	3,455 ft	13,805 ft
Hard Turf	0.05	0.4	4,210 ft	3,205 ft	4,155 ft	3,225 ft	2,960 ft	3,515 ft
Firm Dirt	0.04	0.3	4,320 ft	3,785 ft	4,265 ft	3,810 ft	3,050 ft	4,180 ft
Soft Turf	0.07	0.2	4,905 ft	4,925 ft	4,840 ft	4,960 ft	3,405 ft	5,475 ft
Wet Grass	0.08	0.2	5,025 ft	4,925 ft	4,955 ft	4,960 ft	3,470 ft	5,475 ft

B. Mission Segment Performance Analysis

A performance analysis software was developed to calculate the the important aerodynamic, propulsion, and weights at every stage of the mission. The code uses altitude step integration for climb and descent and distance step integration for cruise. Instead of designing multiple missions with a specific number of drops, the drop portion of the mission is calculated as a fuel allocation, allowing the drop operator to configure an optimal drop segment of the mission. This fuel allocation does not take advantage of weight loss due to fuel burn and assumes flying at a constant altitude (5,000 ft and 300 ft AGL) is configurable, allowing for compatibility with a configurable multi-drop system, variable distance to fire, and different fuel capacities. The team plans to be able to perform two complete missions on one tank of fuel, thus allowing for hot (the aircraft engines still on, but set to idle) refill of fire retardant. The fuel requirement also includes fuel for warm up, a five minute taxi, takeoff, and another five minute taxi back at the end of the flight. This is summarized as the Warm Up, Taxi, and Takeoff (WUTTO) mission segment.

To determine the a desirable time on station, which sets the fuel allocation for the fire fighting portion of the mission, historical fire data was used. CAL FIRE publishes a list of fires along with their size. The area of each fire was assumed to be a square and a perimeter was found. The size of the three largest fires each year from 2013 until 2021, were used to inform the distance needed to fly around the entire fire. Wildfires are increasing in size yearly, therefore the trend from 2013 to 2021 was continued to 2030, the EIS date of Valkyrie. Following the trend outlined allowed for the estimation of the fire perimeter Valkyrie could be deployed in response to. This trend is shown in Figure 44. Of course, an aircraft cannot make an instantaneous change of direction, so load limited turns were added, with a load limit $n_z = 1.75$. The sample flight path is shown in Figure 45 and the designed total distance of the firefighting portion of the mission is 150 nmi.
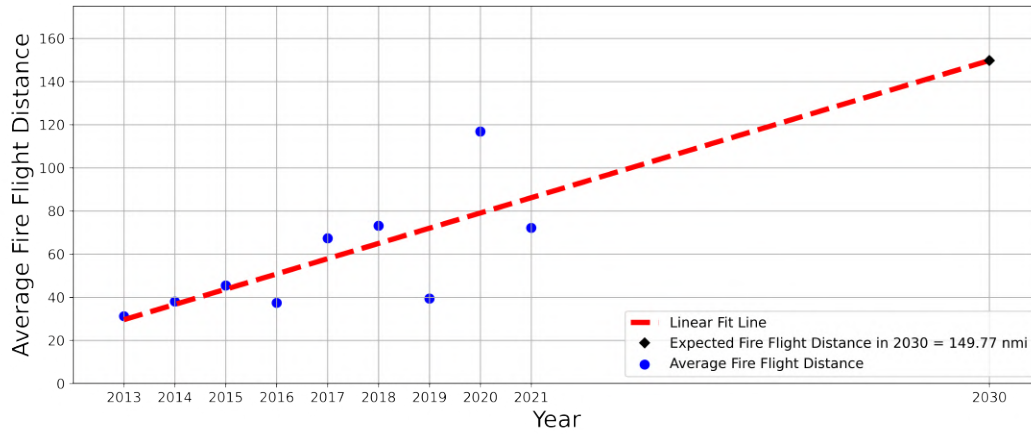
Fig. 44   Predicted Fire Flight Distance for 2030
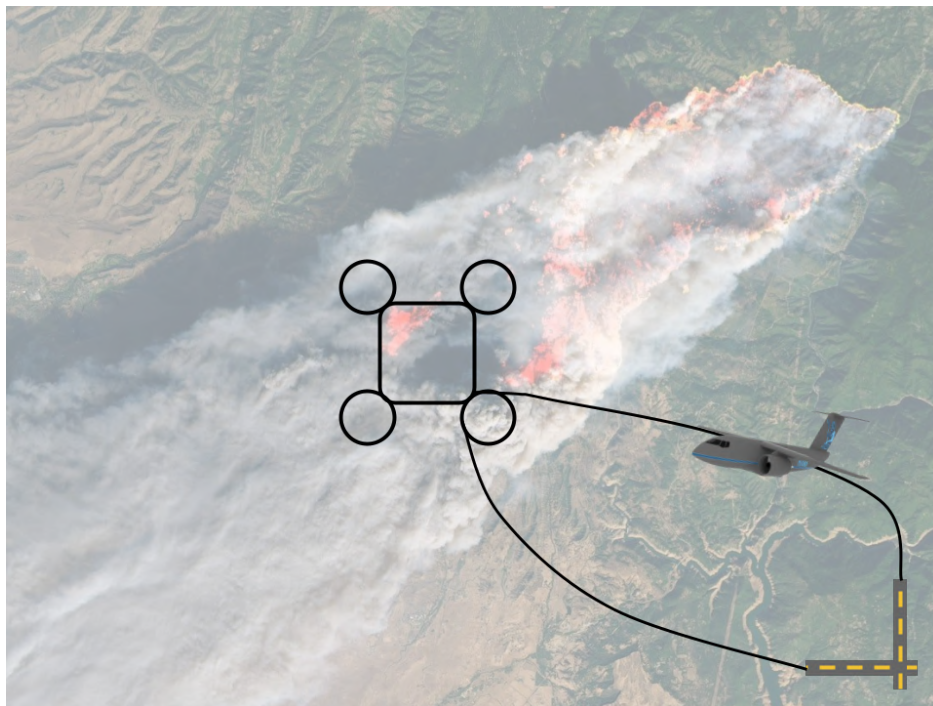
Fig. 45   Sample Firefighting Flight Path

The reserve mission consists of four parts: climb, cruise, loiter, and descent. If the aircraft is unable to land at the planned airport, the reserve mission allows for a diversion. The cruise portion of the reserve mission allows for a 200 nmi diversion. Upon reaching the alternate airport, the aircraft then has reserves for a one hour loiter period. After diverting to the alternate airport and loitering for an hour, the aircraft has enough fuel to descend to the alternate airport.

1. 400 nmi Drop Mission

The 400 nmi drop mission consists of seven mission segments and four reserve mission segments. The mission profile, shown in Figure 2, provides a visual representation of the mission. The payload is carried through the payload drop portion of the flight at which point is assumed to have been dropped. The fuel required during each flight segment is shown in Table 18.

Table 18   Fuel Requirement by Mission Segment for 400 nmi Mission Profile

Mission Segment	Fuel Burn [lb]	Fuel Fraction
WUTTO	560	2.02%
Climb	2,765	10.02%
Cruise	4,575	16.58%
Descent	2,045	7.40%
Fire Flight	5,270	19.10%
Climb	1,100	3.99%
Cruise	3,505	12.71%
Descent	1,220	4.42%
Reserves Climb	1,325	4.80%
Reserves Cruise	1,935	7.01%
Reserves Loiter	2,145	7.78%
Reserves Descent	1,150	4.17%
Total	**27,595**	**100%**

The drag for each flight segment is shown in Table 19. The values reported in the table are found by taking the average of the parameter of interest over the flight segment. As expected, the drag is much higher for the earlier portion of the mission before the payload is dropped.

Table 19   Segment Drag Summary for 400 nmi Drop Mission Profile

Mission Segment	C_D	L/D	Drag [lb]
Climb	0.07454	14.90	14,093
Cruise	0.02994	17.64	11,544
Descent	0.07116	15.06	13,471
Fire Flight	0.11433	12.28	16,027
Climb	0.03667	16.48	7,241
Cruise	0.03518	16.47	6,992
Descent	0.03518	16.47	6,992
Reserves Climb	0.03463	16.44	6,890
Reserves Cruise	0.02054	14.39	7,922
Reserves Loiter	0.03094	17.04	6,570
Reserves Descent	0.03319	16.38	6,630

2. Two 200 nmi Drop Missions

The 2×200 nmi drop mission consists of two 200 nmi drop missions run in sequence, without refilling fuel. The mission is comprised of fourteen mission segments and four reserve mission segments. If the aircraft has to divert after the first 200 nmi drop mission, the second 200 nmi drop mission will be aborted. The mission profile, shown in Figure 3, provides a visual representation of the mission. The payload is carried through the payload drop portion of each 200 nmi drop mission at which point is assumed to have been dropped. The payload is refilled between missions. The fuel required during each flight segment is shown in Table 20. There is an mission segment (taxi and refill), which includes fuel for a five minute taxi, a thirteen minute fire retardant refill at idle, and another five minute taxi.

Table 20   Fuel Requirement by Mission Segment for 2×200 nmi Mission Profile

Mission Segment	Fuel Burn [lb]	Fuel Fraction
WUTTO	560	1.41%
Climb	2,735	6.92%
Cruise	1,750	4.43%
Descent	2,065	5.23%
Fire Flight	5,330	13.48%
Climb	1,255	3.18%
Cruise	1,580	3.99%
Descent	1,420	3.59%
Taxi and Refill	685	1.73%
Climb	2,405	6.09%
Cruise	1,625	4.11%
Descent	1,795	4.55%
Fire Flight	4,620	11.69%
Climb	1,090	2.76%
Cruise	1,485	3.76%
Descent	1,230	3.12%
Reserves Climb	2,995	7.57%
Reserves Cruise	1,930	4.89%
Reserves Loiter	2,135	5.41%
Reserves Descent	1,145	2.90%
Total	**39,830**	**100%**

The drag for each flight segment is shown in Table 21. The values reported in the table are found by taking the average of the parameter of interest over the flight segment. As expected, the drag is much higher for the earlier portion of each mission, before the payload is dropped. The second 200 nmi drop mission has a lower drag due to the fuel burned by the first drop mission.

Table 21   Segment Drag Summary for 2 × 200 nmi Drop Mission Profile

Mission Segment	C_D	L/D	Drag [lb]
Climb	0.07366	14.94	13,934
Cruise	0.02992	17.64	11,537
Descent	0.07187	15.03	13,598
Fire Flight	0.11554	12.22	16,196
Climb	0.04172	16.45	8,153
Cruise	0.02225	15.71	8,579
Descent	0.04065	16.50	7,981
Climb	0.06455	15.43	12,294
Cruise	0.02777	17.45	10,710
Descent	0.06305	15.50	12,013
Fire Flight	0.10040	12.93	14,074
Climb	0.03637	16.47	7,188
Cruise	0.02096	14.77	8,081
Descent	0.06305	15.50	12,013
Reserves Climb	0.49346	13.19	13,281
Reserves Cruise	0.02050	14.34	7,906
Reserves Loiter	0.03080	17.03	6,540
Reserves Descent	0.03303	16.37	6,600

3. Ferry Mission

The ferry mission is comprised of three mission segments and four reserve mission segments. The mission profile, shown in Figure 4, provides a visual representation of the mission. The constraining version of the ferry mission, is the ferry cargo mission where the 20,000 lb payload is carried through the entirety of the flight. The fuel required during each flight segment is shown in Table 22.

Table 22   Fuel Requirement by Mission Segment for Ferry Mission Profile

Mission Segment	Fuel Burn [lb]	Fuel Fraction
WUTTO	560	1.24%
Climb	1,965	4.36%
Cruise	33,845	75.01%
Descent	1,375	3.05%
Reserves Climb	1,475	3.27%
Reserves Cruise	2,120	4.70%
Reserves Loiter	2,445	5.42%
Reserves Descent	1,335	2.96%
Total	**45,120**	**100%**

The drag for each flight segment are shown in Table 23. The value reported in the table is found by taking the average of the parameter of interest over the flight segment.

Table 23   Segment Drag Summary for Ferry Mission Profile

Mission Segment	C_D	L/D	Drag [lb]
Climb	0.05464	15.95	10,513
Cruise	0.02321	16.23	9,255
Descent	0.04059	16.50	7,974
Reserves Climb	0.03988	16.50	7,844
Reserves Cruise	0.02141	15.22	8,537
Reserves Loiter	0.04467	16.61	7,684
Reserves Descent	0.03807	16.52	7,513

C. Aircraft Performance Coefficients

Performance analysis can also be used to calculate important aircraft performance coefficients. This is accomplished by using the top of climb weight of the different mission profiles and analyzing various cruise velocities and altitudes, holding weight constant.

For a turbofan powered aircraft, $(C_L/C_D)_{\max}$ represents the optimal speed for aircraft endurance. When C_L/C_D is maximized, drag and, as a result, thrust required are minimized. Range is maximized at $\left(C_L^{1/2}/C_D\right)_{\max}$. Maximum loiter occurs when $\left(C_L^{3/2}/C_D\right)$ is maximized.

The trade study was conducted sweeping over Mach numbers from 0.4 to 0.67 and cruise altitudes from 25,000 ft to 35,000 ft. The upper bound of the Mach number range allows for the use of low speed airfoils during the firefighting portion of the mission, while still allowing for high speed operation. With these restrictions applied the maximum value for each of the aircraft performance coefficients is found for the mission profiles. These are summarized in Table 24.

Table 24   Maximum Aircraft Performance Coefficients

	400 nmi Mission				2 × 200 nmi Mission				Ferry Mission			
	Altitude	Mach Number	C_L	Value	Altitude	Mach Number	C_L	Value	Altitude	Mach Number	C_L	Value
C_L/C_D	28,750 ft	0.67	0.53	17.8	28,750 ft	0.67	0.53	17.8	28,750 ft	0.67	0.44	17.6
$C_L^{1/2}/C_D$	28,000 ft	0.67	0.52	24.7	28,000 ft	0.67	0.51	24.7	28,000 ft	0.67	0.42	26.3
$C_L^{3/2}/C_D$	29,000 ft	0.50	0.97	15.1	29,000 ft	0.50	0.97	15.1	29,000 ft	0.45	0.98	15.0

Valkyrie flies at 28,000 ft and Mach 0.67 for the cruise portions of all missions and at 29,000 ft and Mach 0.50 for the loiter portions of the firefighting missions and Mach 0.45 for the loiter portion of the ferry mission.

D. Payload-Range Diagram

A payload-range diagram, shown in Figure 46, confirms that the aircraft is able to carry the payload required for the mission. The upper line of the payload-range diagram represents the payload limit of the aircraft. The first sloped portion represents a trade of payload for range while maintaining the maximum takeoff weight limit. The final sloped portion, represents a trade along a line of constant maximum fuel weight, limited by fuel capacity.
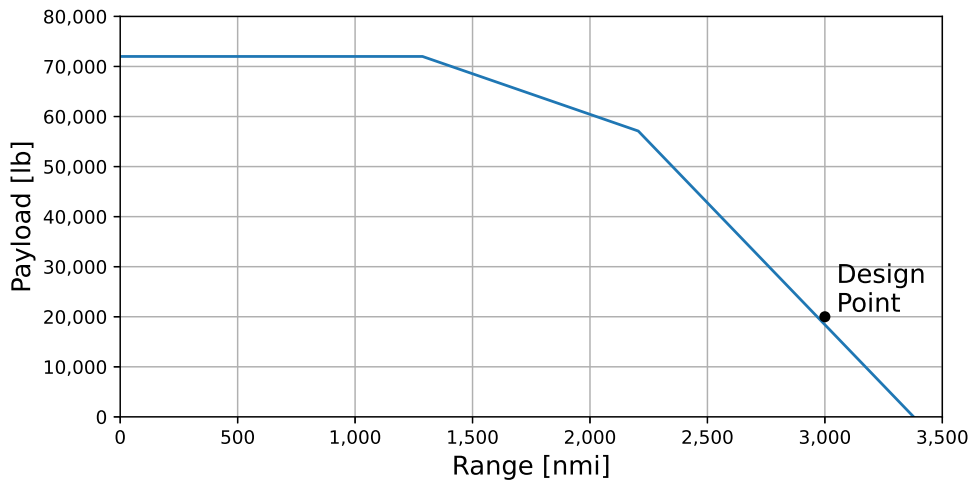
Fig. 46   Payload-Range Diagram

E. Payload-Radius Diagram

Similar to the payload-range diagram, the payload-radius diagram shown in Figure 46 depicts the same trade of payload for range but within the constraints of a firefighting mission. The fuel allocation for the firefighting portion of the mission is kept constant while the mission radius is adjusted. The payload-radius diagram allows operators to determine the maximum amount of fire retardant Valkyrie can transport over a given distance.
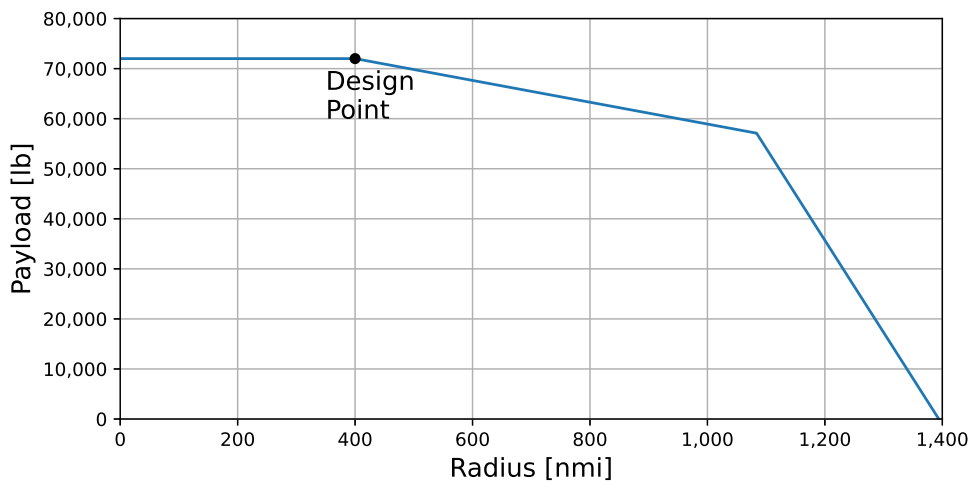
Fig. 47   Payload-Radius Diagram

F. Payload-Time on Station Diagram

The payload-Time on Station (TOS) diagram, shown in Figure 48, depicts the trade of payload for time on station. In this diagram, the radius to the fire is held at 400 nmi, while the duration of the firefighting portion of the mission is adjusted. The payload-TOS diagram allows operators to use one plane as a spotter aircraft or lead plane for another aircraft in the fleet. By sending out an aircraft with a just above 30,000 lb of payload, Valkyrie can act as a spotter aircraft for five hours. Alternatively, Valkyrie can act purely as a spotter aircraft and fly for over six hours on station before needing to return to base and refuel.
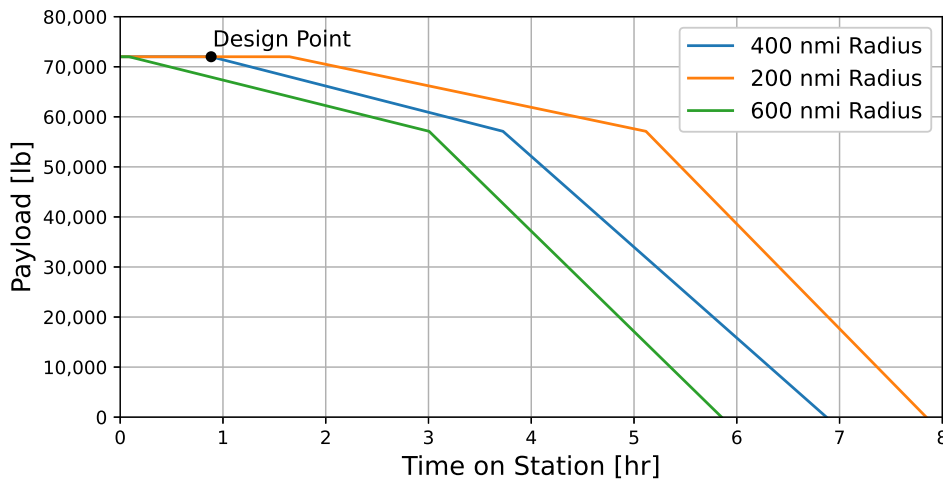
Fig. 48   Payload-Time on Station Diagram

G. Flight Envelope Diagram

The flight envelope diagram shows the safe operating region of the aircraft. Documentation of this safe operating region is imperative to the certification of Valkyrie as §25.671 (b) stipulates that flight testing must demonstrate the safety of operation within this region without exceptional pilot skill, thus validating the theoretically obtained flight envelope. The flight envelope diagram is largest when Valkyrie is flying with minimal fuel. This flight envelope is shown in Figure 49. The limits of the flight envelope are comprised of stall velocity, minimum velocity, structural altitude limit, structural speed limit, and bird strike speed limit. The bird strike limit was developed in keeping with 14 CFR Part 25 §25.631.
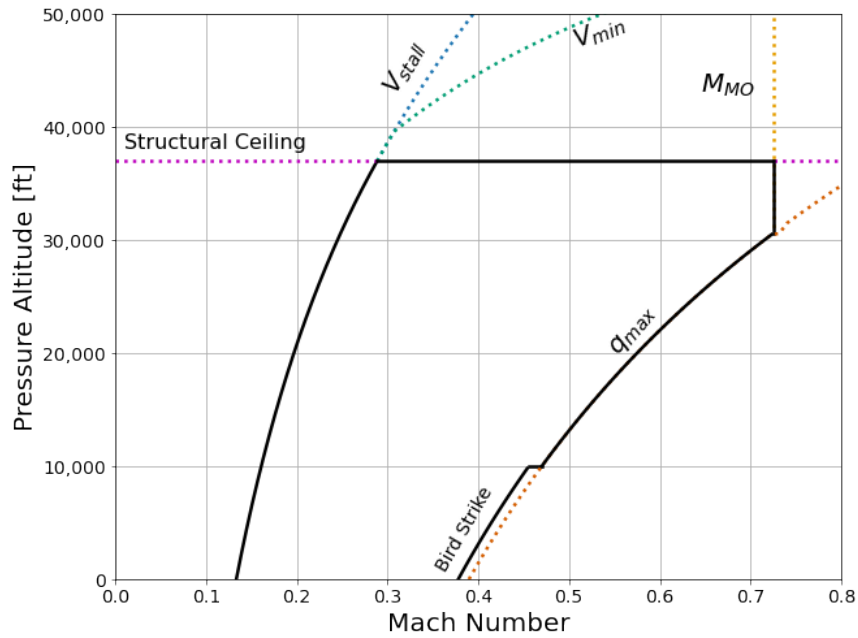
Fig. 49   Flight Envelope Diagram

H. Specific Excess Power Diagram

The specific excess power diagram in Figure 50 shows the aircraft's ability to increase its specific energy over the entire flight envelope. The flight envelope is outlined in solid black. The red line shows that Valkyrie is able to satisfy the 300 knots dash speed requirement above 10,000 ft pressure altitude. Valkyrie is also able to satisfy the 400 knots objective requirement above 27,000 ft.
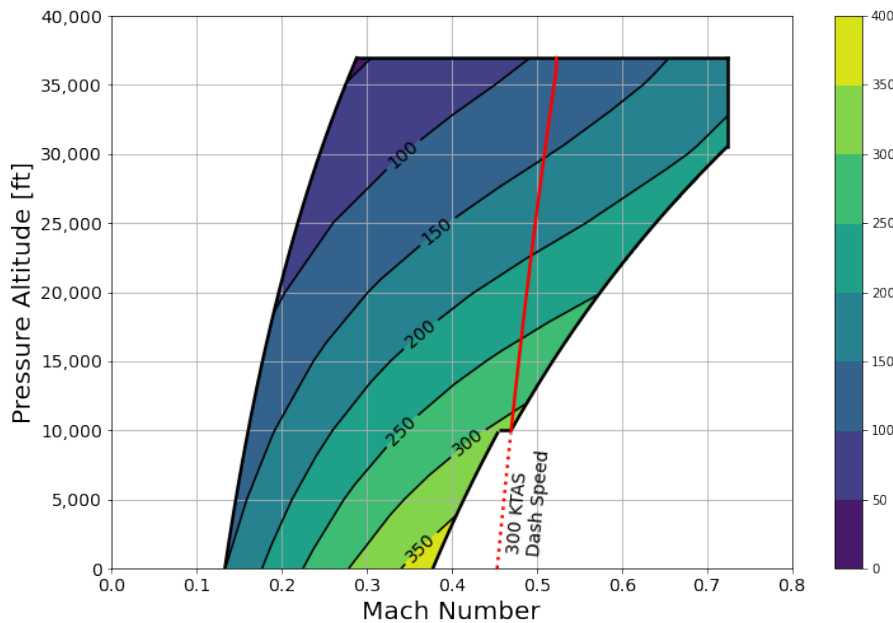
Fig. 50   P-s Diagram

IX. Stability and Control

A. Tail Morphology

The design of the tail was aimed at minimizing trim drag and weight and ensuring that tail stall occurs after wing stall to enable a recovery maneuver. Figure 25 shows that the total CG travel during normal mission operation falls within a narrow range. A fixed-incidence tail is suitable and is also lighter than a variable-incidence tail. Additionally, a variable-incidence tail introduces more failure modes like runaway trim.

1. Airfoil Selection

A host of symmetrical, cambered, and supercritical airfoils were analyzed using VLM to calculate their tail incidence angles required to trim the aircraft at top of climb as well as their drag produced in the trimmed state. For the purposes of the airfoil study, the optimal tail size for each candidate was set by a 5% aft static margin constraint. This method inherently biases toward airfoils with higher lift-curve-slopes because the static margin constraint is met with a smaller tail area and thus less drag, all else being equal. The results of the study are visualized in Figure 51.
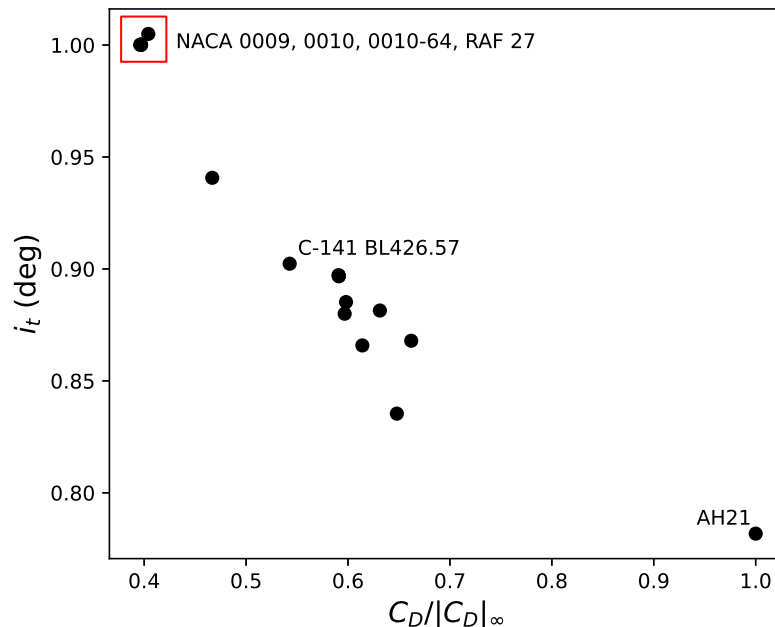
Fig. 51   Tail incidence angle against tail trim drag scaled to a maximum value of one.

Several airfoils stood out for their low relative drag. These airfoils also happened to have the greatest tail incidence angles (positive leading-edge down), which is a favorable trait given that their reduced geometric angle of attack makes them less likely to stall at high α where the wing may be stalled. The performance differences between these airfoils are small to where they are graphically indistinguishable. In the interest of achieving a greater stall angle of attack and structural strength, the thicker, larger leading-edge radius NACA 0010-64 was selected for the horizontal stabilizer.

The vertical tail airfoil was selected among symmetrical airfoils to have a stall side slip angle above that expected of the aircraft to trim in takeoff OEI conditions. Full-scale wind tunnel testing of AR 6 wings by NACA demonstrated that the NACA 0012 yielded a stall angle of attack in excess of 18.9° at Reynolds numbers above 3 million[22]. Meeting the team's needs, the NACA 0012 was chosen for the fin.

2. Tail Sizing

The airfoil selection process sized tails to satisfy a minimum aft static margin constraint. However, there are other factors that drive the horizontal tail size. They are the ability for the tail to produce a moment about the main landing gear at takeoff sufficient to pitch the nose up and for the tail to not stall in out-of-trim conditions due to local flow variation[23]. The latter is an active constraint as can be seen in Figure 52 and set the tail-to-wing area ratio to 0.181 ($V_H = 0.616$). This lower-than-typical tail volume compared to the seed aircraft in Table 4 is due to an increased tail lift effectiveness from a reduction in horizontal tail sweep. Valkyrie takes advantage of its fixed incidence tail by connecting both elevators, giving its stabilizer an unswept hinge line and a quarter-chord sweep of 7.8°. For comparison, the C-390's V_H adjusted for a stabilizer sweep reduction from the 30.2° to 7.8° is 0.638, which is very near Valkyrie's V_H.
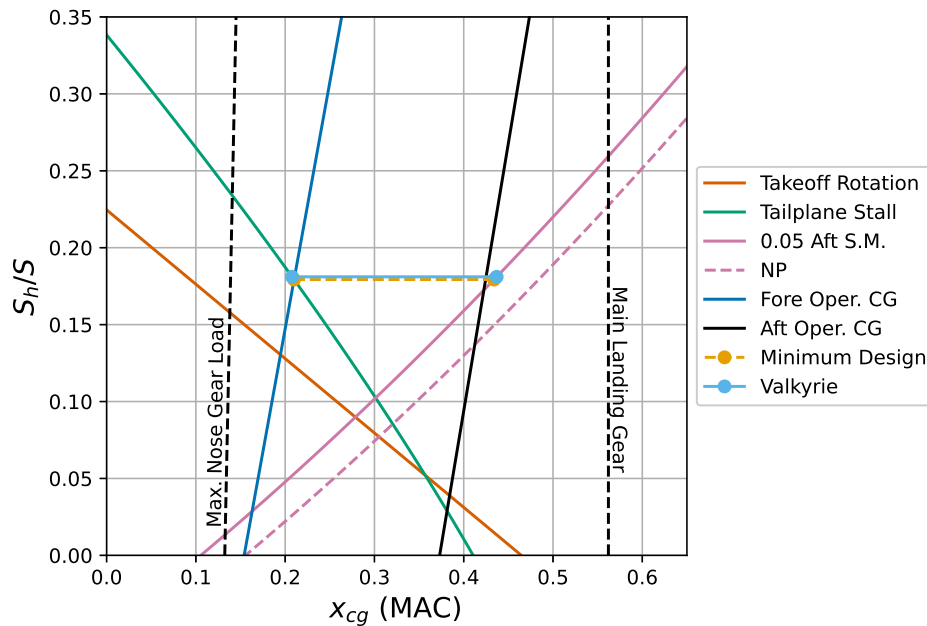
Fig. 52   Scissor/Notch Diagram Used to Size the Horizontal Stabilizer

The vertical tail size was determined using vertical tail volume derived from the similar aircraft in Table 4. At the subsonic Mach numbers Valkyrie operates at, the sweep of the fin was able to be reduced to increase its lift effectiveness. A sweep angle of 25° was retained to give the horizontal stabilizer a sufficient moment arm and a lower vertical tail volume was designed for to account for the reduced sweep. Using the C-2 and C-17's tails as references, the precise differences from trigonometry average to give Valkyrie's tail volume of 0.084.

The elevators were sized to overcome the aircraft's pitch stiffness. The rudder and ailerons were sized accordingly to the takeoff OEI condition with the ailerons additionally constrained by roll rate. The trimmed aircraft deflections for OEI are presented alongside the stability and control data in the sections to follow. The aileron dimensions were provided in the aircraft 3-view in Figure 37. The details of the tail geometry are shown in the tail drawing in Figure 53.
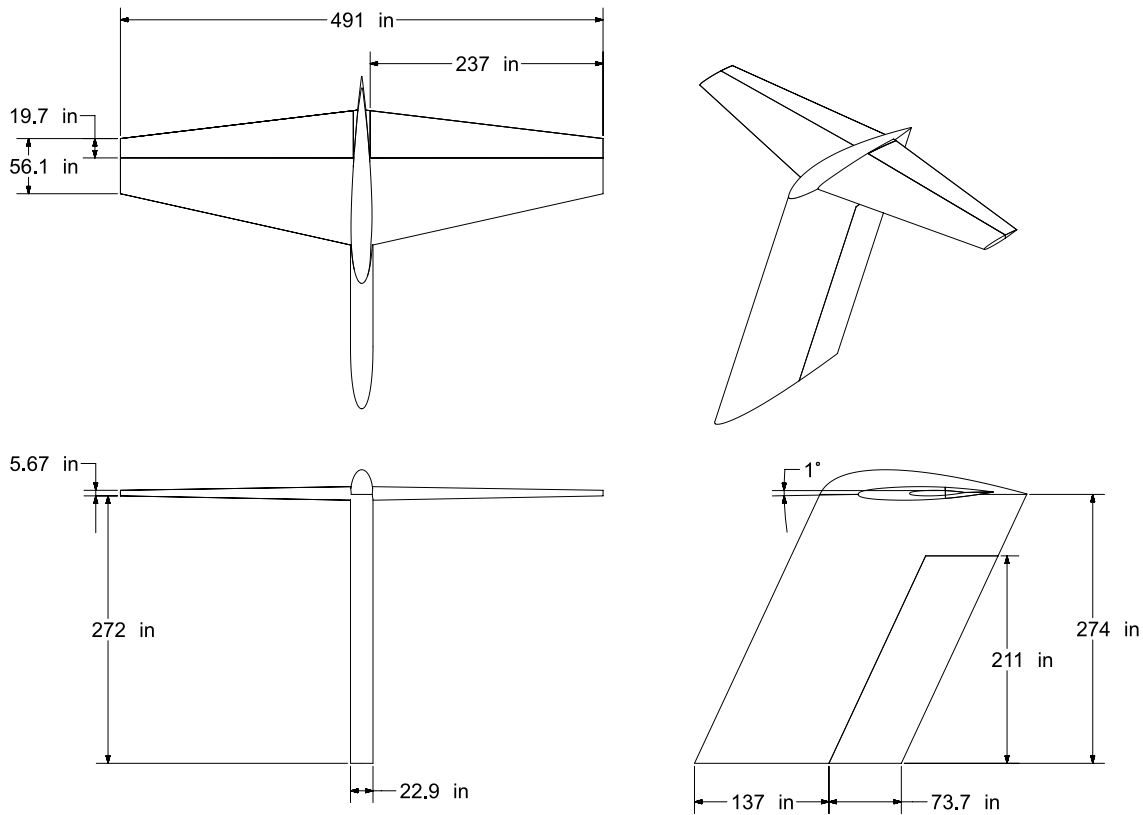
Fig. 53   Dimensioned 3-view of the tail

B. Design Evaluation

1. Method

The stability and control characteristics of Valkyrie were evaluated using data from the VLM solver AVL and validated with equations. For each flight condition, the locations of the wing body, stabilizer, and full aircraft aerodynamic centers and C_{L_α} of each body were acquired from AVL. These were sufficient to calculate the downwash derivatives using Eq. (2.3,18) in Etkin and Reid and the neutral point from Eq. (2.3,23).[24] The absolute location of the neutral point given by AVL was within 1% difference of that from equations. Subsequently, a comprehensive selection of control, stability, and body derivatives were taken from AVL and are presented in Tables 25-27. The α and $\dot{\alpha}$ body derivatives were calculated using Equations (5.2,1)-(5.2,4) and (5.5,10)-(5.5,12) in Etkin and Reid[24].

Table 26 Stability Derivatives

Table 25 Control Derivatives

Condition	Takeoff	TOC	Landing
h (ft)	5,000	28,000	0
ΔISA (°F)	35	0	0
M_∞	0.25	0.67	0.17
α (deg)	10.0	0.385	0.862
$C_{L_{\delta e}}$	0.5068	0.6104	0.5159
$C_{m_{\delta e}}$	-1.783	-2.097	-1.7304
$C_{y_{\delta a}}$	-0.0108	-0.0214	-0.0161
$C_{l_{\delta a}}$	0.1438	0.1743	0.1487
$C_{n_{\delta a}}$	0.0160	0.0061	0.0101
$C_{y_{\delta r}}$	-0.2954	-0.3667	-0.3467
$C_{l_{\delta r}}$	-0.0440	-0.0609	-0.0545
$C_{n_{\delta r}}$	0.1204	0.1536	0.1434

Condition	Takeoff	TOC	Landing
ϵ_α	0.242	0.319	0.248
C_{L_α}	4.793	6.531	5.167
C_{m_α}	-1.918	-1.0264	-1.309
C_{L_q}	7.857	11.447	8.044
C_{m_q}	-21.604	-23.573	-19.742
C_{y_β}	-0.6711	-0.8452	-0.8262
C_{l_β}	-0.1757	-0.1667	-0.1792
C_{n_β}	0.1629	0.2027	0.1961
C_{y_p}	0.2921	-0.0128	0.0684
C_{l_p}	-0.4436	-0.5738	-0.4884
C_{n_p}	-0.1608	-0.0131	-0.0648
C_{y_r}	0.6721	0.8506	0.7724
C_{l_r}	0.4488	0.2387	0.3765
C_{n_r}	-0.3050	-0.3243	-0.3165

Table 27 Body Derivatives

Condition	Takeoff	TOC	Landing
C_{x_u}	-0.0209	-0.0201	-0.1914
C_{x_α}	1.1525	0.1860	0.7051
C_{x_q}	0.3565	-0.2997	-0.4582
$C_{x_{\dot\alpha}}$	0	0	0
C_{z_u}	-3.256	-0.9895	-2.935
C_{z_α}	-4.793	-6.531	-5.165
C_{z_q}	-7.915	-11.449	-8.052
$C_{z_{\dot\alpha}}$	-0.0341	-0.0228	-0.0152
C_{m_u}	0.1799	0.1699	0.0197
$C_{m_{\dot\alpha}}$	-0.1162	-0.0776	-0.0518

2. Static Stability

From Table 26, it can be observed that $C_{m_\alpha} < 0$, $C_{n_\beta} > 0$, and $C_{l_\beta} < 0$, which proves that Valkyrie is directionally statically stable. Static longitudinal stability can also be determined by checking for a positive static margin. Table 28 shows the static margins associated with different flight modes.

Table 28   Valkyrie Static Margins

Condition	NP (%MAC)	CG (%MAC)	S.M. (%MAC)
MTOW Takeoff	60.03	32.91	27.12
TOC	50.49	34.78	15.71
Max. Fore CG	48.69	21.06	27.63
Max. Aft CG	48.69	42.51	6.18

3. Aircraft Trim

To trim the aircraft at TOC with no elevator deflection, the stabilizer was fixed at a 1° leading-edge down incidence angle. Evaluating the aircraft at TOC with this incidence angle yielded a trim elevator deflection less than one-twentieth of a degree, which is within the mathematical uncertainty in using numerical methods. This can be seen visually in Figure 54 and numerically in Table 29 where the trim C_L with zero elevator deflection is effectively the required 0.517. The angle of attack at takeoff was driven by the $C_{L_{TO}}$ required to make BFL. While the optimal climb is performed at maximum excess power, it is still useful to calculate the configurations necessary for a steady climb. Also tabulated, the trim states for steady climb are seen in Figure 55. The specific elevator deflection of -3.35° trims Valkyrie at its MTOW during takeoff.

Table 29   Trim Conditions

	TOC $M = 0.67$, $h_p = 28{,}000$ ft, ISA				Takeoff $V_{\text{LOF}} = 283.7$ ft/s, $h_p = 5{,}000$ ft, +35 °F ΔISA			
δ_e (deg)	-4	-2	0	2	-5	-3.35	0	2
$C_{L_{\text{trim}}}$	1.378	0.950	0.522	0.094	1.675	1.473	1.062	0.817
α (deg)	8.307	4.369	0.431	-3.507	5.547	3.215	-1.523	-4.352
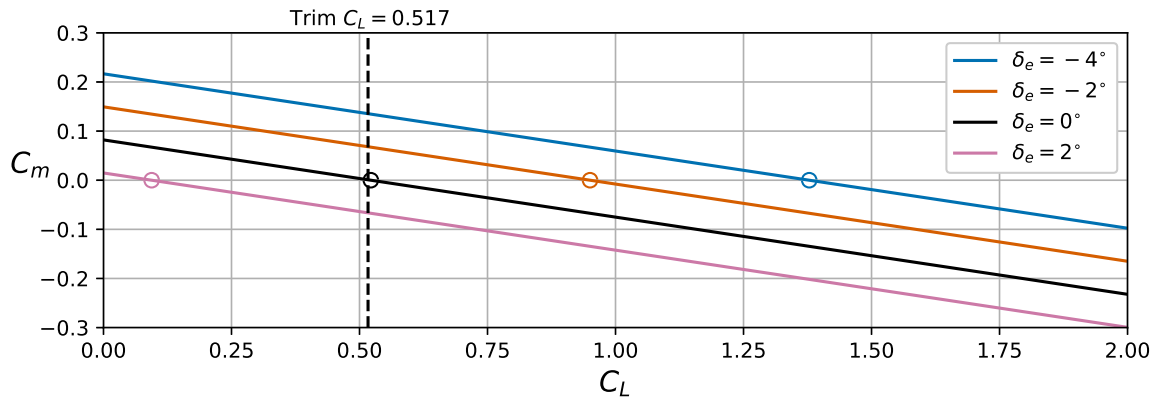
Fig. 54   Trim Diagram for Steady Level Flight at Top of Climb
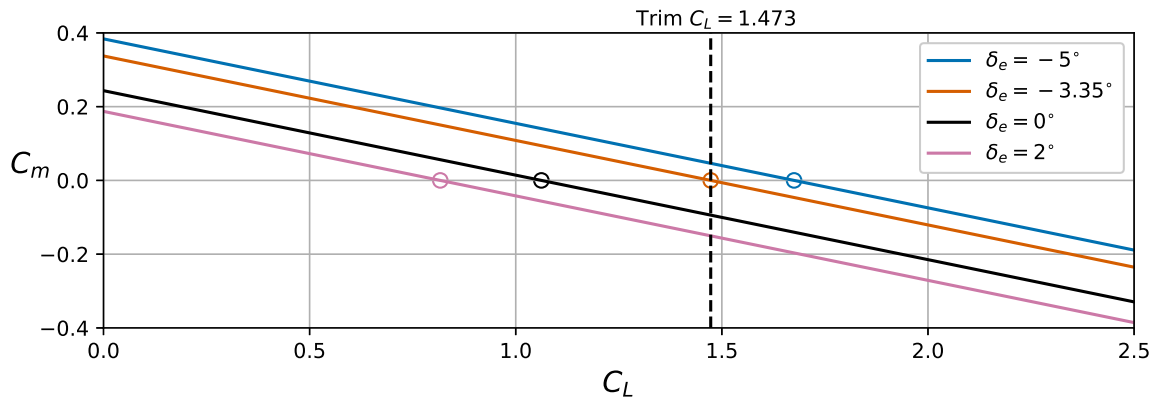
Fig. 55   Trim Diagram for Steady Climb at Takeoff Conditions

The β, δ_a, and δ_r derivatives in Tables 25 and 26 determine the trim states of the aircraft under continuous perturbation (i.e. crosswind, OEI). The equilibrium side force, roll moment, and yaw moment as functions of bank, sideslip, aileron deflection, and rudder deflection angles is a system of 3 equations and 4 unknowns. Figure 56 shows all possible orientation and deflection angles to trim for OEI at takeoff condition from sideslip angles of 0 through 14°. This satisfies the aircraft trim requirements outlined in §25.175(a) - 25.175(d) for longitudinal stability and §25.177(a) - 25.177(d) for lateral stability.
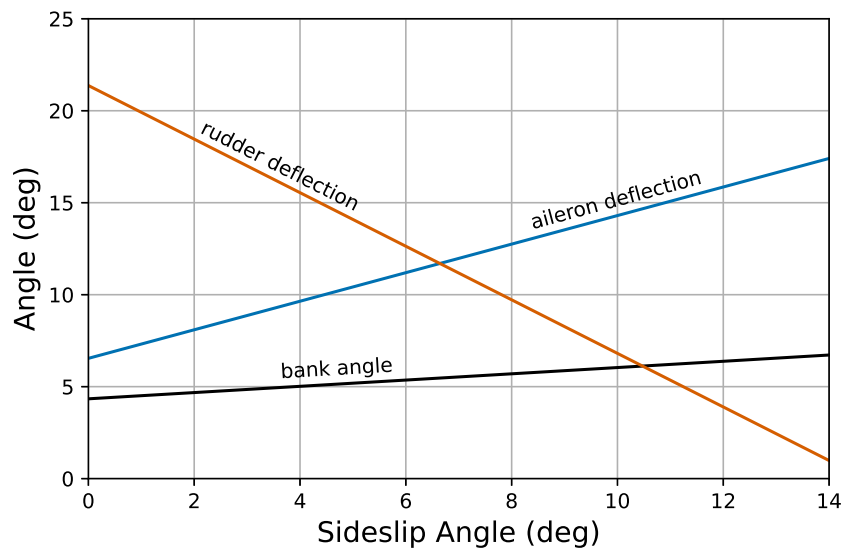
Fig. 56   Aircraft Orientation and Control Surface Deflections to Trim in OEI at Takeoff

4. Dynamic Longitudinal Stability

The longitudinal modes were found through eigenvalues of the plant matrix defined in Eq. (4.9,18) in Etkin and Reid[24] where $\lambda = n \pm \omega i$. To complete the plant matrix, the principal moments of inertia were approximated using Raymer's historically-based Eq. (16.52)-(16.54) for jet heavy bomber class aircraft[8], and the dimensional derivatives were calculated from the definitions in Table 4.4 of Etkin and Reid[24] using stability and body derivatives from Tables 26 and 27. The calculated eigenvalues are as follows:

Mode 1 (Phugoid mode): $\qquad \lambda_{1,2} = -0.0009527 \pm 0.10931i$

Mode 2 (Short-period mode): $\quad \lambda_{3,4} = -0.92995 \pm 2.08901i$

Etkin and Reid expressions in Eq. (6.1,12)[24] calculate the time and cycles to half and damping ratio used to construct the transfer function. Valkyrie's pitching impulse response for the long-period phugoid and short-period modes are shown in Figure 57. The time and cycles to half are given in Table 30. The negative real-parts of the eigenvalues and the decaying amplitudes in the impulse response are each sufficient conditions for dynamic longitudinal stability.
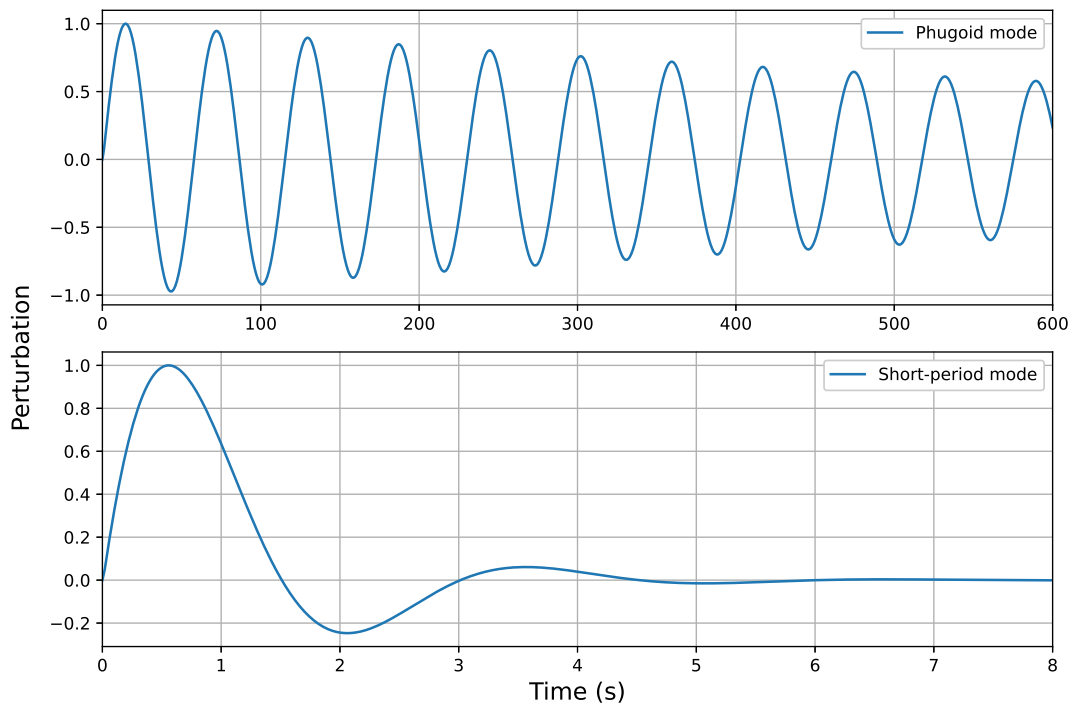
Fig. 57   Impulse Response of Phugoid and Short-Period Modes Scaled to Unit Maximal Perturbation

5. Dynamic Lateral Stability

The lateral modes were found similarly to the longitudinal modes from the plant matrix for the lateral dynamics in Etkin and Reid Eq. (4.9,19)[24]. The matrix was completed using an estimate of I_{xz} from the example aircraft in Roskam Part 6[25]. The dimensional derivatives were calculated using stability derivatives in Table 26 from definitions in Table 4.5 of Etkin and Reid[24]. The resulting eigenvalues are:

Mode 1 (Spiral mode): $\lambda_1 = -0.001923 \pm 0i$

Mode 2 (Rolling convergence): $\lambda_2 = -1.001333 \pm 0i$

Mode 3 (Dutch roll): $\lambda_{3,4} = -0.16127 \pm 1.51277i$
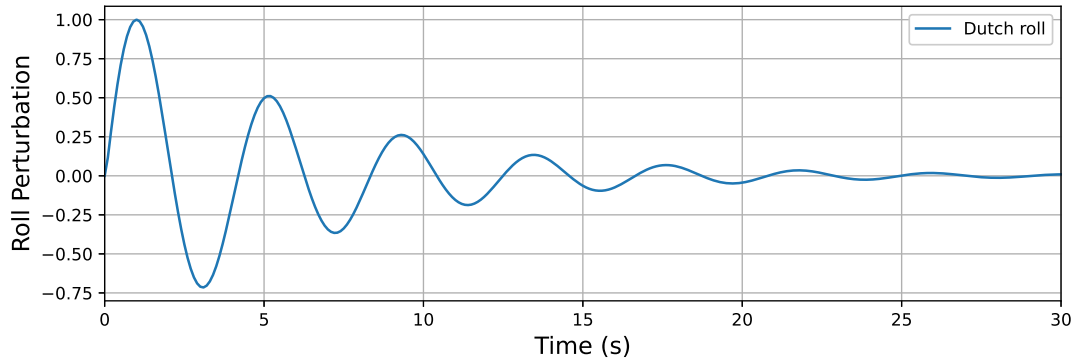
Fig. 58   Impulse Response of Dutch Roll Scaled to Maximal Unit Roll Perturbation

The roll impulse response is plotted in Figure 58. By inspection of the real parts of the eigenvalues and amplitude transient, Valkyrie is determined to be roll stable and spirally stable. A summary of all of Valkyrie's dynamic modes is presented in Table 30.

Table 30   Summary of Valkyrie Dynamics

Mode	Damping Ratio, ζ	Natural Frequency, ω_n (rad/s)	t_{half} (s)	N_{half}	Period, T (s)
Short-period	0.4067	2.287	0.745	0.247	3.008
Phugoid	0.008716	0.1093	727.4	12.62	57.48
Dutch roll	0.1060	1.521	4.297	1.032	4.153
Rolling	N/A	N/A	0.692	N/A	N/A
Spiral	N/A	N/A	360.3	N/A	N/A

X. Structures and Loads

A. V-n diagram

The V-n diagram for Valkyrie was plotted in accordance with 14 CFR §25.333 and §25.341 and is shown in Figure 59. The V-n diagram shows the region in which the aircraft can safely be operated before encountering structural limitations. While regulations mandate a minimum maximum positive load factor of between 2.5 and 3.8, the decision was made to use a positive load factor of 4.5 due to the increased likelihood of Valkyrie encountering turbulence or other high load inducing environments during operation. Due to the increased maximum positive load factor used to design Valkyrie, the influence of gusts is significantly diminished as can be seen by the gust diagram being nearly entirely encapsulated by the V-n diagram.
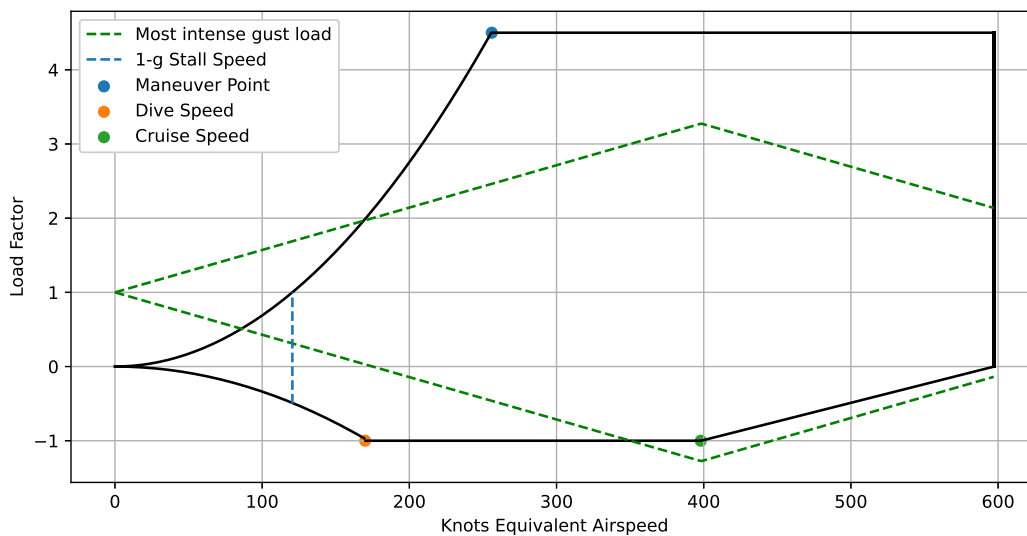
Fig. 59   V-n Diagram

B. Load distribution and path

The spanwise lift distribution for the half-span of Valkyrie was plotted using VLM simulation data obtained using an OpenVSP model of the aircraft with a 0°angle of attack. While geometrically accurate, this model did not have engines nor did it result in a lift distribution that accounted for the weight of the wing, engine, or fuel tanks, all of which were accounted for manually using the top of climb fuel weight for the 400 nmi radius firefighting mission profile, as this is the main design mission for Valkyrie. The resulting lift distribution is shown in Figure 60. The shear force distribution, shown in Figures 61 and 62, is obtained by the first integration of the lift distribution and the spanwise bending moment, shown in Figures 63 and 64, is obtained by taking the second.
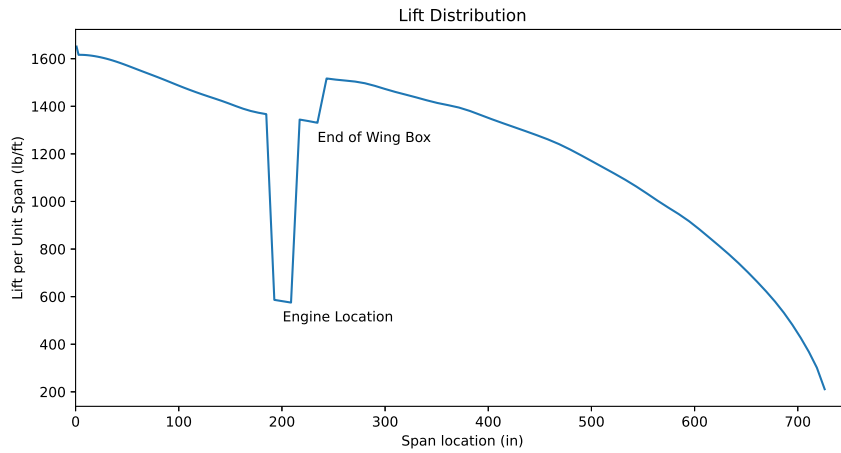
Fig. 60   Elliptical Wingload
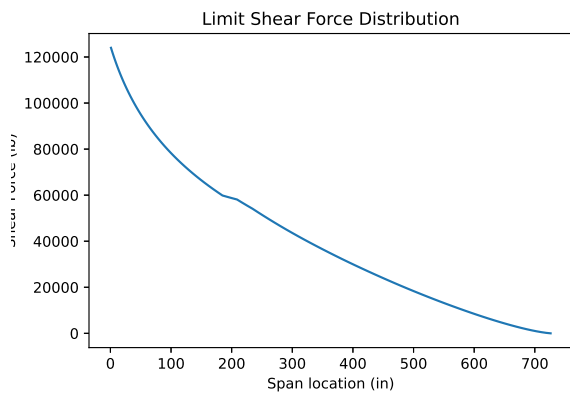
Fig. 61   Limit Shear Force Diagram
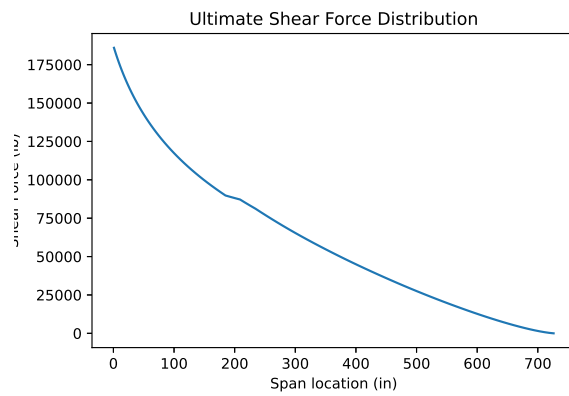
Fig. 62   Ultimate Shear Force Diagram
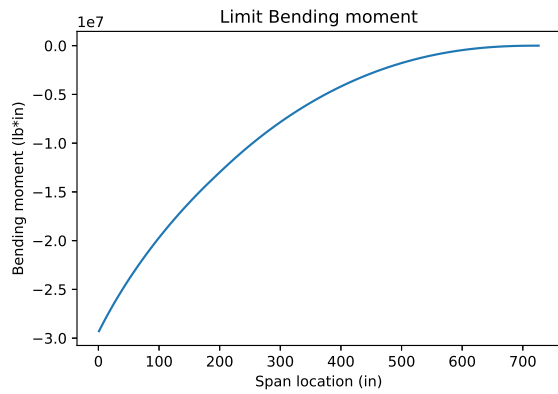
Fig. 63   Limit Bending Moment Diagram
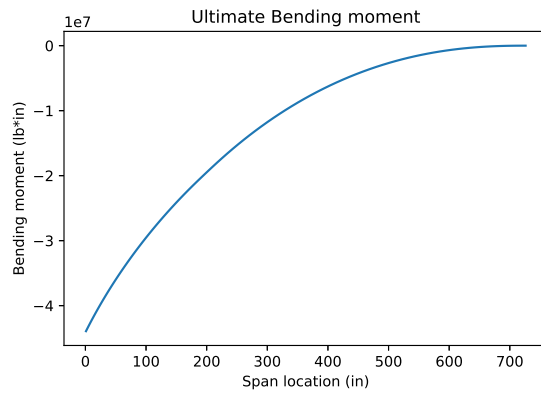
Fig. 64   Ultimate Bending Moment Diagram

59

C. Structures

1. Material Selection

To reduce cost and increase repairability at remote airfields without access to the tools and skill-set associated with the more complex composite repair methods, the structure of Valkyrie avoids composite components. Additionally, composites do not absorb impact from debris as well as metal alloy structures such as large embers leading to structural damage. Due to cost and manufacturing difficulties, titanium alloys will only be used where necessary, such as landing gear components which need a high yield strength and are required to be fire resistant per CFR 14 Part 25 §25.729(c) due to friction resulting from braking during landing. Research was conducted surveying a variety of metal alloys used in commercial and cargo aircraft. The most common types of aluminum found in these aircraft are Aluminum Alloy 7075 (AA7075) and AA6061. Due to its lessened corrosion resistance from the alloying process, AA7075 is often covered with a thin layer of pure aluminum[8], a technique that the proposed aircraft will use for all alloyed external components. The material properties for considered alloys are shown in Table 31[26].

Table 31   Comparison of Metal Alloys

Metal Alloy	σ_{Yield} (psi)	σ_{Ultimate} (psi)	ρ (lb/in^3)	General Properties
AA7178	78,000	88,000	0.1019	High compressive strength-to-weight ratio
AA7075-T6	63,000	74,000	0.1015	Corrosion and cracking resistance
AA 7075	86,000	97,000	0.1033	Superior stress and corrosion resistance
AA6061-T6	35,000	42,000	0.0975	Easy to machine; high corrosion resistance
AA2024-T351	41,000	68,000	0.1004	High strength-to-weight, fatigue resistance; poor corrosion
Ti 6Al-4V	133,000	138,000	0.1631	Lightweight, strong, and robust

This trade study confirmed that all alloys used have yield stresses within the bounds set by the limit and ultimate shear force and bending moment, shown in Figures 61 - 64. As a result of this trade study, the following decisions were made regarding the material selection for the various components of the structure, as outlined in Table 32.

Table 32   Comparison of Common Aircraft Metal Alloy Properties

Material	Component
AA7178	Spars
AA7075	Wing Ribs, Stringers
AA7055	Wing Skin
AA6061	Fuselage Skin, Frames
Ti 6Al-4V	Landing Gear Components

2. Pressurization

Pressurization is required for aircraft flying above 15,000 ft. Due to the altitude at which Valkyrie will be flying at in cruise, pressurization is necessary. Like most commercial aircraft, Valkyrie will be designed for an 8,000 ft altitude pressurization, which is 10.92 psi. This is the maximum allowable pressure altitude before supplemental oxygen is required per 14 CFR Part 25 §25.841(a). However, as the flight deck is the only part of the aircraft carrying humans, only the flight deck will be pressurized as shown in Figure 65. The pressure differential is used to size the AA7055 nose skin thickness and to define the structural limits on the operating ceiling, with a maximum pressure differential of 7.77 psi. A semi-hemispherical bulkhead will be used to support the pressure at the end of the nose section and a smaller flat bulkhead will be used at the tip to ensure space for a radar, enclosing the flight deck. A semi-hemispherical bulkhead was chosen for the rear of the flight deck as they are lighter than flat bulkheads, easier to manufacture than hemispherical bulkheads, which have better pressure distribution characteristics than flat bulkheads. Sizing the bulkheads was done using the methods outlined in Niu[27], and then further validated using FEM analysis, as shown in Figure 66. The analysis used a constant pressure across the inside surface of the bulkhead with the boundary condition consisting of the outside lip, where the bulkhead would mount the the fuselage.
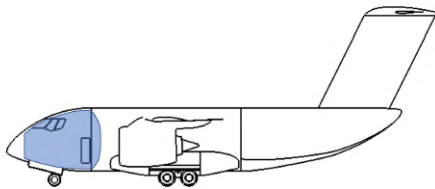
Fig. 65   Pressurized Flight Deck
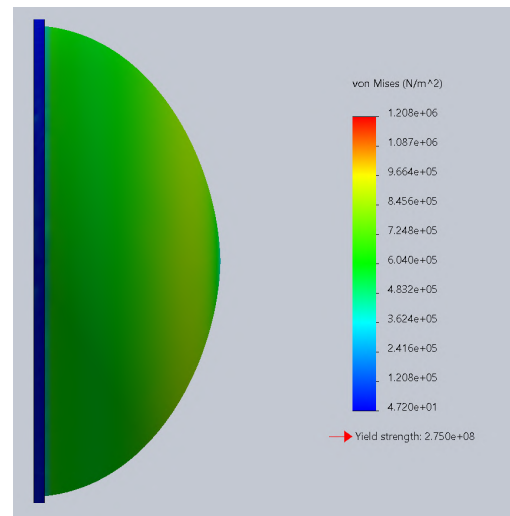
Fig. 66   Bulkhead

3. Structural Layout

The wing will consist of ribs attached to a forward and aft spar. The C-channel spar was chosen for its ability to resist both bending and shear stress similarly to I-beams, but allows for greater space for fuel within the wet wing and easier maintenance checks due to the seams being visible from the interior of the wing.

These C-channel spars are sized using the methods outlined in Roskam III[28] and further validated using FEA. The main spar is located at 18% of the chord and the aft spar is located at 65% of the chord. This will leave the recommended 25% chord necessary for the flaps, ailerons, and related control mechanisms[8]. Valkyrie requires 28% of the chord for flaps, and the 7% extra serves as a buffer zone for the flap mechanisms. This will also allow for a larger wing torque box, resulting in thinner ribs as the bending and shear stresses will be better distributed. The spars will be attached in the middle with bolted AA7178 plates to a main keel beam, constructed out of AA2024 due to its high fatigue resistance and strength to weight ratio. Due to the lack of quarter chord sweep, it was decided that the ribs will be placed in the same direction as flight. The ribs will be evenly spaced at 26 in to assist in ease of maintenance, manufacturing, and stress distribution[8], with a total of 56 ribs used.

Engine mounts are designed and validated using FEA with a maximum load factor of 4.5 and are constructed out of AA7178 with a protective layer of pure aluminum. These mounts will be attached to the two main spars 200 in from the center of the wing, as the result of a rotor burst analysis, ensuring only a 5% chance of a rotorburst on one engine causing critical failure in the other. This is in keeping with the rotorburst engine spacing requirements outlined in §25.903(b). Depicted in Figure 67 is the FEA results for the engine mount at maximum operational conditions. The loads used for the FEA included a force of 67,000 lb to represent the maximum sea level thrust ad the exit of the nozzle and the force from the weight of the engine and nacelle.
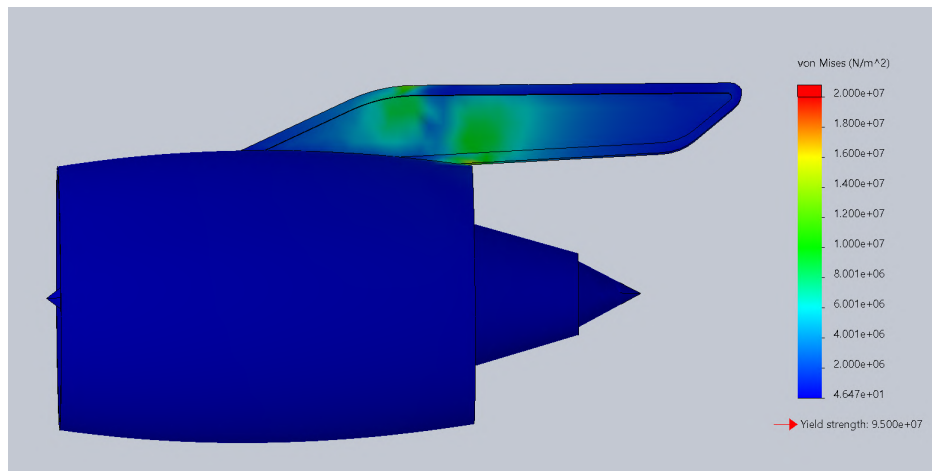
Fig. 67   Engine Mount FEA Results

Valkyrie uses a wet wing for a lighter resulting wing structure. Lightening holes, vent holes, and mouse holes, which are sized using FEM analysis, are put in the ribs to save weight and allow fuel to easily flow within the wing box. Figure 68 below details the FEA results used to size the cutouts, showing a pressure load of 15 psi on the surfaces where the wing skin mounts, and fixtures at the spar cutouts. It should be noted that the section of the rib behind the aft spar will be cut out for all but eight of the ribs to allow space for the flaps and associated subsystems.
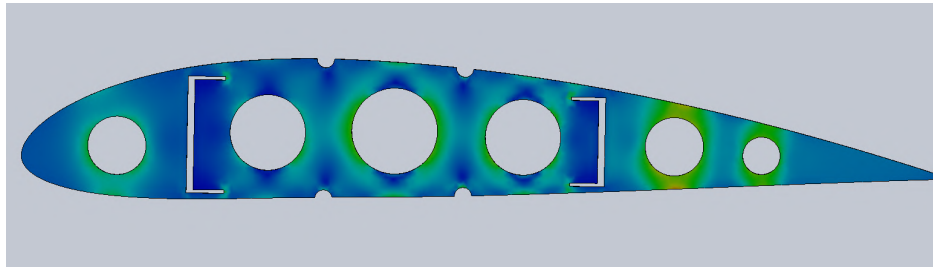
Fig. 68   Rib FEA Validation

Skin thickness was sized using the methods outlined in Niu[27]. The values for the different components are outlined in Table 33.

Table 33   Skin Thicknesses

Component	Thickness (in)
Pressurized Nose	0.090
Wings	0.083
Tail	0.083
Fuselage	0.060

A trade study was conducted to determine the style of stringers necessary. Data for the selection was obtained in Niu[27]. The important criteria to consider are how easy it is inspect the stringer for corrosion, how structurally efficient the stringer is, how many fasteners can be placed, and the weight of the stringer, as shown in Table 34.

Table 34   Stringer Style Trade Study

Criteria	Weight	Scale	J-style	Z-style	Y-style	I-style	Hat-style
Corrosion Inspectability	0.5	5 = Highest Inspectability	5	5	1	5	1
Structural Efficiency	1.0	5 = Highest Structural Efficiency	3	4	5	3	4
Fastener Method	0.25	5 = Highest Number of Fasteners	4	3	4	3	4
Material Weight	0.5	5 = Lowest Weight	3	5	3	4	1
Total			**8**	**9.75**	**8**	**8.25**	**6**

Based on this trade study, the z-style stringer with a spacing of 12 in had the highest total, therefore it was selected. These stringers will be riveted to the skin and follow the splice style assembly as outlined in Niu[27].

Depicted in Figure 69 is a simplified depiction of the structural layout of the fuselage, wings, and tail for the proposed aircraft.
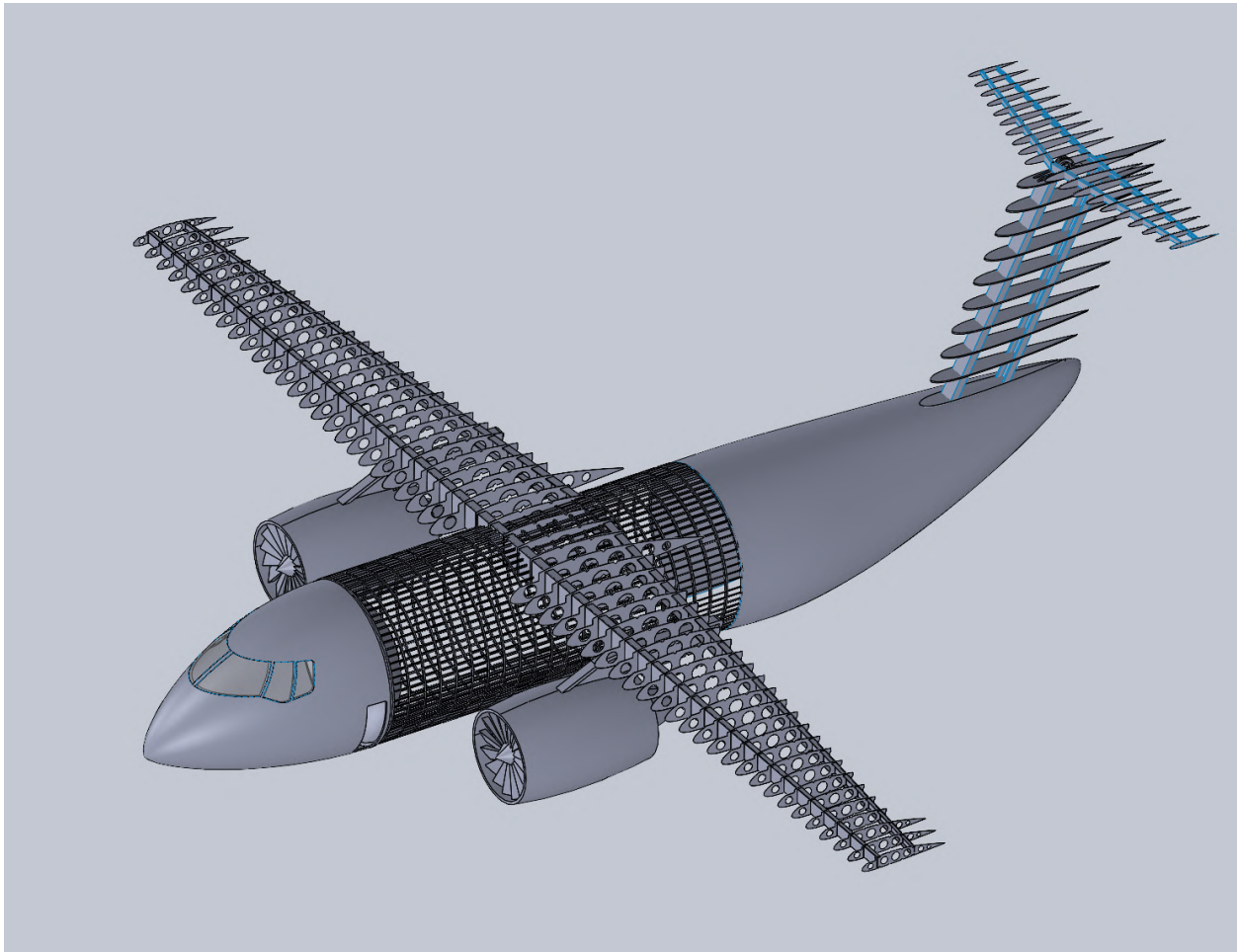
Fig. 69   Simplified Structural Layout

The SOLIDWORKS FEA solver was used to simulate the lifting load of the wing in level flight. By applying the load distribution on the the selected material and geometry properties, FEA simulated and derived the load and the displacement as shown in Figure 70 and Figure 71.
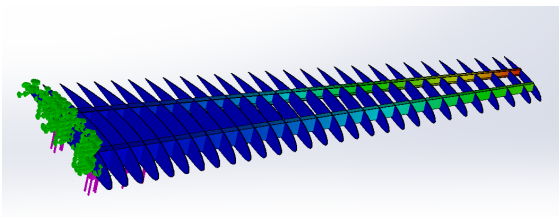
Fig. 71   Load FEA

Fig. 70   Displacement FEA
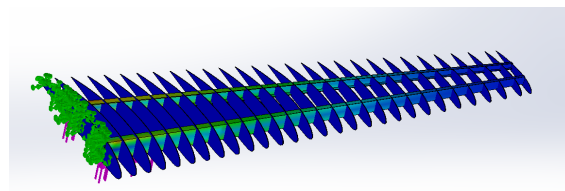
D. Landing Gear

1. Overview

The landing gear for the proposed aircraft will be a tricycle layout in a similar configuration to the Kawasaki C-2 and Dornier 238. This setup is used almost exclusively for this class of aircraft, as it has stable payload loading, taxiing, and takeoff characteristics. As described in Raymer §11.2[8], for an aircraft with a MTOW between 200,000 and 400,000 lb, a four-wheeled bogey is employed for the main gear. At a design MTOW near 200,000 lb, it was decided to use the four wheeled bogey as opposed to a two wheeled bogey. This is to better distribute the weight on rough fields and have greater redundancy in the event of a blowout. The landing gear can accomodate landing at MTOW to alleviate concerns that arise from the exclusion of a fuel jettison system. While the payload can be jettisoned in an emergency, this system could fail in an event where emergency landing at MLW is required. Both of the seed aircraft use a standard retractable nose wheel and sponsons on each side of the fuselage for the retractable main gear. It was determined that due to the speed of the aircraft at cruise, retractable landing gear was necessary to improve performance. A trade study was conducted to determine the optimal retraction position, summarized in Table 35.

Table 35   Sponson vs. Wing Retraction Trade Study

Criteria	Weight	Scale	Sponson Retraction	Wing Retraction
Cost	0.25	5 = Lowest Cost	3	4
Drag	0.5	5 = Lowest Drag	1	5
Structural Load	1.0	5 = Lowest Load	5	2
Maintenance	0.5	5 = Lowest Maintenance	4	3
Complexity	0.75	5 = Lowest Complexity	4	1
Weight	0.5	5 = Lowest Weight	3	2
Total			**12.75**	**8.75**

Although these sponsons increase the drag on the fuselage during flight, the larger footprint on the ground results in a much more stable aircraft which is necessary for the loading of fire retardant and potential rough field operations. The choice to use external sponsons also allows for greater interior space in the fuselage for the retardant tanks or cargo and associated systems. Both the nose and main gear are supported by Oleo struts to provide smoother landings and allow for the ability to operate on rougher, unprepared airstrips[8]. Although this is not a requirement, the team deems it a necessity due to the remote locations that fires can spread.

2. Components

Nitrogen filled tires will be used to support the higher load of the aircraft. Using the preliminary statistical sizing process described in Raymer it was determined that the diameter and width of the nose tires will be 38 in and 11 in, respectively. A recommended 30% increase for rough field landing results in tires with a width of 49 in and a diamter of 16 in for the main tires. The maximum static load equations in Raymer are also used in the selection of tires. Table 36 details the specifications of the chosen tires.[8]

Table 36   Tire Selection

Tire Manufacturer	Tire Part Identification	Location	Quantity	Max Load Rating
Dunlop	DR19926T	Nose	2	16,100 lb
Dunlop	DR22728T	Main	8	51,900 lb

As recommended by Raymer table 11.3[8], the tires will be inflated between 45-70 psi for rough runways. Raymer Eq. (11.1) - Eq. (11.4)[8] are used to place the gear in a manner such that the nose gear will support 10% of the static load and the main gear will support the remaining 90% to allow for optimal weight distribution and to ensure the nose wheel is controllable. A trade study was conducted to determine the appropriate materials for the landing gear components. The material choice for the landing gear beam is AA7175, chosen for its high tensile strength. The rest of the gear will be constructed from Ti 6Al-4V, a lightweight and high strength titanium alloy. The aircraft will use carbon brakes, which are significantly lighter, last longer, and have greater energy absorption compared to traditional steel brakes[29]. These carbon brakes will have a deceleration factor of 0.5g[30] and an overall braking coefficient of 0.3 to ensure the aircraft can stop within the imposed LFL. FEA was run on the landing gear with a load factor of 4.5. Figure 72 depicts the load paths for the main landing gear bogey and nose gear.
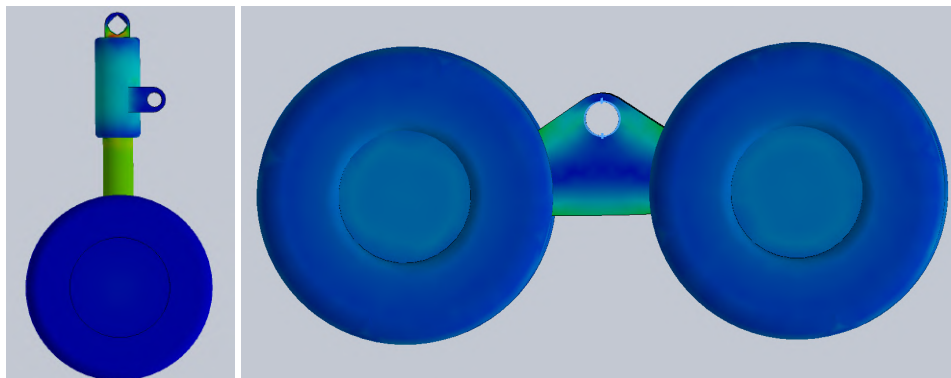
Fig. 72   Landing Gear FEA

3. Retraction

The nose gear will retract in the direction of flight, allowing for the airspeed to assist in blowing the gear down in the event of hydraulic failure. As opposed to rotating in or folding sideways, the main gear will retract forward in relation to the direction of flight which will allow the emergency pneumatic deployment system to be less complex and lightweight. This emergency landing gear deployment system was added to ensure compliance with §25.729(a) of 14 CFR Part 25, which requires an emergency landing gear deployment system. This will also assist in preventing the gear from shearing during landing. A drag link geometry will be used to retract the main gear, as this system allows for a larger distance between the extended and retracted position and results in less space needed within the landing gear bay as the gear folds as it rotates up as shown in Figure 73.
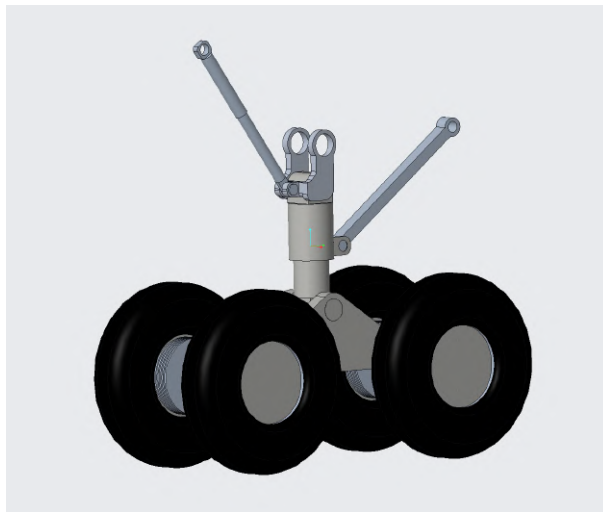
Fig. 73   Main Gear Drag link Geometry

The industry standard electric powered hydraulic cylinders will be used to power both the retraction system and the landing gear doors. Depicted in Figure 74 is the landing gear retraction sequence.
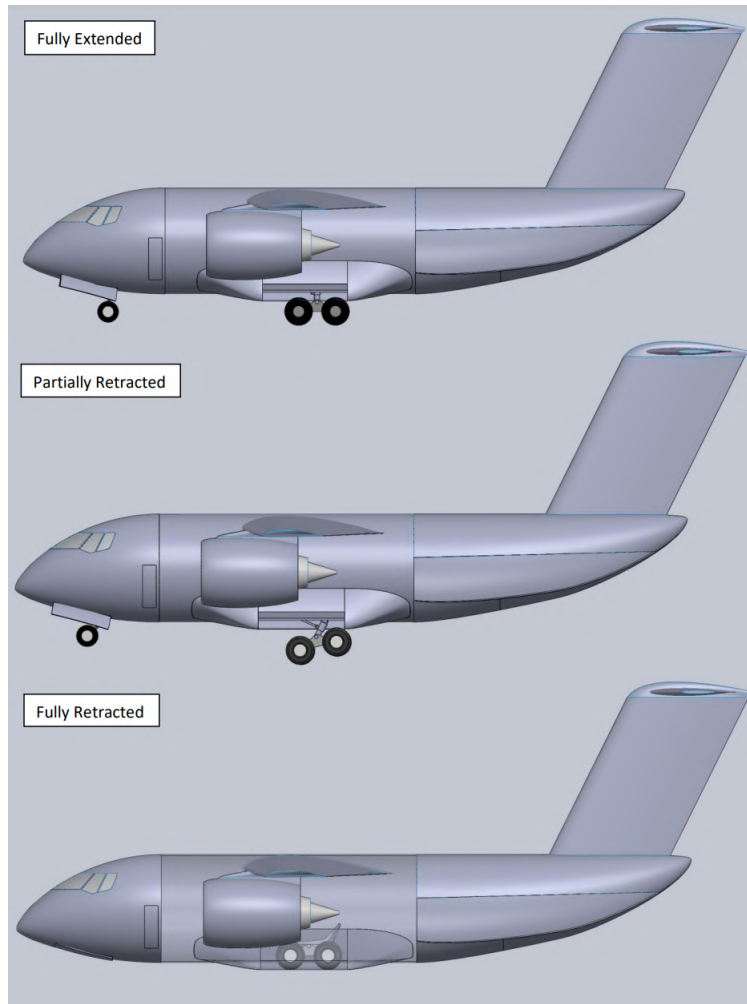
Fig. 74   Landing Gear Retraction Sequence

4. *Landing Gear Angles*

Figure 75 and Figure 76 depicts the longitudinal tip over and tail strike angles of the aircraft in both the compressed and uncompressed states as well as the overturn angle. Compressed values for the Oleo shocks were determined using methods outlined in Raymer[8].
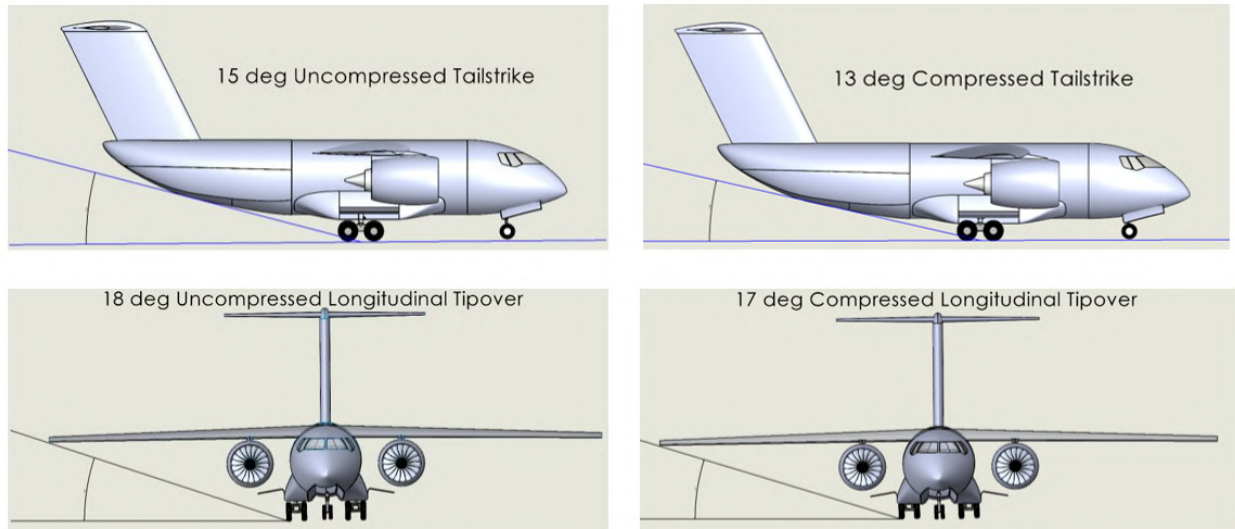
Fig. 75   Landing Gear Angles
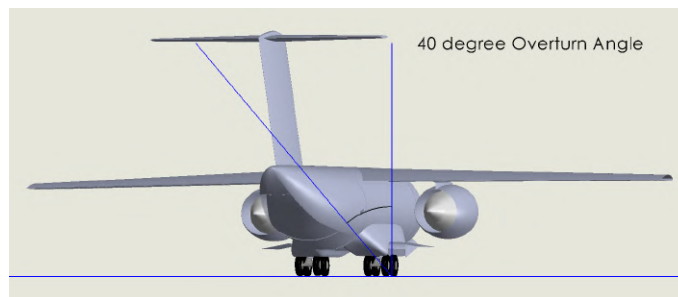
Fig. 76   Overturn Angle

XI. Systems

A. Subsystems

1. Flight Controls

To ensure pilot concentration during payload drop, the flight controls are designed to minimize work loads on the pilots. The fly-by-wire system interprets control inputs from the yoke or flight computer and deflects the ailerons, elevators, and rudder via hydraulics. The yokes and rudder pedals for both pilots have shared feedback, meaning pilots can physically observe the inputs of the other.

Control surface actuation systems depend on a central hydraulic reservoir to regulate internal control line pressure through a pump system for actuation. The leading and trailing edge flap system is also controlled by this system, but separate in function as the flaps are not generally used for course alteration. The outlined means of control for hydraulic systems is in compliance with hydraulic control by flight crew requirements outlined in 14 CFR Part 25 §25.1435.

The aircraft will be fitted with a Collins Aerospace FCS-7000 flight control system allowing for autonomous capabilities during some mission segments. This system will allow for autopilot to be used in periods where the pilots can take a less involved approach to flying, letting the on board computer system handle the course alterations. This satisfies the RFP requirement of flight with an autopilot being a possibility for the proposed system, while still allowing the pilot to disengage the autopilot at any point at which it becomes necessary. This requirement is stipulated in §25.1329(a), (b), (j), and (i). Additionally, the FCS-7000 is already known to be certifiable by the FAA. This system is robust and capable of handling harsh environments to meet the demands of a firefighting mission. It is currently is use on the KC-135, showing this system already has proven operational capabilities. The dual computer system and third monitoring processor to control the autopilot prevents flight control anomalies. It is also designed to operate over a wide range of missions that include airdrops, which can be utilized for added retardant drop capabilities. The FCS-7000 system is capable of aiding in navigation in any environment, with a proven record on current aircraft operated globally.

2. Engine Controls

Throttle controls will be electrically driven based on the movement of the two throttle levers, each lever controlling the power demanded from each of the two engines based on the rotational position. The fuel flow and other parameters that dictate the operating condition of the engines are determined by the Full Authority Digital Electronic Control (FADEC) system. This control system allows for optimal flight parameters to be set for the Engine Control Unit (ECU) depending on the demands input by the pilots, which can elongate the life of the engines and improve efficiency at every point within the mission. Manual override is an option in the case of a failure to give pilots the ability to create a less optimal operating condition for the engines, which may be needed in certain cases within specific missions as is required by 14 CFR Part 25 §25.1329(l).

3. Fuel System

To hold fuel on Valkyrie, the wing's skin, rib, and spar structure will be used as a tank exterior through a wet wing construction. The ribs running normal to the leading-edge along the span of the wing are being used as tank walls which split the tanks into section. The main center tank is housed in the top of the fuselage within the wing structure that runs through the inside of the cylindrical section of the fuselage. Two secondary tanks will be fixed near the root of the wing, outside of the fuselage with direct fuel feeds to the engine as this will allow for minimal piping from the center tank. These feed tanks will be accompanied by secondary tanks with venting at the end to allow for ideal pressure to be maintained with the entire tank system. These outermost tanks will act, in part, as reserve tanks to allow for unexpected flight time. The whole tank system will have fuel feed valves between each of the tank sections to allow for fuel to be pumped from one tank to another for ideal weight and fuel distribution. The fuel tank system schematic of Valkyrie is shown below in Figure 77 with the main tanks highlighted in yellow, feed tanks in blue, outer partial reserve and secondary tanks in red.
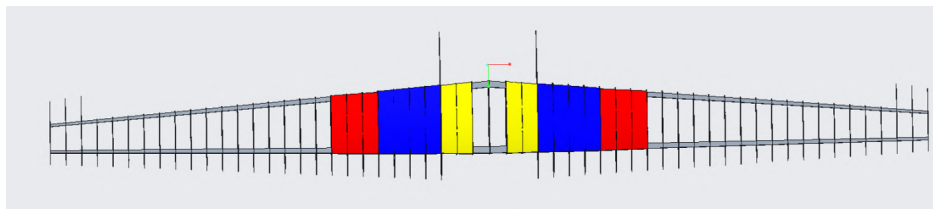
Fig. 77   Schematic of Fuel Tank Placement in the Wing

4. Hydraulics System

Three individual hydraulic lines drive the control surfaces, flaps actuation, and landing gear deployment. At least two lines power each control surface, with triple redundancy for the rudder, due to its importance in an OEI condition. Hydraulic pressure is supplied by two engine driven pumps with a backup electric motor pump. To keep the hydraulic fluid clean and consistent, the hydraulic system is fitted with filters on the supply and return lines. This system will also incorporate integrated checking systems, such as relief valves to make sure the hydraulic lines do not become over pressurized, which can lead to catastrophic failure in certain, demanding circumstances. Should the hydraulic line that powers all control surfaces be severed, plug valves will ensure that the hydraulic fluid does not leak out. These can be seen in Figure 78.
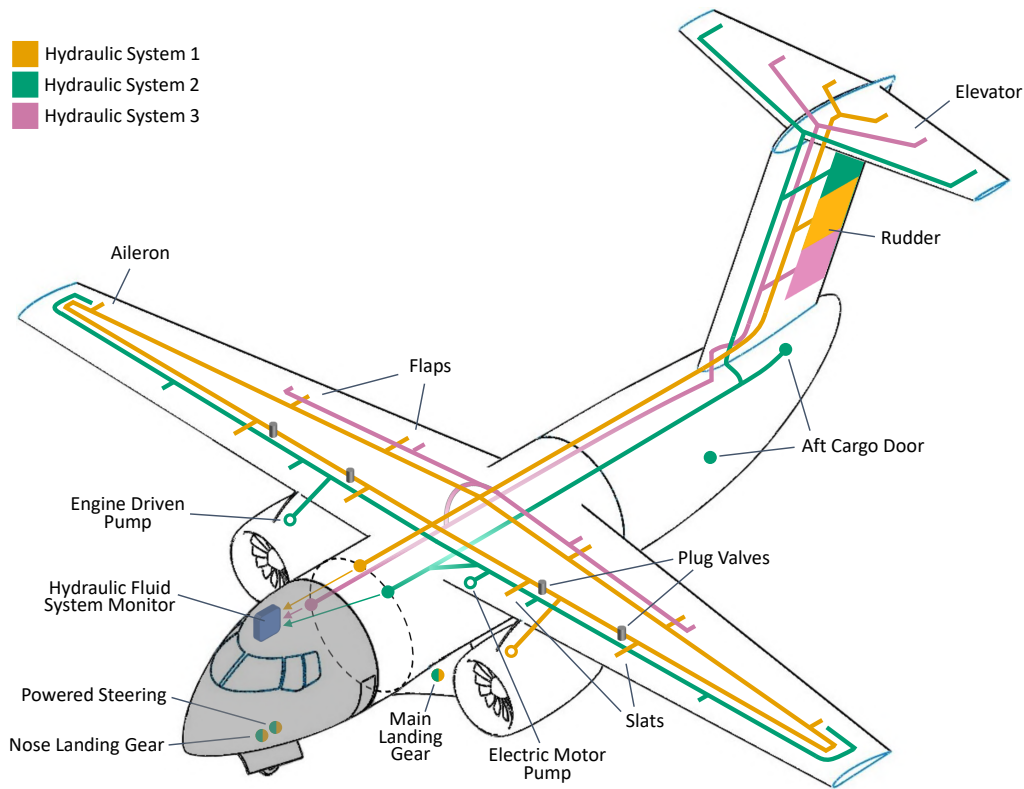
Fig. 78 Hydraulic System Diagram

5. Electric System

To provide the power needed for various electrical systems, Valkyrie is fitted with redundant energy generation systems. The main energy generation comes from the engines themselves, powering the various flight deck systems. The electric system regulates the hydraulic, engine control, and flight control systems, which are fed by this main electrical power supply. The spatial awareness systems, like the weather radar and aircraft tracking system, will also be powered by this main power feed. These systems include a RTA-4100 MutiScan weather radar manufactured by Collins Aerospace to accurately display oncoming weather patterns to the pilots.

To start the plane, initial electrical power is provided by the on board Auxiliary Power Unit (APU), which acts as a smaller turbine engine to provide energy when the engines have been turned off. Valkyrie employs a traditional centralized method for power distribution where the APU and engine generators feed into a common electronics bay that distributes the power to the on-board electrics. This system is diagrammed in Figure 79.
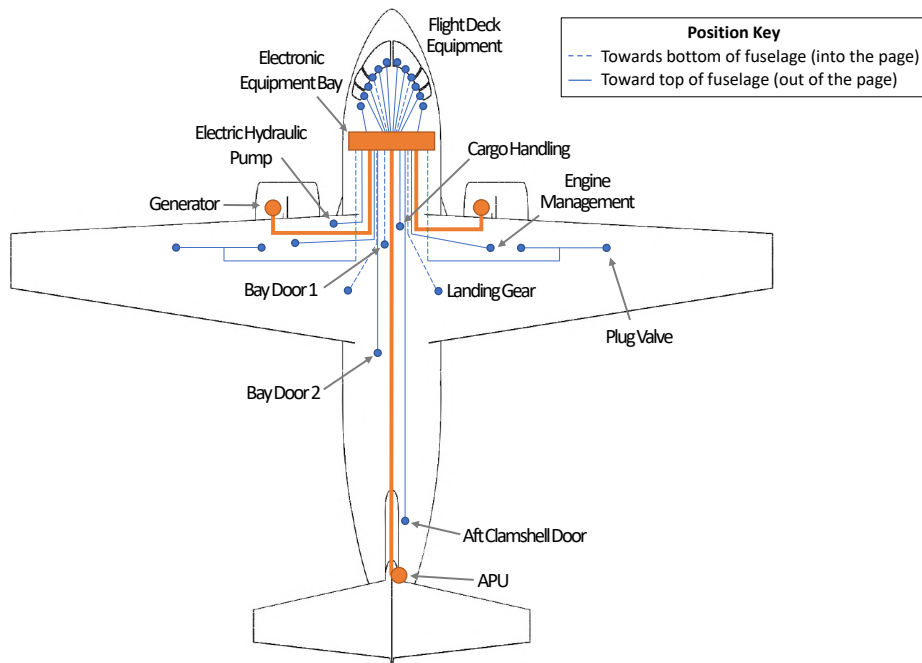
Fig. 79   Electrical systems schematic

6. Pneumatic System

Valkyrie's onboard pneumatic systems consist of pressurized air feed from engine bleed off supply for the pressurized flight deck. Low pressure bleed air is bled off of the final stage of the booster and high pressure bleed air is bled off of the third stage of the high-pressure compressor as can be seen in Figure 80.This pressurized air bleed off is also used for wing deicing in keeping with the flight into known icing capability required by the RFP, and are certifiable under 14 CFR Appendix O to Part 25(a). Along with this environmental control air feed, there is a closed-loop pressurized air tank system used for backup deployment of the landing gear.

73

7. Environmental Control System

Since Valkyrie does not carry passengers in the main hold of the fuselage, to reduce weight and internal structure needed, only the flight deck section is pressurized. A climate control system with air conditioning, heating, and a HEPA filter ensures that the flight deck will not become an unworkable setting. The pressurization is achieved using bleed air from the engine low-pressure and high-pressure compressor stages. These air are first cooled through a precooler, which is an open loop heat exchanger using fan air as the cold fluid that exhausts to atmosphere. The output air is further cooled through air conditioning packs before passing through a HEPA filter and entering the cabin. The pressurization schematic of Valkyrie is shown below in Figure 80. Additionally, per CFR 14 Part 25 §25.1447, supplemental oxygen is stored in the flight deck in the event of loss of pressure.
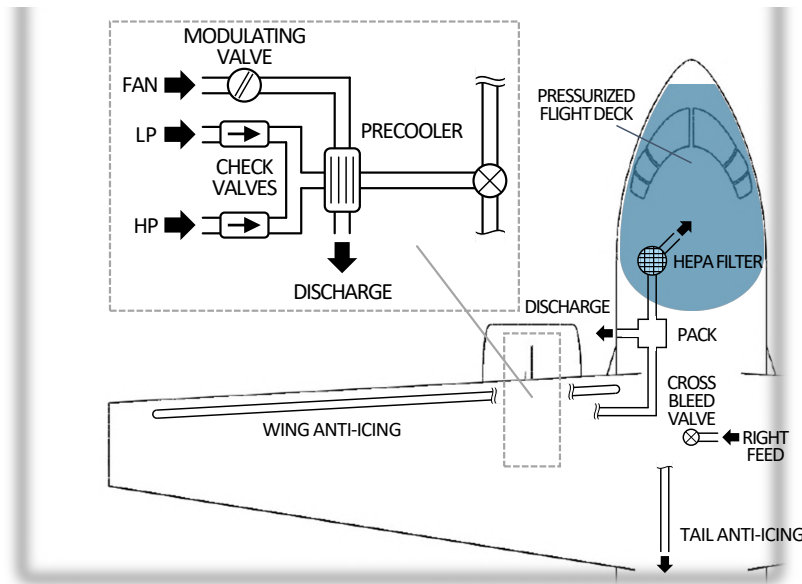
Fig. 80　Schematic of Pneumatic and Environmental Systems

8. Emergency System

In the case of flight control failure, there will be redundancy built into this plane's hydraulic systems with backup pumps. In the case of a that the landing gear is unable to be deployed due to primary hydraulic system failure, a backup compressed air system will be available to the pilots to fire the landing gear into the down and locked position. In another case, if the hydraulics system fails, a secondary set of lines and redundant pump will be included to allow for continued flight control, even if the primary system fails.

Targeting a rotor burst case, electrical and hydraulic routing have redundancy built-in through top and bottom mounting as show in Figure 81. In this case, if a rotor burst were to occur, the change of total systems failure would be within 5%. This redundancy is implemented to ensure Valkyrie is certifiable under 14 CFR Part 25 §25.1461. In the event of an unlikely catastrophe, a black box data recording system is fitted.
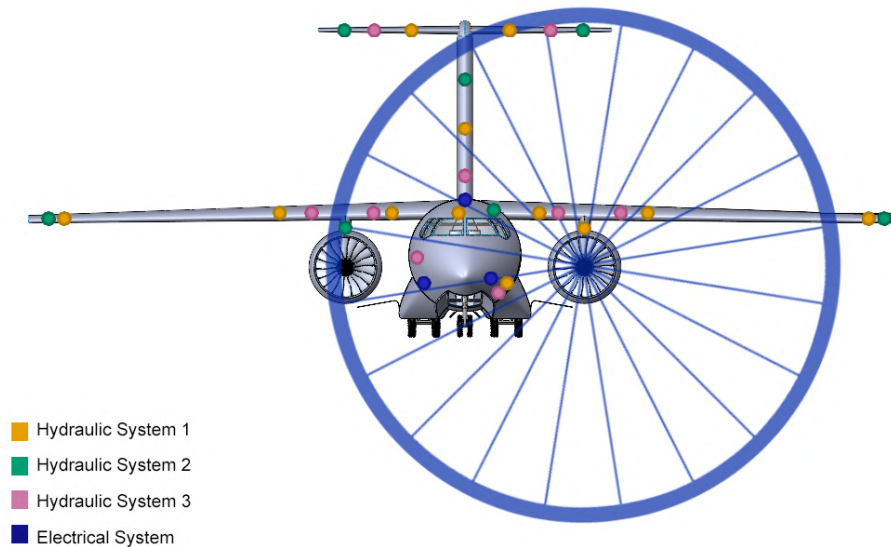
Fig. 81   Rotor Burst Considerations for Hydraulic Lines

B. Avionics

The RFP requires VFR and IFR capable flight with an autopilot. The specific avionics were chosen in compliance to this and with the philosophy of rugged dependability given the harsh operating environment. The team has opted to not tackle fully autonomous operations due to its infeasibility in dynamic environments such as aerial firefighting given the current state of technology. The limitations to full autonomy are largely to do with software. The state-of-the-art in sensor technology can provide accurate measurements of the environment, but environmental factors can cause discontinuous data streams and misinterpreted state estimates. An example is if the aircraft were flying in a mountainous region where GPS communication can be severed. Without a means to get absolute positional data, navigation would have to rely solely on relative measurements (i.e. using an Inertial Navigation System (INS)). Issues from inconsistent streams of GPS data can be somewhat alleviated with sophisticated filtering algorithms like the Kalman or Madgwick filters, although pure inertial navigation remains a difficult and active area of research. Even years down the line, the risk of an unmanned hull loss may still likely be high enough to where full aerial firefighting autonomy is infeasible. However, Valkyrie has been designed as a fully autonomous ready aircraft, meaning full autonomy is possible using only its current hardware. That is, Valkyrie is only software limited. To accomplish this, Valkyrie is equipped with sensors and systems supporting satellite, inertial, and terrain based navigation and computer vision. At present, partial autonomy is retained in the form of an autopilot as per the RFP.

Table 37   Avionics

System	Manufacturer	Product	Details
Flight Controls	Collins Aerospace	FCS-7000	Autopilot FBW ILS No cooling air required Dissimilar processors in each computer
APU	Honeywell	HGT400	60 kVA output Fireproof mounts
Cargo Handling	Collins Aerospace	ACLADS	Loadmaster station Electronic cargo handling Airdrop
Engine Management	BAE Systems	FADEC 3	Supports GEnx-2B engine model
Air Data	Collins Aerospace	ADS-3000	Internal Standard Atmosphere calibration Reduced Vertical Separation compliant
Navigation	L3Harris	TACAN+	Geographical navigation
	Honeywell	H-764	Embedded GPS/INS
Safety	L3Harris	TCAS 3000SP	Traffic collision avoidance
		TAWS	Controlled flight into terrain prevention
Imaging	Collins Aerospace	MS-110	Multiple visible/IR imaging bands
Weather Radar	Collins Aerospace	RTA-4100 MultiScan	Accurate weather and turbulence hazards
Flight Data Recording	L3Harris	FA2300 MADRAS	Up to 2 hrs of audio recording Records at least 25 hrs of flight data

Table 37 details the avionics equipped on Valkyrie. The FCS-7000 was the ideal flight control system to tackle aerial firefighting. Much of the selection rationale was explained in Section XI.A.1, but additionally, it accommodates for a wide range of digital sensors (including the selected EGI) and has built-in room for upgradability that will support software enabling of full autonomous operations in the future. The Honeywell APU was selected based on its power requirements. Historical trends between APU power and aircraft weight project 56.4 kVA for the APU, which was most closely provided by the HGT400. The critical navigation components were chosen to provide absolute, reference, and inertial positioning. Because inertial navigation is unstable with time, absolute positioning is required to calibrate the aircraft's position periodically. Especially in low visibility conditions, proximity-based navigation can be useful to navigate around terrain. Building on the systems that use relative proximity, safety measures in the form of TAWS and TCAS are equipped on Valkyrie.

XII. Payload, Drop, and Refill

A. Design Process

Valkyrie is a purpose-built firefighting aircraft, thus, the payload drop system is a very important part of its operation. The goal of a firefighting aircraft is to be able to drop retardant around a fire so as to slow its growth. Table 38 summarizes the benefits and drawbacks of both custom and pre-built drop systems.

Table 38   Existing vs. Novel System Trade Study

Parameter	Weight	Scale	Novel System	Existing System
Cost	0.5	5 = Lowest cost	1	4
Certification	0.5	5 = Easiest to certify	2	5
Customization	0.5	5 = Easiest to customize	5	3
Reliability	0.5	5 = Highest degree of proven reliability	2	5
Repair & Maintenance	0.5	5 = Easiest to repair and maintain	2	5
Total			**6**	**11**

The retardant system on Valkyrie must be certified as required by the United States Department of Agriculture (USDA)[31]. Since there is no cost requirement the difference in cost between a designed and existing system is not a driving factor for Valkyrie. For a designed system the performance may not be known until the aircraft is ready to fly. It is possible to test the system in another aircraft prior to using it in Valkyrie but this will raise the cost. Overall, choosing an existing system is more beneficial for performance, repair and maintenance, certification, and cost making it a better choice than designing a system.

When using an existing system it is important to conduct a similarity analysis. Two retardant systems were considered: RADS and MAFFS. Other systems, such as the Boeing 747 Supertanker's drop system and the DC-10's drop system are similar to the MAFFS (Supertanker) or are modifications that don't optimize the overall performance of the aircraft (DC-10 belly-mounted tank).

B. Requirements and Existing Systems

The latest RADS and MAFFS systems are compared to the RFP requirements in Table 39.

Table 39   Requirements, RADS-XXL and MAFFS II Comparison

Parameter	Requirements	RADS-XXL	MAFFS II
Retardant Capacity (gal)	8,000 gal	4,000 per tank	3,600 gal per tank
Multi-drop Capable, minimum 2,000 gal per drop	Minimum 2,000 gal per drop	Multi-drop capable	Multi-drop capable
Retardant Reload Rate, >= 500 gal/min	>= 500 gal/min	>= 500 gal/min	>= 500 gal/min
Retardant Density, >=9 lbs/gal	>= 9lbs/gal	Any USDA approved retardant	Any USDA approved retardant
Compressed Air	-	No	Yes
Emergency Drop System	-	Yes	Yes
Maximum Flow Rate (gal/s)	-	1,600	700
System Weight (lb)	-	2,300	15,000
Purpose	-	Firefighting	Firefighting, Chemical/Oil Spills, Fumigation, Agricultural Applications

To meet the total capacity, two RADS-XXL tanks or MAFFS II systems can be used with the latter resulting in a slightly lower total capacity. RADS-XXL is much lighter than the MAFFS II. This is because the MAFFS II is not purpose-built for firefighting and carries extra weight for its other capabilities. The RADS-XXL offers a much higher maximum flow rate without carrying any compressed air. Overall, the RADS outperforms the MAFFS II whilst also being a lighter system. The RADS has been used on multiple C-130s by CAL Fire and has been approved by the FAA and Transport Canada. The RADS-XXL system is depicted in 82[10].

Fig. 82   RADS-XXL Tank

C. Modifications

The use of a two RADS-XXL tanks necessitates certain modifications. The tanks are placed two feet apart, as shown in Figure 18. Between the two tanks will be a passive pipe system consisting of a lower pipe and an upper pipe, which will allow retardant to flow between the two tanks. This system protects against the failure of one tank, as retardant can still be used through the other tank. The pipe system also keeps both tanks at the same level meaning the CG will not be affected by dropping retardant. Since there is no pressurized air, the pipe system will only need to be able to withstand the pressure from the retardant in the tanks. Modifying the tanks will be a joint collaboration between the Coulson Aviation Group and the team. The Coulson Aviation Group has modified and fitted multiple RADS-XXL systems so the team has chosen to use Coulson's expertise for any modifications and re-certification.

D. Transportation & Containment

1. Corrosion

Corrosion is a major factor in the design process of the fire retardant system. The pipe system will be made of 6061-T6 Alclad Aluminum[32]. As part of corrosion prevention, frequent maintenance and inspection of the tanks will be required. Fire retardants that are approved by the US Forest Service already contain inhibitor additives, thus protective coating is not required in the tanks[32]. All electrical wires shall be placed such that any risk of them coming into contact with fire retardant is mitigated in compliance with the Electrical Wiring Interconnect System (EWIS) protection requirements given in 14 CFR §25.1721.

2. Sloshing

Sloshing contributes to mechanical stress and changes in CG during flight neither of which are desired. Mathematical analysis shows that the addition of walls from the top of the capsule can mitigate the effect of sloshing[33]. At this point it is unknown whether the RADS XXL has measures to prevent sloshing. Modifications will be made if the RADS does not have a relevant solution.

3. Payload Integrity

Fire retardant approved by the US Forest Service must be recirculated every 24 hours to prevent component settling[34]. The airport base or retardant supplier would be expected to take care of the storage and re-circulation of the retardant. As a result, there is no need for mixing instruments on board.

E. Refill

The fire retardant will arrive from a supplier, such as Perimeter Solutions. At the base there must be a mixing station in which liquid concentrate is mixed with water to produce the mixed retardant. This process may take around 15 minutes so it must be done beforehand. Once the mixed retardant is ready it can be transported to the aircraft.[34]

Electric motors or internal combustion engines will be used to drive the delivery pumps on ground[35]. Gasoline-engine driven pumps will be kept on ground as backup[35]. According to the US Forest Service retardant delivery rate for existing pumps are 500 gal/min[35]. To transfer the retardant into the tank, the aft cargo door will be opened and a hose will connect directly to the forward tanks, this is preferable to underside reloading as the pumps would need to be extremely powerful given the 4,000 gal capacity. The tanks can be loaded simultaneously or in series depending on the availability of pumps and mixing retardant stations.

F. Payload Drop

Onboard the aircraft there will be a drop system operator. The operator communicates with the pilot and the leadplane to conduct the drop. The operator will have an digital interface system to configure and facilitate payload drops via the RADS-XXL constant flow control system. Inside each tank are a number of sensors that relay information to the interface. Both the operator and the pilots have the ability to jettison all the retardant in the case of an emergency. The RADS-XXL tanks are connected via a chute bay doors that open to facilitate the drop.

XIII. Cost Analysis

A. RDTE and Unit Cost

The Development and Procurement Cost of Aircraft (DAPCA-IV) model was used to forecast the RDTE and flyaway costs initially[8]. It was then decided to compare the methods outlined in Roskam VIII[36] and Zijp's top down life cycle cost model[37] to obtain the RDTE and flyaway cost. Both methods are more in-depth than the DAPCA-IV cost model and provide a framework for estimating unit and operational costs in addition to RDTE and flyaway, making both a more practical choice for rigorous cost analysis. The unit cost of the Kawasaki C-2 and Embraer C-390, the two seed aircraft, was estimated using the two models and compared to known values. The results of this comparison are shown below in Table 40.

Table 40   Cost Forecasting Model Validation

Aircraft	Actual Unit Cost	Roskam Model Unit Cost	Error	Zijp Model Unit Cost	Error
Kawasaki C-2	$176M[38]	$193M	9.66%	$166M	5.68%
Embraer KC-390	$50M[39]	$55.1M	10.1%	$52.2M	4.44%

While both methods predict the cost of existing aircraft to within a satisfactory margin of error, it is apparent that Zijp's model is superior to Roskam VIII for this application. This could be due to the fact that the Zijp model was developed in 2012 while the Roskam VIII model was developed in 1990. Although inflation has been factored into the costs in the above table, and indeed into every cost presented using the US Consumer Price Index (CPI), it is possible that the newer model takes into account technological improvements impacting cost beyond inflation.

The Zijp model was implemented to obtain the RDTE and flyaway cost as a function of engine and avionics, interior, manufacturing, materials, tooling, and quality control costs[37]. Special attention was given to the development of the interior cost, which adapted the Zijp model to estimate the cost associated with the interior of a commercial aircraft to account for the purchase, modification, and installation of the RADS-XXL payload drop system. The cost of engines and avionics in this model accounts for the purchase cost of all engines and avionics packages for the full production run in addition to the cost of engineering and integration. RDTE and flyaway cost was initially calculated for a production run of 50 aircraft over five years. Given the aircraft's potential use in non-firefighting environments, it was decided to use the upper limit of the four to ten aircraft per year production rate outlined in the RFP. The estimated RDTE and flyaway cost for Valkyrie is $8.137B, the breakdown for which is shown below in Figure 83. Assuming a profit margin to the manufacturer of 15%, the unit cost of Valkyrie is $187.2M.

Valkyrie RDTE & Flyaway Cost Breakdown
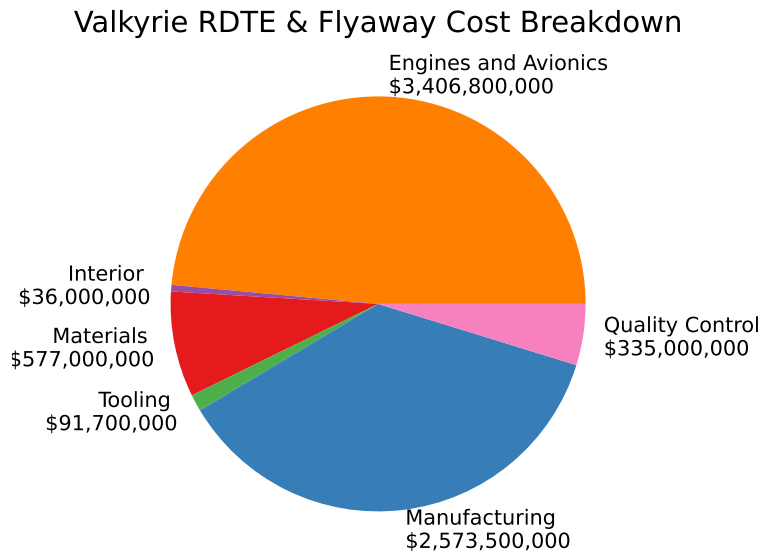
Fig. 83   Breakdown of RDTE and Flyaway cost

B. Operating Costs

The Zijp model was used to determine the operating cost per mission profile, which can then be averaged to obtain a cost per flight hour for Valkyrie. In these calculations, the cost of fire retardant is assumed to be three dollars per gallon, which is accurate for both Fire-Trol and Phos-Chek fire retardant however is far higher than the cost of using water[40]. The operational cost of Valkyrie takes into account fuel and retardant costs, as well as crew, ground, and auxiliary salary, depreciation, the use of a leadplane for firefighting missions, California state landing fees per 1,000 lb of maximum landing weight[41], and California state ramp tower fees. The conceptual breakdown of Valkyrie's operational cost for both firefighting missions can be seen below in Figure 84. As shown in the figure, the fuel cost is the highest cost associated with operation. This figure does not include the cost of retardant as this is a variable cost.
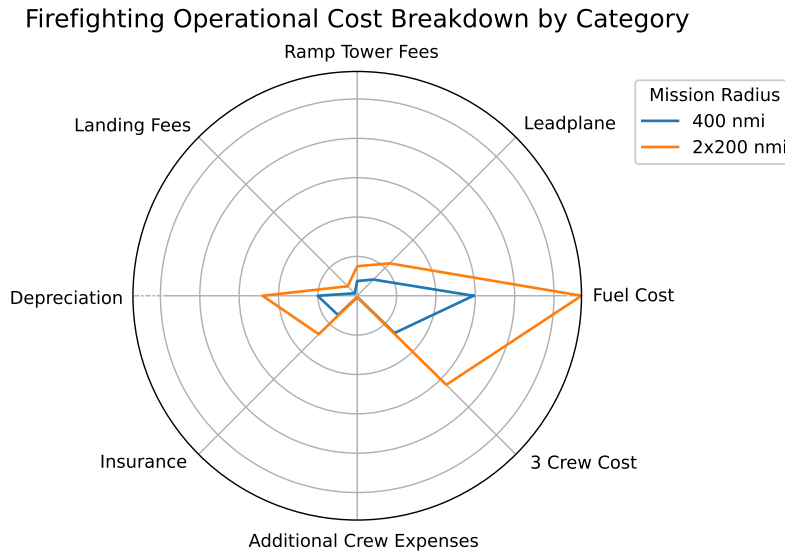
Fig. 84   Breakdown of Operational Cost

Minor differences exist between the calculation of operational cost for firefighting and ferry missions. Notably, the ferry mission operational cost is not dependent on the cost of fire retardant or a lead plane. The cost associated with each mission, as well as the approximate cost per hour and operational cost breakdown of two existing systems as a point of comparison, can be seen in Table 41.

Table 41   Operational Cost Breakdown

Mission Profile	Operating Cost	Operating Cost Less the Cost of Retardant	Operating Cost Less the Cost of Retardant and Fuel	Cost per Hour (neglecting retardant cost)	Cost per Hour (including retardant cost)	Cost per Hour (neglecting retardant and fuel costs)
Ferry & Cargo	$19,700	–	$7,420	$2,580.00	–	$1,000.00
400 nmi Firefighting	$38,250	$14,250	$8,300	$4,600.00	$12,400.00	$2,700.00
2 x 200 nmi Firefighting	$69,770	$30,170	$18,770	$5,500.00	$12,700.00	$3,400.00
Boeing 747 Supertanker Firefighter	$260,100	$204,300	$16,300	–	–	–
DC-10 Firefighter	$155,200	$119,200	$10,700	–	–	–

Assuming Valkyrie operates according to the RFP at 1,200 flight hours per year following the allocation shown in Figure 6, the cost per flight hour associated with each mission profile can be used to calculate the yearly operational cost of Valkyrie. Assuming all training missions and half of all firefighting missions are 400 nmi firefighting missions, the yearly operational cost of Valkyrie neglecting the variable costs of fuel and retardant comes to $2.49M.

C. Operator Profit

Valkyrie is intended to be owned by a private company and leased to firefighting bodies following the model used by existing VLAT companies such as 10Tanker and Global Supertanker. The leasing cost model employed by these companies is shown conceptually for the Boeing 747 Supertanker, as leased by Global Supertanker.

The cost model consists of a reservation fee and flight hour fee, with the cost of fuel and retardant being purchased by the owning company, but being the financial responsibility of the operator. The reservation fee is typically for a period of three days, and in the case of Global Supertanker's lease with CAL FIRE, $175,000. In this same case, the cost per flight hour was $17,500 with a minimum of three flight hours[42]. In order to determine what costs drove these prices, the operational costs associated with the firefighting missions of the DC-10, as operated by 10Tanker, and the Boeing 747 Supertanker, as operated by Global Supertanker were determined as shown in Table 41.

Comparing the operational costs to the reservation and flight hour leasing costs, a profit margin can be determined and used to predict a reasonable lease cost for Valkyrie. By simply comparing the values, the face-value profit margin of Global Supertanker is approximately 580%. This, however, does not account for aircraft ownership as Global Supertanker must also continuously pay back the loan initially taken out in order to purchase the company's fleet of Boeing 747 Supertankers. Maintaining this margin, an appropriate three day reservation cost for Valkyrie would be $85,000 and an appropriate cost per flight hour would be $8,500.

D. Cost Saving Measures

Valkyrie's unit and RDTE costs were calculated assuming a production run of 50 aircraft over five years. This is based on values outlined in the RFP, namely that a realistic production quantity would be four to ten aircraft per year. Due to Valkyrie's ability to double as a cargo carrier, using the upper bound of this limit is justified. Sweeping the number of aircraft produced over five years from 20 to 200, the following trends in RDTE and unit cost are observed.
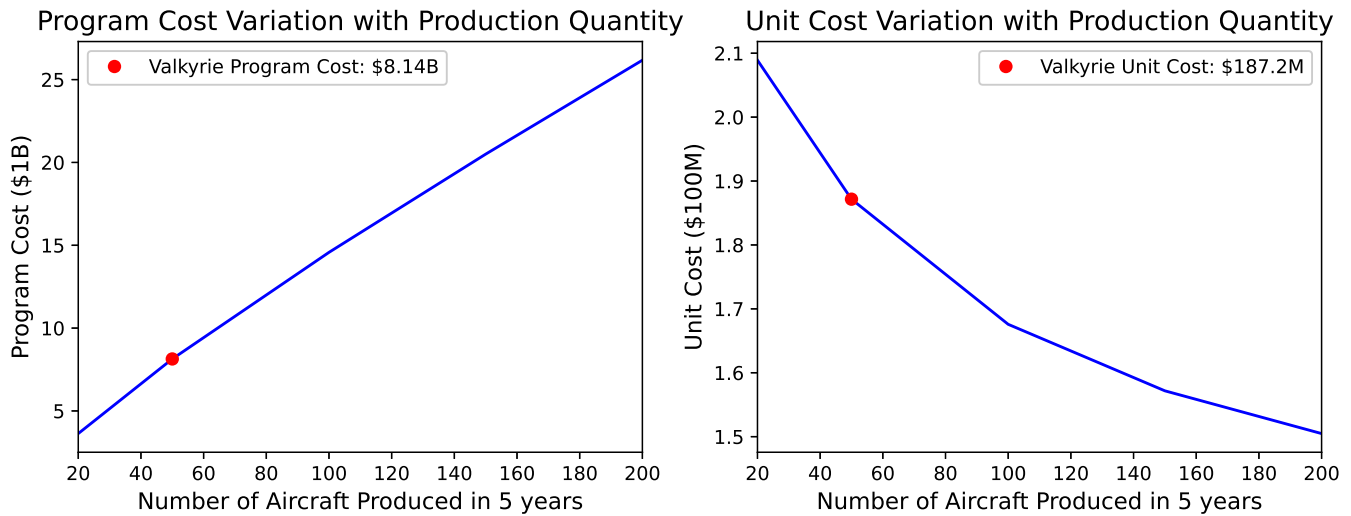
Fig. 85   RDTE and Unit Cost Variation with Production Quantity

Increasing the quantity of aircraft produced in five years linearly increases the RDTE cost, however it causes the unit cost to sharply decrease. From the trends observed in the variation of unit cost with respect to production quantity, it is clear that a slight increase in production quantity significantly decreases the unit cost, making Valkyrie far more financially competitive and justifying the increased initial investment by the company manufacturing the aircraft. Valkyrie was designed to be able to justify such a production increase – the production run of 4-10 aircraft per year is realistic for a purpose built firefighting aircraft, however Valkyrie is highly modular and can operate as a remote-location cargo carrier and could easily be provisioned to be a conventional tanker aircraft.

The effective cost of Valkyrie can be further decreased by taking measures to decrease the operational cost of the aircraft. As previously discussed, the VLAT owning company that leases out Valkyrie takes out a loan for the initial purchase and uses profit generated by Valkyrie to pay for the aircraft. Maintaining the lease costs outlined in the previous section, decreasing the operational cost of the aircraft would allow the owning company to make higher profits while maintaining a competitive market position, thus enabling the company to pay back the initial loan faster and make more overall profit. Valkyrie has been designed to allow for the decrease in operational costs in two ways.

Firstly, while Valkyrie is not fully autonomous at this juncture, the Collins Aerospace FCS-7000 avionics package was selected in part due to the fact that this capability could be achieved in the future with a relatively inexpensive software upgrade. Specifically, the ability to perform ferry and cargo missions autonomously would likely be realized by Valkyrie's 2030 EIS date, if not shortly thereafter. This significantly reduces the personnel cost associated with Valkyrie's operations. Additionally, the operational cost could be further decreased in the event that firefighting missions can be performed autonomously as this would decrease the cost of insurance associated with operating Valkyrie.

Another means of decreasing the operational cost of Valkyrie is through the use of Sustainable Aviation Fuel (SAF). SAF is a drop in fuel, meaning it burns the same as conventional Jet A-1 fuel in an engine, however it is more responsibly sourced. While the cost of SAF is comparable to that of Jet A-1, companies operating aircraft using SAF are eligible for a credit between \$1.25 and \$1.75 per gallon of SAF used, depending on the level of greenhouse gas reduction associated with the fuel as part of the Sustainable Aviation Fuel Act[43].

E. Model Uncertainties

The top down Zijp model for aircraft cost estimation was used for Valkyrie's RDTE and flyaway, unit, and operational cost. This method was selected due to a demonstrated higher level of accuracy than the Roskam model for aircraft similar to Valkyrie. While more accurate, the Zijp model consistently had a 5% error associated with it, adding some uncertainty to the model. Additionally, the Zijp model, as well as Roskam and DAPCA-IV, rely on the use of factors to quantify costs associated with a more sophisticated design. The Zijp model, utilizes three factors to determine the level of technological complexity present in the design process: the use of CAD in the aircraft design, general design difficulty, and stealth. The values of these factors were determined through similarity analysis and Valkyrie was priced using the values corresponding to comparable aircraft. This introduces another level of uncertainty to the model.

XIV. Repair and Maintenance

Valkyrie will be flown in a challenging environment. The firefighting mission cycles the aircraft repeatably, especially when performing a multiple-drop mission. Additionally, the forward operating airports whence the proposed aircraft shall operate have minimal repair capabilities.

Valkyrie is expected to be privately owned and leased to operators, therefore there will not be a six month off-season during which maintenance would be possible. Instead maintenance will need to be performed throughout operation. This means that the aircraft will need to be easily accessible to maintenance crews and modularly designed, allowing for quick and easy replacement of parts which have been degraded over multiple missions. When operated in a fleet, if one aircraft is out of service due to scheduled maintenance another aircraft will be able to meet the demand.

Aircraft maintenance is broken up into a series of checks: A Checks, B Checks, C Checks, and D Checks. A Checks are one step above the pre-flight check that is performed before every flight. A Checks include checking emergency lights, lubricating nose gear retract actuator, and checking parking brake accumulator pressure. B checks are less common in the modern world of aviation, instead airlines typically opt to perform what used to be a B Check during the A Check. B Checks typically happen every six to eight months. During a B Check, the aircraft will be taken to a hanger and will require 180 labor hours. B Checks check for landing gear alignment as well as checking for hydraulic leaks or corrosion. The harsh environment in which Valkyrie operates necessitates B checks being performed every six months rather than being combined with another lettered check. C Checks are the start of the heavy maintenance portion of the

maintenance plan. Performed every two to three years, a C Check requires six-thousand labor hours. During a C Check, the structure will be checked for corrosion and damage, the electric system will be checked, and all fittings and cables will be lubricated. The aircraft is typically out of service for one to two weeks for a C Check. D Checks are a complete and comprehensive inspection of the entire aircraft. The aircraft is typically taken apart and inspected for damage and corrosion. D Checks only happen every six to ten years, but take 40,000 labor hours and close to a million dollars to complete. The maintenance schedule is summarized in Table 42. Providing a maintenance schedule such as that which is summarized below is required under the maintenance instruction part of 14 CFR Appendix H to Part 25(b).

Table 42   Maintenance Schedule

Maintenance Check	Schedule
A Check	Every 500 Flight Hours
B Check	Every Six Months
C Check	Every 4,000 to 6,000 Flight Hours
D Check	Every 24,000 to 40,000 Flight Hours

Valkyrie is capable of carrying repair supplies to assist with fleet up keep. The 20,000 lb cargo mission was designed for this purpose. A summary of the repair and supplies and their respective weights is shown in Table 43. Valkyrie has the capacity for three RADS-XXLs, which allows – when operating in a three aircraft fleet – the ability to designate one aircraft to carry repair and maintenance supplies while the other two aircraft each carry one of the repair aircraft's RADS-XXL.

Table 43   Repair Supplies and Weights

Item	Weight [lb]
Spare Engine	12,400
Spare Tires (2 Nose Gear & Eight Main Gear Tires)	2,123
Spare Hydraulic Fluid (Complete Refill)	66
Spare Engine Oil (Complete Refill)	50
Engine Winch	250
Engine Dolly Cart	1,500
Repair Tools	3,500

XV. Conclusions

The deployment of Valkyrie against the wildfires projected for 2030 is a vital hedge against the increasingly catastrophic impacts of climate change. Valkyrie is designed to not only maximize firefighting capability, but also to minimize environmental impact, all while maintaining relevance across multiple areas of aviation. No two wildfires are the same, which is why Valkyrie maximizes both its flexibility and capability with the inclusion of a highly configurable firefighting system – either a single 400 nmi, 8,000 gal retardant mission or two 200 nmi 6,500 gal retardant missions can be performed on a single refueling, and the RADS-XXL payload system, controlled by a designated drop operator, allows for highly tactical delivery of fire retardant to the affected area. The wildfire crisis is affecting millions today, and projected to impact millions more by Valkyrie's EIS date. This crisis, at its root, is caused by the impacts of climate change, which can be neutralized or reversed if global carbon neutrality is achieved. As such, Valkyrie was designed to minimize any negative environmental impact associated with operation. This is achieved by selecting a highly efficient power plant that is also compatible with the environmentally friendly drop in fuel, SAF. Firefighting is a vital, yet incredibly specialized area of aviation, yet the aircraft developed for these roles are often expected to perform duties outside of their area of expertise. This is why the team developed capabilities which not only make it possible, but incredibly simple for Valkyrie to transport up to 20,000 lb cargo at the 3,000 nmi ferry range. This ability, coupled with Valkyrie's 5,000 rough field BFL, allows the aircraft to fill another vital niche by serving as a cargo carrier capable of landing in extremely remote locations, or transporting specialized repair and maintenance equipment to remote bases of operation. By prioritizing these core tenets of Valkyrie's design philosophy, the team was able to design an aircraft capable of combating a range of growing global issues while remaining both financially and ecologically viable.

References

[1] AIAA, "Undergraduate Team Aircraft Design RFP – Responsive Aerial Firefighting Aircraft," `https://www.aiaa.org/get-involved/students-educators/Design-Competitions`, 2021. Accessed: 02-08-2022.

[2] Oregon Department of Forestry, "Aviation Procedures Manual," `https://www.fs.fed.us/r6/fire/pnwcg/aviation/2008/08MasterAPM-Edition.pdf`, 2020. Accessed: 04-28-2022.

[3] Embraer, "C-390 Millennium," `https://defense.embraer.com/global/en/c-390`, 2022. Accessed: 02-08-2022.

[4] Acquisition, T. . L. A., "C-2 Transport Aircraft Reference Guide," `https://www.mod.go.jp/atla/en/policy/pdf/defense_equipment_C-2_reference_guide.pdf`, 2022. Accessed: 02-08-2022.

[5] Boeing, "C-17 Globemaster III," `https://www.boeing.com/defense/c-17-globemaster-iii/`, 2022. Accessed: 03-05-2022.

[6] Airbus Defence and Space, "A400M - Delivery to the Point of Need," `https://web.archive.org/web/20151018162055/http://militaryaircraft-airbusds.com/Aircraft/A400M/A400MSpec.aspx`, 2015. Accessed: 10-18-2015.

[7] Green, W., *Observer's Book Of Aircraft: 1976*, Penguin Putnam, London, 1976.

[8] Raymer, D. P., *Aircraft Design: A Conceptual Approach*, 6th ed., AIAA education series, American Institute of Aeronautics and Astronautics, Incorporated, 2018.

[9] Roskam, J., *Airplane Design Part V: Component Weight Estimation*, DARcorporation, Lawrence, KS, 2018.

[10] Coulson Aviation, "RADS-XXL," `https://www.coulsonaviationusa.com/rads-technology`, 2018. Accessed: 04-26-2022.

[11] FAA, "TCDS NUMBER E00087EN," `https://rgl.faa.gov/Regulatory_and_Guidance_Library/rgMakeModel.nsf/0/74e4c2086661f360862584120046b423/\protect\T1\textdollarFILE/E00087EN_Rev6.pdf`, 2019. Accessed: 03-04-2022.

[12] FAA, "TCDS NUMBER E00090EN," `https://rgl.faa.gov/Regulatory_and_Guidance_Library/rgMakeModel.nsf/0/c2c82eb65c1ce09c8625835900601474/\/E00090EN_Rev_8.pdf`, 2018. Accessed: 03-04-2022.

[13] FAA, "TCDS NUMBER E00088EN," `https://rgl.faa.gov/Regulatory_and_Guidance_Library/rgMakeModel.nsf/0/ae71cf81844093f98625836600766d81/\protect\T1\textdollarFILE/E00088EN_Rev_4.pdf`, 2018. Accessed: 03-04-2022.

[14] FAA, "TCDS NUMBER E00078EN," `http://large.stanford.edu/courses/2016/ph240/ginsberg2/docs/E00078NERev3.pdf`, 2011. Accessed: 03-04-2022.

[15] Meher-Homji, C. B., Chaker, M. A., and Motiwala, H. M., "Gas Turbine Performance Deterioration," *Proceedings of the 30th Turbomachinery Symposium*, Texas A&M University, 2001. URL `https://oaktrust.library.tamu.edu/bitstream/handle/1969.1/163330/t30pg139.pdf`, Accessed: 05-08-2022.

[16] *50 Years of Engine Improvements*, Pacific North West AIAA Symposium, AIAA, Seattle, Washington, 2009.

[17] Elsiver, B., "Data B : Engine Data File : General Electric Engines," `https://booksite.elsevier.com/9780340741528/appendices/data-b/table-2/default.htm`, 2001. Accessed: 02-08-2022.

[18] Kurzke, J., and Halliwell, I., *Propulsion and Power - An Exploration of Gas Turbine Performance Modeling*, 1st ed., Springer, 2018.

[19] Herrmann, S., "Untersuchung des Einflusses der Motorenzahl auf die Wirtschaftlichkeit eines Verkehrsflugzeuges unter Berucksichtigung eines optimalen Bypassverhaltnisses," Ph.D. thesis, TU Berlin, Berlin, 2010.

[20] Howe, D., *Aircraft Conceptual Design Synthesis*, 1st ed., Wiley, 2005.

[21] Abbott, I. H., and Doenhoff, A. E. V., *Theory of Wing Sections*, Dover Publications, 1959.

[22] Goett, H. J., and Bullivant, W. K., "Tests if NACA 0009, 0012, and 0018 Airfoils in the Full-Scale Tunnel," Tech. Rep. NACA-TR-647, National Advisory Committee for Aeronautics, Jan. 1939.

[23] Torenbeek, E., *Synthesis of Subsonic Airplane Design: An Introduction to the Preliminary Design of Subsonic General Aviation and Transport Aircraft, with Emphasis on Layout, Aerodynamic Design, Propulsion and Performance*, 1st ed., Springer, Dordrecht, Kluwer, Boston, 1982.

[24] Etkin, B., and Reid, L. D., *Dynamics of Flight: Stability and Control*, 3rd ed., Wiley, New York, 1996.

[25] Roskam, J., *Airplane Design Part VI: Preliminary Calculation of Aerodynamic Thrust and Power Characteristics*, DARcorporation, Lawrence, KS, 2017.

[26] ESAB, "Understanding the Aluminum Alloy Designation System," `https://www.esabna.com/us/en/education/blog/understanding-the-aluminum-alloy-designation-system.cfm`, 2022. Accessed: 02-08-2022.

[27] Niu, M. C. Y., *Airframe Stress Analysis and Sizing*, 3rd ed., Adaso/Adastra Engineering Center, 2011.

[28] Roskam, J., *Airplane Design Part III: Layout Design of Cockpit, Fuselage, Wing and Empennage: Cutaways and Inboard Profiles*, DARcorporation, Lawrence, KS, 2018.

[29] Allen, T., Miller, T., and Preston, E., "Operational Advantages of Carbon Brakes," *Aero Magazine*, 2009. URL `https://www.boeing.com/commercial/aeromagazine/articles/qtr_03_09/pdfs/AERO_Q309_article05.pdf`, Accessed: 02-08-2022.

[30] Roskam, J., *Airplane Design Part IV: Layout Design of Landing Gear & Systems*, DARcorporation, Lawrence, KS, 2018.

[31] USDA Forest Service, "Standards For Airtanker Operations," `https://www.fs.usda.gov/sites/default/files/2020-08/fs_standards_for_airtanker_operations_-_final_08192020.pdf`, 2020. Accessed: 04-26-2022.

[32] USDA Forest Service, "Guidelines for Preventing Fire Retardant Corrosion," `https://babel.hathitrust.org/cgi/pt?id=umn.31951d03009806e&view=1up&seq=1&skin=2021`, 1986. Accessed: 03-05-2022.

[33] Claire Chasse, M. J., "SLOSHING IN A TANK : DEVELOPMENT OF A WATER BOMBING SYSTEM FOR FIRE-FIGHTING," `https://hmf.enseeiht.fr/travaux/bei/beiep/book/export/html/881`, 2013. Accessed: 03-05-2022.

[34] USDA Forest Service, "FIRE RETARDANT STANDARD MIXING SYSTEM," `https://www.fs.fed.us/t-d/pubs/pdf/99511204.pdf`, 1999. Accessed: 03-05-2022.

[35] USDA Forest Service, "Interagency Retardant Base Planning Guide," `https://www.fs.fed.us/t-d/pubs/pdf/06511803.pdf`, 2006. Accessed: 03-05-2022.

[36] Roskam, J., *Airplane Design Part VIII: Airplane Cost Evaluation*, DARcorporation, Lawrence, KS, 2018.

[37] Zijp, S., "Development of a Life Cycle Cost Model for Conventional and Unconventional Aircraft," *T.U. Delft*, 2014.

[38] Insinna, V., "Japan's C-2 airlifter makes its international debut," *DefenseNews*, 2017.

[39] International, F., "The Market for Military Transport Aircraft," *Forecast International*, 2010.

[40] US Forest Service, "Fire & Aviation Management DC-10 Briefing Paper," `https://www.nifc.gov/nicc/administrative/nmac/L-14-13%201_DC-10BriefingPaper.pdf`, 2019. Accessed: 03-06-2022.

[41] Los Angeles World Airports, "Landing Fees and Other Charges," `https://www.lawa.org/-/media/lawa-web/group-and--division/files/air-carrier-operating-permit-acop-lax/landing-fees-at-lax.ashx`, 2019. Accessed: 03-06-2022.

[42] Saunders, D., and Rokos, B., "Massive - and pricey - 747 joins Cal Fire's arsenal to battle wildfires," *The Sun*, 2017. URL `https://www.sbsun.com/2017/09/02/cal-fires-new-firefighting-aircraft-is-pricey-but-worth-it-officials-say/`, Accessed: 02-08-2022.

[43] 117th Congress, "Sustainable Aviation Fuel Act," `https://www.congress.gov/bill/117th-congress/senate-bill/1608/text`, 2020. Accessed: 04-28-2022.

[44] Leslie A. Richardson, J. B. L., Patricia A. Champ, "The hidden cost of wildfires: Economic valuation of health effects of wildfire smoke exposure in Southern California," *Journal of Forest Economics*, 2012.

[45] Leland M. Nicolai, G. E. C., *Fundamentals of Aircraft and Airship Design*, 2nd ed., AIAA education series, American Institute of Aeronautics and Astronautics, Incorporated, 2010.

[46] USDA Forest Service, "Fire Statistics," `https://www.fs.usda.gov/managing-land/fire/wofambrief/firestats`, 2017. Accessed: 03-05-2022.

[47] Congressional Research Service, "Wildfire Statistics," `https://sgp.fas.org/crs/misc/IF10244.pdf`, 2021. Accessed: 03-05-2022.

[48] Perimeter Solutions, "PHOS-CHEK LCE20-Fx," `https://www.perimeter-solutions.com/wp-content/uploads/2021/07/PERI9590_LCE20_Fx_Product_Sheet_v8.pdf`, 2021. Accessed: 03-05-2022.

[49] USDA Forest Service, "Modular Aerial Fire Fighting System," `https://www.fs.fed.us/rm/fire/pubs/pdfpubs/user_gd/ug-02.pdf`, 2006. Accessed: 03-05-2022.

[50] Anderson, J. D., *Introduction to Flight*, 8th ed., McGraw-Hill series in aeronautical and aerospace engineering, McGraw-Hill Education, New Yord, NY, 2016.

[51] Eshelby, M. E., *Aircraft Performance: Theory and Practice*, 1st ed., AIAA Education Series, American Institute of Aeronautics and Astronautics, Incorporated, 2000.

[52] Rockwell Collins, "FCS-7000 Flight Control System," `https://www.collinsaerospace.com/-/media/project/collinsaerospace/collinsaerospace-website/product-assets/files/public/products/product-brochures/controls/flight-controls/fcs-7000-data-sheet.pdf?rev=f90c14d8b18846e39ef25bc9c86e2339`, 2022. Accessed: 03-06-2022.

[53] Goodyear Aviation, *Goodyear Aviation Data Book*, The Goodyear Tire & Rubber Company, 2021.

[54] Under Secretary of Defense, "Memorandum for Under Secretary of Defense for Acquisition and Sustainment," `https://www.dla.mil/Portals/104/Documents/Energy/Standard%20Prices/Petroleum%20Prices/E_2019Oct1PetroleumStandardPrices_190928.pdf?ver=2019-09-30-072433-663`, 2019. Accessed: 03-06-2022.

[55] Federal Aviation Administration, "Aircraft Operating Cost," `https://www.faa.gov/regulations_policies/policy_guidance/benefit_cost/media/econ-value-section-4-op-costs.pdf`, 2019. Accessed: 03-06-2022.

[56] Kroo, I., and Shevell, R., *Aircraft Design: Synthesis and Analysis*, Desktop Aeronautics Inc., Stanford, CA, 2001.

[57] United States Department of Agriculture, "Fire Retardant Standard Mixing System," Tech. rep., Forest Service, Aug. 1999. URL `https://www.fs.fed.us/t-d/pubs/pdf/99511204.pdf`, Accessed: 02-08-2022.

[58] *DR29622T Specification*, Dunlop Aircraft Tyres, June 2007.

[59] *DR25821T Specification*, Dunlop Aircraft Tyres, June 2007.

[60] Site, B. . T., "Boeing 737 - Trailing Edge Flaps," `http://www.b737.org.uk/flightcontrols.htm#Trailing_Edge_Flaps`, 1999. Accessed: 02-08-2022.

[61] Division, N. H., "FAR Landing And Takeoff Field Lengths," `https://history.nasa.gov/SP-468/app-h.htm`, 2022. Accessed: 02-08-2022.

[62] Jeziorski, A., "Jet age dawns for 328," `https://www.flightglobal.com/jet-age-dawns-for-328/19508.article`, 1998. Accessed: 02-08-2022.

[63] Abbott Aerospace Canada Ltd., "V-n Diagram Spreadsheet," `http://www.abbottaerospace.com/whats-new/v-n-diagram-spreadsheet/`, 2016. Accessed: 02-08-2022.

[64] Lavietes, M., "Western U.S. Wildfires Cost Insurers up to \$13 billion in 2020," *Reuters Breaking and International News*, 2020. URL `https://www.reuters.com/article/us-usa-wildfires-insured-losses-trfn/western-u-s-wildfires-cost-insurers-up-to-13-billion-in-2020-idUSKBN28P2NQ`, Accessed: 02-08-2022.

[65] Roman, J., Verzoni, A., and Sutherland, S., "Greetings from the 2020 Wildfire Season: Five Undeniable Truths from a Pivotal Year in the World's Growing Struggle with Wildfire," *NFPA Journal*, 2020. URL `https://www.nfpa.org/News-and-Research/Publications-and-media/NFPA-Journal/2020/November-December-2020/Features/Wildfire`, Accessed: 02-08-2022.

[66] Filikov, A. I., Ngo, T., Matthews, S., Telfer, S., and Penman, T. D., "Impact of Australia's catastrophic 2019/20 bushfire season on communities and environment. Retrospective analysis and current trends," *Journal of Safety Science and Resilience*, 2020. URL `https://www.sciencedirect.com/science/article/pii/S2666449620300098`, Accessed: 02-08-2022.